Old Dominion University
ODU Digital Commons

Physics Theses & Dissertations | Physics

Spring 2016

Plasma Processing of Superconducting Radio Frequency Cavities

Janardan Upadhyay
Old Dominion University

Follow this and additional works at: https://digitalcommons.odu.edu/physics_etds

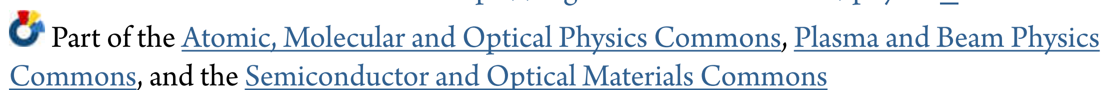
Part of the Atomic, Molecular and Optical Physics Commons, Plasma and Beam Physics Commons, and the Semiconductor and Optical Materials Commons

Recommended Citation

Upadhyay, Janardan. "Plasma Processing of Superconducting Radio Frequency Cavities" (2016). Doctor of Philosophy (PhD), dissertation, Physics, Old Dominion University, DOI: 10.25777/cf7w-b797
https://digitalcommons.odu.edu/physics_etds/98

This Dissertation is brought to you for free and open access by the Physics at ODU Digital Commons. It has been accepted for inclusion in Physics Theses & Dissertations by an authorized administrator of ODU Digital Commons. For more information, please contact digitalcommons@odu.edu.

PLASMA PROCESSING OF SUPERCONDUCTING RADIO FREQUENCY CAVITIES

by

Janardan Upadhyay
B.Sc. June 1999, Gorakhpur University, India
M.Sc. July 2001, Gorakhpur University, India
M.S. June 2008, Old Dominion University

A Dissertation Submitted to the Faculty of
Old Dominion University in Partial Fulfillment of the
Requirements for the Degree of

DOCTOR OF PHILOSOPHY

PHYSICS

OLD DOMINION UNIVERSITY
May 2016

Approved by:

Leposava Vuskovic (Director)

H. Lawrence Phillips (Member)

Alexander L. Godunov (Member)

Jean R. Delayen (Member)

Mileta Tomovic (Member)

ABSTRACT

PLASMA PROCESSING OF SUPERCONDUCTING RADIO FREQUENCY CAVITIES

Janardan Upadhyay
Old Dominion University, 2016
Director: Dr. Leposava Vuskovic

The development of plasma processing technology of superconducting radio frequency (SRF) cavities not only provides a chemical free and less expensive processing method, but also opens up the possibility for controlled modification of the inner surfaces of the cavity for better superconducting properties. The research was focused on the transition of plasma etching from two dimensional flat surfaces to inner surfaces of three dimensional (3D) structures. The results could be applicable to a variety of inner surfaces of 3D structures other than SRF cavities. Understanding the Ar/Cl_2 plasma etching mechanism is crucial for achieving the desired modification of Nb SRF cavities. In the process of developing plasma etching technology, an apparatus was built and a method was developed to plasma etch a single cell Pill Box cavity. The plasma characterization was done with the help of optical emission spectroscopy. The Nb etch rate at various points of this cavity was measured before processing the SRF cavity. Cylindrical ring-type samples of Nb placed on the inner surface of the outer wall were used to measure the dependence of the process parameters on plasma etching. The measured etch rate dependence on the pressure, rf power, dc bias, temperature, Cl_2 concentration and diameter of the inner electrode was determined. The etch rate mechanism was studied by varying the temperature of the outer wall, the dc bias on the inner electrode and gas conditions. In a coaxial plasma reactor, uniform plasma etching along the cylindrical structure is a challenging task due to depletion of the active radicals along the gas flow direction. The dependence of etch rate uniformity along the cylindrical axis was determined as a function of process parameters. The formation of dc self-biases due to surface area asymmetry in this type of plasma and its variation on the pressure, rf power and gas composition was measured. Enhancing the surface area of the inner electrode to reduce the asymmetry was studied by changing the contour of the inner electrode. The optimized contour of the electrode based on these measurements was chosen for SRF cavity processing.

Copyright, 2016, by Janardan Upadhyay, All Rights Reserved.

DEDICATED TO MY PARENTS

ऋग्वेद श्लोक्

को अद्धा वेद क इह प्र वोचत्कुत आजाता कुत इयं् विसृष्टी: ।
अर्वाग्देवा अस्य विसर्जनेनाथा को वेद यत् आबभूव ॥
इयं् विसृष्टीर्यत् आबभूव यदि वा दधे यदि वा न ।
यो अस्याध्यक्ष्: परमे व्योमन्त्सो अन्ङ्ग वेद यदि वा न वेद ॥

Who verily knows and who can here declare it, whence it was born and whence comes this creation?
The Gods are later than this world's production. Who knows then whence it first came into being?
He, the first origin of this creation, whether he formed it all or did not form it,
Whose eye controls this world in highest heaven, he verily knows it, or perhaps he knows not.

Rig Veda 10:129

ACKNOWLEDGMENTS

I am finally coming to the end of my educational journey and would like to express my gratitude and appreciation to all of countless individuals who have been part of my journey for all these years.

I would like to begin by thanking my Ph.D. advisor, Dr. Lepsha Vuskovic, for providing guidance, having patience and being calm during all the ups and downs of this journey and giving me freedom to pursue different experimental ideas. A big thanks to Dr. Svetozar Popovic, for his guidance in the lab, his passion for experiments and enthusiasm for new ideas. Thanks to my research advisors at Jefferson laboratory, Dr. Larry Phillips and Dr. Anne-Marie Valente-Feliciano for guiding me through my Ph.D. work related to th SRF cavity. A huge thanks to my thesis committee members: Dr. Alex Godunov, Dr. John Delayen and Dr. Mileta Tomovic for their continuous feedback during my Ph.D. progrom. Special thanks to Dr. Charles Sukenik for always helping me including on the weekends and Dr. Gail Dodge for smoothing out all the challenges, a graduate student faces. Thanks to Dr. Larry Weinstein for having confidence in me and giving me the opportunity to join the Ph.D program at ODU.

Thanks to Dr. Ari Palczewski, Ms. Tina Harris, Ms. Olga Trofimova, Mr. Steve Castagnola and Mr. Thurman for their ongoing technical supports during the cavity testing and surface analysis. I would like to express my sincere gratitude to Ms. Lisa Okun, Mrs. Annette Guzman-Smith and Mrs. Delicia Malin for all the numerous support during my Ph. D. work.

Thanks to Do Im, who without his keenness and effort on all the hard experimental work my accomplishments would not have been possible. Thanks to my lab mates Dr. Ana samolov, Dr. Milka Nikolic, Milos Basovic, and Jeremy peshl for making lab a nice and pleasant place to work. In the same vein, I would also like to thank my classmate Dr. Bill Ford, Dr. Mike Mayer and Dr. Mike Spata.

Thanks to Dr. Senthilraja for helping me transition to life in Norfolk. Many thanks to my roommates, Vardhan and Raghu, for making me feel right at home and also my friends Srujana, Sirisha, Asma, vinutha and Nakul for their exciting conversations.

Thanks to Dr. Aye Lu Win and Jack for regular lunch and coffee sessions with interesting conversations which always cheered me up and kept me motivated. A huge

thanks to Dr. Subashini De silva for all the technical help and friendship during all these years.

I would also like to thank to my professors and friends in India: Dr. Vivek Tiwari and Dr. Shantanu Rastogi for inspiring me to pursue research work and Praveen, Sachchidananda, Dr. Durgesh, Kailash, Sameer, Pradeep, Mritunjay and Dr. Amitava for their constant support.

I would especially like to thank my mom and dad for supporting me throughout this journey and for placing very high importance on my education. A special thanks to my elder brother Dr. Karunakar Upadhyay for kindling my interest in physics and encouraging me to pursue a Ph.D. A huge thanks to my sister in law, Rekha, nephew Kaustubh ans sister Asha. A big thanks to my younger brother Vijay (Veenoo), who has always been supportive of me. I am indebted to my grandmother (Aiya) for all the love and support, without her it would not have been possible.

The list is endless, but I would like to thank all who have helped me in every way during this journey.

This work is supported by the Office of High Energy Physics, Office of Science, Department of Energy under Grant No. DE-SC0007879 and DE-SC0014397. I would like to acknowledge financial support received from Jefferson Laboratory through Graduate Student Research Assistantship [1].

[1]Jeeferson Laboratory is opeated by Jefferson Science Associates under DOE No. Contract No. DE-AC05-06OR23177

TABLE OF CONTENTS

Page

LIST OF TABLES ix

LIST OF FIGURES x

Chapter

1. INTRODUCTION 1
   1.1 ORGANIZATION OF THE DISSERTATION 2

2. SRF CAVITY BASICS 5
   2.1 RF CAVITY BASED ACCELERATOR 5
   2.2 ACCELERATING VOLTAGE 6
   2.3 FIGURES OF MERIT 6
   2.4 SUPERCONDUCTIVITY 7
   2.5 THEORY OF SUPERCONUCTIVITY 8
   2.6 SURFACE RESISTANCE 11
   2.7 LOSSES IN SRF CAVITY 13
   2.8 CAVITY PROCESSING 15

3. BASIC PLASMA PROCESSING 18
   3.1 PLASMA PARAMETERS 18
   3.2 TYPES OF PLASMA 20
   3.3 PLASMA PROCESSING 22
   3.4 ETCHING MECHANISM 24
   3.5 ELECTRONEGATIVE PLASMA 26
   3.6 OBSERVABLES 26
   3.7 PROCESS PARAMETERS 27
   3.8 PLASMA DIAGNOSTICS 29

4. RF PLASMA 32
   4.1 SYMMETRIC PLASMA 33
   4.2 ASYMMETRIC PLASMA 34
   4.3 SUMMARY 41

5. EXPERIMENTAL SET UP FOR NIOBIUM SAMPLES 43
   5.1 FLAT SAMPLE EXPERIMENT 43
   5.2 RING SAMPLE EXPERIMENT 44

6. EXPERIMENTAL RESULTS FOR RING SAMPLES 55
6.1 DEPENDENCE OF THE ETCH RATE ON THE PROCESS PARAMETERS 57
6.2 DETERMINATION OF THE ETCH RATE MECHANISM AND DEPENDENCE OF ETCH RATE UNIFORMITY ALONG THE GAS FLOW DIRECTION ON PROCESS PARAMETERS 61
6.3 VARIATION OF THE SELF BIAS POTENTIAL WITH PROCESS PARAMETERS AND OTHER ASYMMETRY MEASUREMENTS .. 78
6.4 OPTIMIZATION OF THE ELECTRODE SHAPE TO REVERSE THE ASYMMETRY IN PLASMA 89

7. EXPERIMENTAL SET UP FOR SINGLE CELL SRF CAVITY 102
7.1 SINGLE CELL PILL-BOX CAVITY EXPERIMENT 103
7.2 SUMMARY 111

8. RF TEST OF THE PLASMA ETCHED CAVITY AT CRYOGENIC TEMPERATURE 113
8.1 EXPERIMENT AND METHOD 113
8.2 RESULTS AND DISCUSSIONS 114
8.3 CONCLUSION 118

9. SUMMARY AND CONCLUSIONS 119

BIBLIOGRAPHY 122

VITA 130

LIST OF TABLES

Table Page

1. Etch rate variation at fixed pressure and different flow rates achieved using the gate valve. 69

2. Etch rate variation at a given pressure and different flow rates achieved with and without turbo molecular pump. 70

3. Etch rate variation of the second ring with/ without the first Nb ring. Etching conditions are the same. 78

LIST OF FIGURES

Figure Page

1. Scheme of plasma sheath potential distribution in symmetric and asymmetric discharge. 33

2. Illustration of formation of self-bias potential 35

3. Scheme of the experimental setup for the flat Nb sample etching 44

4. Atomic force micrograph of a sample processed with BCP technique. Surface roughness was 286 nm. 45

5. Atomic force micrograph of a plasma etched BCP sample. Surface roughness was 215 nm. 46

6. Photo of the cylindrical processing cavity. 48

7. Cylindrical cavity and inner electrodes with varying diameter. In clockwise direction: the disassembled arrangement and three end on views of the assembled electrode configuration, starting with the lowest diameter of the electrode. 49

8. Pumping system for corrosive gases. 50

9. Photo of experimental setup for cylindrical plasma processing. 51

10. Photos of etching samples: (a) Flat sample (b) Ring samples. 51

11. Photo of experimental set-up for temperature variation during etching cylindrical cavity. 53

12. Schematic diagram of atmospheric pressure rf power feedthrough. 54

13. Spreading of plasma inside the cylindrical cavity at different conditions: top left, lower pressure; top right, medium pressure; bottom left, higher pressure at low power; and bottom right, higher pressure and higher power. 56

14. Etching rate and self-bias dependence on the diameter of the driven electrode. Solid lines are visual guidelines. 58

15. Etching rate dependence on the gas pressure. Solid line is visual guideline. 59

16. Etching rate dependence on rf power. Solid line is the exponential fit. . . . 60

17. Etching rate dependence on concentration of chlorine (% Vol) diluted in argon. Solid line is visual guideline. 62

18. Cross-sectional images and schematic of coaxial rf electrode, plasma, and sheath potentials: (a) Image of coaxial electrodes (b) Image of coaxial plasma (c) Plasma sheath potential distribution in coaxial rf plasma (d) Plasma sheath potential distribution in coaxial rf plasma with positive dc bias on the inner electrode. 64

19. Etching rate dependence on the Nb temperature. Solid line represents exponential fit. 65

20. Etching rate dependence on the dc bias at the inner electrode. Solid line is a visual guideline. 67

21. Etching rate dependence on gas composition and indicated etching parameters. 68

22. Schematic and image of the Nb ring sample placed on inner surface of the outer cylinder: (a) Cross sectional view of two ring samples placed on the inner surface of the outer cylinder indicated with arrows (b) Schematic of axial view of the two ring samples (c) Schematic of loading effect with inner electrode and two ring samples when plasma is on. Arrows show the direction of the gas and rf power flow. 71

23. Etch rate ratio of two rings versus temperature of the substrate. Solid line is a visual guideline. 72

24. Etch rate ratio of two rings versus the positive bias on the inner electrode. Solid line is a visual guideline. 73

25. Etch rate ratio of two rings versus rf power in the system. Solid line is a visual guideline. 74

26. Etch rate ratio of two rings versus pressure of the system. Solid line is a visual guideline. 75

27. Etch rate ratio of two rings versus Chlorine percentage in Ar/Cl_2 gas mixture. Solid line is a visual guideline. 76

28. Etch rate ratio of two rings versus diameter of the inner electrode in the system. Solid line is a visual guideline. 77

29. Schematic layout of two coaxial cylindrical electrodes. 79

30. Schematic layout of coaxial cylindrical dischrages with different diameter inner electrodes. 80

31. Self-bias potential dependence in the Ar plasma on the pressure for different diameter inner electrodes. Solid lines are visual guideline. 82

32. Self-bias potential dependence in the Ar plasma on the rf power for different diameters inner electrodes. Solid lines are visual guideline. 83

33. Self-bias potentail dependence on the rf power for different diameter inner electrodes in Ar and Ar/Cl_2 plasma. Solid lines are visual guideline. 84

34. Self-bias potential dependence on the rf power for electrode diameter of 5.0 cm for pure Ar and Ar/Cl_2 mixture. Solid lines are visual guideline. . . 85

35. Self-bias dependence on the gas pressure for electrode diameter of 5.0 cm for pure Ar and Ar/Cl_2 mixture. Solid line is a visual guideline. 86

36. The dc current variation with pressure for 5.0 cm diameter electrode for Ar and Ar/Cl_2 plasma. Solid line is a visual guideline. 87

37. The dc current variation on the dc bias voltage at fixed pressure and fixed rf power for Ar and Ar/Cl_2 plasma. Solid line is a visual guideline. 88

38. Illustration of various structured inner electrodes in coaxial plasma: (a) disc loaded corrugated structure (DLCS), (b) small pitch bellows, (c) large pitch bellows, and (d) straight cylindrical tube. 91

39. Illustration of various structured inner electrodes in coaxial plasma: (a) strait tube, (b) large pitch bellows, and (c) disc-loaded corrugated structure (DLCS). 93

40. Self-bias potential dependence on the pressure for various structured electrodes in the Ar plasma. Solid lines are visual guidelines. 94

41. Self-bias potential dependence in the Ar plasma on the rf power for various structured electrodes in the Ar plasma. Solid lines are visual guidelines. . . 95

42. Self-bias potential dependence on pressure in the Ar/Cl_2 plasma for various structured electrodes. Solid lines are visual guidelines. 96

43. Self-bias potential dependence in the Ar/Cl_2 plasma on the rf power for various structured electrodes. Solid lines are visual guidelines. 97

44. The dc current variation with rf power for various structured electrodes and two different gas compositions. Solid lines are visual guidelines. 98

45. Self-bias potential dependence on the rf power in the Ar/Cl_2 plasma for various structured electrodes. Solid lines are visual guidelines. 99

46. The etch rate variation with differently structured electrodes for the same plasma conditions. 100

47. Schematic diagram of the single cell pill-box cavity experiment. 104

48. Cylindrical single cell pill-box cavity 105

49. Photos of variable diameter Nb ring samples to be placed in the pill-box cavity (left) and Nb ring samples inside the pill-box cavity (right). 105

50. Arrangements of the inner electrode length in the pill-box cavity (a) variable shape electrode for full length cavity (b) full length electrode (c) shortened electrode in the pill-box cavity. 107

51. Image of the Nb sample closest to the gas flow inlet: before plasma etching (left) and after plasma etching (right). 108

52. Image of moving gas flow inlet setup. 109

53. Pill-box cavity with movable inner electrode and movable gas flow inlet. . 110

54. Pill-box cavity with plasma. 110

55. Schematic diagram of the inner electrode, gas flow inlet and pill-box cavity during plasma processing. 111

56. Experimental setup to plasma etch single cell SRF cavity. 114

57. Images of a single cell cavity (left) plasma etched (right) (BCP). 116

58. Images of surface analysis of residue from plasma etched cavity. 116

59. rf test results of the plasma etched SRF cavity. Black, green, blue and yellow markers indicate performence data of the plasma etched single cell SRF cavity at various stages of the test. 117

CHAPTER 1

INTRODUCTION

Many particle accelerators currently in use or planned to be built in the future, use superconducting radio frequency (SRF) cavities based technology. High frequency electromagnetic fields are generated in these electrodynamic resonant cavities, made of bulk superconducting materials, typically niobium. Niobium (Nb) is a superconducting material with a critical temperature of 9.18 K. In order for these cavities to perform, the mechanically damaged layer formed during fabrication has to be removed from the inner surfaces. To improve the rf performance of SRF niobium cavities, the cavity surface should be prepared by a process that enhances surface smoothness, removes impurities, and creates less sharp grain boundaries. Buffered chemical polishing (BCP) or electro polishing (EP) are currently used technologies based on the use of hydrogen fluoride (HF) in liquid acid baths, which poses major environmental and personal safety concerns.

Plasma etching technology developed for the semiconductor industry represents a new and exciting method for making precise features in insulators, semiconductors, and metals. Plasma etching technology, like rf sputtering, ion beam milling and reactive ion etching is widely used as a tool for the fabrication of most microelectronic components. Sice the dimension usually considered in the semiconductor industry is in the nm scale, there is a potential to achieve improved surface features and to lower the surface roughness resulting in superior rf performance and higher-gradient SRF cavities by a simplified and cleaner manufacturing process, that is by plasma etching compared with conventional wet chemical etching processes.

HF-free plasma-based (dry) technologies would be much more controllable, less expensive, and more environment-friendly. A successful application of plasma etching to Nb cavities have major benefits in the cost reduction of the next generation of particle accelerators. There is also a possibility, since the final stage of plasma etching produces a pure Nb surface free from sub-oxides and residue from wet chemistry, that a variety of superior high quality surfaces may be intentionally created through plasma processing, such as pure niobium pentoxide without suboxides, or superconducting niobium nitride. Such surface modifications can be done in the same process

cycle with the plasma etching process.

We are developing a method to etch the inner surfaces of SRF cavities made of Nb by using a coaxial capacitive rf plasma of an argon/ chlorine (Ar/Cl_2) gas mixture. We have adopted a stepwise approach by choosing smooth coaxial cylinder electrodes as an intermediary geometry, where the outer, grounded electrode is to be etched. The discharge is obviously asymmetric due to differences in the surface area of the inner and outer electrodes. The sheath voltage asymmetry is compensated by applying a positive dc bias to the inner electrode. In developing the cavity etching technology, we were using a sample, which was a ring rather than a flat coupon. The ring sample has proven to allow controlled studies of the etching rate variations in cylindrical geometry of a coaxial asymmetric discharge. In all experiments, one or more ring samples were positioned to fit tightly on the inner surface of the outer electrode, to ensure uniform electric and thermal contact. We have achieved plasma etching by a cylindrical coaxial capacitive rf discharge. Surface augmentation to reduce the sheath voltage asymmetry was adopted and four structures were experimented. The most suitable structure was chosen for cavity processing. To mimic the plasma surface interaction in the SRF cavity, a pill box cavity was adopted and experiments were performed in a pill box cavity. Segmented plasma production by stepwise movement of the gas flow inlet and inner electrode was found suitable for varied diameter structure plasma processing. After lessons learned with the pill box cavity, an actual SRF cavity was plasma etched and rf tested at cryogenic temperatures.

1.1 ORGANIZATION OF THE DISSERTATION

Chapter 2 explains the basics of superconductivity and the SRF cavity. It also points out the problems associated with the SRF cavity in particle accelerators. This chapter describes the currently used chemical processing methods like buffered chemical processing (BCP), electropolishing (EP), centrifugal barrel polishing (CBP) and the steps to prepare the surface of an SRF cavity for use in accelerators.

Chapter 3 introduces the basics of plasma and plasma processing. It explains the basic terms and terminology used in plasma physics and the plasma etching industry. The process parameters, plasma parameters and diagnostic equipment to measure these parameters is explained. It describes different etching mechanisms possible during plasma etching and different etch observables defined by the goals of the processes.

Chapter 4 provides details of the rf plasma, types of plasma depending on the power coupling method of rf power. Inductively coupled rf plasma, capacitively coupled rf plasma and particulary asymmetric capacitively coupled plasma are presented. The relationship between surface area ratio of electrodes and the plasma sheath voltage ratio is explained. A review of the work done to change the plasma potential in rf asymmetric plasma is presented.

Chapter 5 decribes the actual experimental setup regarding the cylindrical cavity etching experiment. The coupling scheme of rf power to inner electrode, the vacuum pumping system and the rf power supply with matching network, and the dc power supply is shown. It describes the gas flow system, ring sample and the arrangement of the ring samples in the cylindrical cavity for the etch rate non uniformity experiment. The method to raise, measure and monitor the temperature of the cylindrical cavity is presented.

Chapter 6 presents the techniques used to compensate for the asymmetry in sheath voltage due to surface area difference by using a positive dc power supply. This chapter also shows the dependence of the etch rate on process parameters based on the ring sample experiment data. The etch rate dependence on the pressure, power, chlorine concentration in the gas mixture, and the diameter of the inner electrode in this type of coaxial discharge is presented. The variation in etch rate due to temperature and dc bias change is shown and the etch rate mechanism determination is determined. The etch rate non uniformity due to depletion of radicals along the gas flow direction on process parameters is reported. The quantitative measurement of the self-bias potential for different diameter electrodes and its variation on process parameters is presented. The self-bias dependence on gas pressure and rf power for Ar and Ar/Cl_2 plasma in coaxial type asymmetry is shown. In this chapter we also present the dependence of the external dc current (required to eliminate the self-bias potential) on gas pressure, rf power, and concentration of chlorine in the gas mixture for different diameters of inner electrodes. It is possible to increase the inner electrode surface area without increasing its diameter. Four differently structured inner electrodes were constructed and their effect on the self-bias potential was measured. The experimental results of the measured self-bias potential and dc current of these four structures in an asymmetric coaxial discharge in Ar and Ar/Cl_2 mixture at different pressures and rf powers are presented and discussed.

Chapter 7 describes the apparatus and method for plasma etching of the inner

surface of a variable-diameter cylindrical cavity like the SRF cavities. To reduce the etch rate non-uniformity due to depletion of the radicals, the simultaneous movement of the gas flow inlet and the inner electrode to produce segmented plasma is implemented and shown in this chapter. The concept of a pill box cavity made of steel of similar dimension to the standard SRF cavity to use for the experiment related to plasma etching is described and the experimental setup is shown. The option to choose the size of the electrode and related complexity due to asymmetric plasma is explained and the chosen electrode size is presented..

Chapter 8 presents the test results of the plasma etched single cell 1497 MHz SRF cavity. The mechanically and buffer chemically etched SRF cavity is rf tested at cryogenic temperatures. The same cavity is plasma etched and tested again at the same cryogenic temperatures. The Q_0 vs E_{acc} graphs are plotted and shown. The meanings of different plots are explained.

CHAPTER 2

SRF CAVITY BASICS

2.1 RF CAVITY BASED ACCELERATOR

The early generation particle accelerators were DC accelerators. The DC accelerators are huge in size and they are limited in energy by corona discharges. The rf cavity based accelerator does not have these limitations. rf cavities are electrodynamic structures resonating at microwave frequency and imparting electromagnetic energy to traversing charged particles. The rf fields in the cavity are obtained from eigenvalues of the equation

$$\left(\nabla^2 - \frac{1}{c^2}\frac{\partial^2}{\partial t^2}\right)\left\{\begin{array}{c}\vec{E}\\ \vec{B}\end{array}\right\} = 0\,, \tag{1}$$

with boundary conditions $\hat{n} \times \vec{E} = 0$ and $\hat{n} \cdot \vec{B} = 0$, where $\hat{n}$ is the unit vector normal to the cavity surface. $\vec{E}$ and $\vec{H}$ are electric and magnetic fields in the cavity with $\vec{B} = \mu_0 \vec{H}$, where μ_0 is the free-space permeability. The boundary conditions ensure the absence of any parallel electric or normal magnetic field at the surface of the cavity.

The simplest example of a cavity is a cylindrical waveguide shorted by a metalic structure at both ends is called a pill box cavity. The rf cavities can have different mode of structures depending on the length and width of the structure. The transverse magnetic (TM) mode, where the magnetic field is transverse to the cavity axis, and the transverse electric (TE) mode, where the electric field is transverse to the cavity axis, are prominant mode inside a rf cavity. TM_{010} is the most used mode for the accelerating cavity. The TM type accelerator cavities are generally half-wave structures, where the accelerating gap in these cavities is $\beta\lambda/2$. The $\lambda/2$ is the half wavelength of the corresponding resonant frequency and β is v/c, the ratio of the velocity of the charged particle to the velocity of light [1].

2.2 ACCELERATING VOLTAGE

Charge particles, during the transit in the cavity, see the time varying electric field. As the electron approaches the velocity of light at low energy, the transit time to traverse the cavity for maximum gain is one half of the rf period.

$$T_{cav} = d/c = \pi/\omega_0, \tag{2}$$

where ω_0 is the angular frequency of the accelerating mode. We can calculate the accelerating voltage, V_c for a cavity to be

$$V_c = \frac{1}{e}(\text{maximum energy gain possible during transit}). \tag{3}$$

This voltage is given by the line integral of E_z as seen by the electron,

$$V_c = \int_0^d E_z(\rho = 0, z)e^{-i\omega_0 z/c}\mathrm{d}z\,. \tag{4}$$

Generally, the average accelerating electric field (E_{acc}), the electron sees during transit is given by

$$E_{acc} = V_c/d. \tag{5}$$

2.3 FIGURES OF MERIT

The cavity shape and size are optimized based on the specific application of the accelerator. There are figures of merit explained below, which are helpful in doing a comparison between different cavity designs.

2.3.1 GEOMETRY FACTOR AND SHUNT IMPEDENCE

Due to the currents within the surface layer of the cavity walls, even a superconducting cavity shows losses at the rf frequency. This dissipated energy is part of one of the important figures of merit for an accelerating cavity called the quality factor Q_0, which is defined as

$$Q_0 = \frac{\omega U}{P_{diss}}. \tag{6}$$

Where U is the stored energy, ω is the frequency of the cavity, and P_{diss} is power dissipation in cavity walls. As the energy oscillates between electrical energy and magentic energy inside the cavity. The stored energy in an rf cavity is given by

$$U = \frac{1}{2}\varepsilon_0 \int_V \mid \vec{E} \mid^2 \mathrm{d}v = \frac{1}{2}\mu_0 \int_V \mid \vec{H} \mid^2 \mathrm{d}v, \tag{7}$$

and power dissipation is given by

$$P_{diss} = \frac{1}{2}R_s \int_S \mid \vec{H} \mid^2 \mathrm{d}s, \tag{8}$$

where $\vec{E}$ and $\vec{H}$ are the electric and magnetic fields in the cavity. The integration is taken over the entire interior cavity surface assuming that R_s is independent of H. Typically R_s is several tens of nano ohms for a well prepared Nb SRF cavity.

The geometrical factor, which is only dependent on the cavity shape is defined as

$$G = Q_0 R_s\,. \tag{9}$$

The geometrical factor is independent of the size and material of the cavity. Another quantity that defines the losses in the cavity is shunt impedence, R_a, defined as

$$R_a = \frac{V_c^2}{P_{diss}}\,. \tag{10}$$

The unit of shunt impedence is ohms per cell. During the optimization of the cavity, the aim is to have as high a shunt impedence as possible. The ratio of $[R_a/Q_0]$ is

$$\left[\frac{R_a}{Q_0}\right] = \frac{V_c^2}{\omega_0 U}\,, \tag{11}$$

which is independent of the surface resistance. The ratio of $[R_a/Q_0]$ is also independent of the cavity size [1].

2.4 SUPERCONDUCTIVITY

Superconductivity is a phenomenon where, below a certain temperature (T_c), the resistivity of the material goes to zero and it shows perfect diamagnetism. It was first discovered by Kammerlingh-onnes in 1911 [2]. Several pure elements, compounds and alloys are superconducting materials at varied critical temperatures. When below the critical temperature (T_c), superconducting material completely expels the

magnetic field from its interior. They behave like a perfect diamagnet and this was first observed by Meissner [3]. There is a current flowing on the surface of the superconducting material which produces a magnetic field in the opposite direction of the applied magnetic field to cancel it. These currents do not decay with time since there is no resistance in superconductors. The exclusion of the magnetic field from the superconducting materials interior differentiates it from the perfect conductors. However, there is a critical magnetic field for each material, H_c, above which the superconductivity is destroyed. This critical magnetic field H_c is related thermodynamically to the free energy difference between the normal and superconducting state. There is a tempertaure dependence of this critical field and it is related to critical temperature, T_c [1, 4, 5]

$$H_c(T) \simeq H_c(0)\left[1-\left(\frac{T}{T_c}\right)^2\right]. \tag{12}$$

2.5 THEORY OF SUPERCONUCTIVITY

Gorter and Casimir, in 1934 [6], interpreted thermodynamically the coexistance of normal and superconducting electrons. London and London, in 1935 [7], derived the electrodynamic equation to describe resistanceless and the perfect diamagnetic nature of the superconductors [8]. This is called the two fluid model of the superconductivity, where the assumption is that the superconductor has two types of electrons, normal conducting and superconducting. In the two fluid model, the normal conducting electron density, n_n, and the superconducting electron density, n_s, have two corresponding velocity components, v_n and v_s.

The two-fluid model separates the electrons into a superfluid component with density, n_s and velocity v_s, and a normal component with density n_n and velocity v_n, and with a total electron density of $n = n_s + n_n$. The super electrons are accelerated by a constant electric field, $\vec{E}$

$$m\frac{\partial \vec{v}_s}{\partial t} = e\vec{E}, \tag{13}$$

which provides the first London equation

$$\frac{\partial \vec{J}_s}{\partial t} = \frac{n_s e^2}{m}\vec{E}, \tag{14}$$

where n_s is the density of the superelectrons, m is the electron mass, and e is the charge of an electron.

The normal conducting electron and superconducting electrons current density are given by

$$\vec{J_n} = -en_n\vec{v_n}\,, \tag{15}$$

$$\vec{J_s} = -en_s\vec{v_s}\,. \tag{16}$$

The superconducting electron component does not face resistance while the normal conducting electron current component does;

$$\vec{J_n} = \sigma_n\vec{E}\,. \tag{17}$$

Using Maxwell equations

$$\vec{\nabla} \times \vec{E} = -\frac{\partial \vec{B}}{\partial t}\,, \tag{18}$$

provides the following

$$\vec{\nabla} \times \vec{J_s} + \frac{n_s e^2}{m}\vec{B} \tag{19}$$

for which, London realised that this quantity has to not only be time independent, but also has to be zero.

$$\vec{\nabla} \times \vec{J_s} + \frac{n_s e^2}{m}\vec{B} = 0\,. \tag{20}$$

Combining this equation with another Maxwell equation

$$\vec{\nabla} \times \vec{B} = \mu_0\vec{J_s}\,, \tag{21}$$

gives

$$\nabla^2\vec{B} - \frac{\mu_0 n_s e^2}{m}\vec{B} = 0\,, \tag{22}$$

which can be also represented as

$$\nabla^2\vec{B} = \frac{1}{\lambda_L^2}\vec{B}\,, \tag{23}$$

where λ_L is the penetration depth. This shows that the current density and magnetic

field in superconducting materials exist in a thin surface layer of thickness λ_L,

$$\lambda_L = \left[\frac{m}{\mu_0 n_s e^2}\right]^{1/2} , \tag{24}$$

thus,

$$B(x) = B(0)exp\left[-\frac{x}{\lambda_L}\right] , \tag{25}$$

where $B(0)$ is the external magnetic field, which drops exponentially inside the superconductor. The depth at which the magnetic field decays by a factor of $1/e$ is called the London penetration depth (λ_L).

The temperature dependence of the penetration depth is given by

$$\lambda_L(T) = \frac{\lambda_L(0)}{\sqrt{1-\left(\frac{T}{T_c}\right)^4}} . \tag{26}$$

There is a discrepency between the calculated and experimental value of λ_L. The explanation of this discrepency required an additional concept, the coherence length (ξ_0). Pippard introduced a characteristic dimension for superconducting wave functions (ξ_0) called coherence length, which could be estimated by the uncertainty principle [9]

$$\xi_0 = a\frac{\hbar v_F}{k_B T_c} , \tag{27}$$

where a is numerical constant, v_F is the Fermi velocity and k_B is the Boltzmann constant. The fit to the experimental data provides the value of a = 0.15. The value of (ξ_0) for Nb is $\approx$ 39 nm.

Ginzburg and Landau explained superconductivity [10] based on an order parameter, and divided the superconductors into two categories. The superconductors are categorized based on the Ginzburg-Landau parameter $\kappa = \frac{\lambda_L}{\xi}$ as

- Type I Superconductors - $\kappa = \frac{\lambda_L}{\xi} < \frac{1}{\sqrt{2}}$
- Type II Superconductors - $\kappa = \frac{\lambda_L}{\xi} > \frac{1}{\sqrt{2}}$

where κ is a roughly constant ratio over temperature.

For type I superconductors there is only one critical magnetic field, B_c, and for type II superconductors there are two critical magnetic fields, B_{c1} and B_{c2}. Type

II superconductors show superconducting properties below B_{c1}, while show normal conducting properties above B_{c2}. In the mixed state of $B_{c1} < B < B_{c2}$, type II superconductors are penetrated by lines of magnetic flux called vortices. The theory of superconductivity based on modern mechanics was successfully explained by the BCS theory [11]. The theory suggests that it is energetically favorable for two electrons to form a Cooper pair at low temperature. This process is assisted by phonons. Each pair consists of electrons of opposite spin and momentum. Though Cooper pairs are energetically favorable below T_c, all of the electrons are paired at T = 0 K. At a finite temperature, $T < T_c$, the fraction of unpaired electrons is given by the Boltzmann factor $\exp(\Delta/k_bT)$. The variation of the energy gap close to T_c is predicted to be

$$\frac{\Delta(T)}{\Delta(0)} \approx 1.74 \left(1 - \frac{T}{T_c}\right)^{1/2} . \tag{28}$$

The energy gap vanishes at the critical temperature, a large number of quasi-particles are thermally excited and the material becomes normal conducting [1, 4, 8, 12, 13].

2.6 SURFACE RESISTANCE

Superconductors have no resistance for direct current propagation. When the current is varying particularly at high frequency like microwave frequency, there is a substantial surface resistance. This resistance can be explained by the two fluid model consisting of superelectrons and normal electrons. In the direct current case, no electric field exists in the metal, as superelectrons would accelerate and the current would increase indefinitely. Since there is no electric field, normal electrons cannot get accelerated and no resistance occur. Normal electrons do not contribute to the dc flow. In the case of rf, the inertial mass of the electrons of the supercurrents creates a lag between the electric field and current. This electric field accelerates normal electrons and some of the currents flow through the normal electrons. In superconductors, the rf currents is carried by both super electrons and normal electrons. The conductivity of the superconductor has both components,

$$\sigma = \sigma_n - i\sigma_s . \tag{29}$$

The conductivity contributed by the normal electrons is given by

$$\sigma_n = \frac{n_n e^2 \tau}{m} , \tag{30}$$

and the conductivity contributed by the super electrons is given by

$$\sigma_s = \frac{2n_s e^2}{m\omega}\,, \tag{31}$$

where n_n and n_s are the densities of the normal and super electrons, τ is the relaxation time between collisions, and e and m are the charge and mass of an electron. The impedance of the superconductor can be written as

$$Z_s = R_s + iX_s\,, \tag{32}$$

where the real part of the impedence is

$$R_s = \frac{1}{2}\sigma_n \mu_0^2 \lambda_L^3 \omega^2, \tag{33}$$

and the imaginary part of the impedence is

$$X_s = \mu_0 \lambda_L \omega. \tag{34}$$

The surface resistance is

$$R_s \propto \lambda_L^3 \omega^2 l \exp\left(-\frac{\Delta(T)}{k_B T}\right)\,. \tag{35}$$

The formula for the surface resistance (R_s) of superconductors, based on the very successful BCS theory, is a function of temperature (T), frequency (ω), and depends on material properties such as the critical temperature (T_c), energy gap (Δ), coherence length (ξ), penetration depth (λ_L), and mean free path (l). A good approximation of surface resistance at $T < T_c/2$ and $\hbar\omega \ll \Delta$ is

$$R_s \sim \frac{A_s}{T}\omega^2 \exp\left(-\frac{\Delta(T)}{k_B T}\right) + R_{res} = R_{BCS}(T) + R_{res}\,, \tag{36}$$

where R_{res} is the residual resistance and R_{BCS} is the BCS surface resistance. The BCS surface resistance can be calculated by numerical programs [14]. A good expression and fit is

$$R_s = 2 \times 10^{-4} \frac{1}{T}\left(\frac{f}{1.5}\right)^2 \exp\left(-\frac{17.67}{T}\right) + R_{res} = R_{BCS} + R_{res} \tag{37}$$

where f is the rf frequency in GHz and T is the operating temperature of an SRF

cavity.

2.7 LOSSES IN SRF CAVITY

Bulk niobium is used in almost all of the superconducting cavities used in accelerators. The rf critical magnetic field for Nb is around 180 mT and T_C is around 9.2 K. The ideal behavior of an SRF cavity would be achieved if the total surface resistance were equal to the BCS surface resistance value. In reality, there are several effects which contribute to the deviation from the ideal Q_0 vs E_{acc} curve. The effects at low fields are residual resistance, flux trapping, adsorbed gases and resistive particles and effects at high fields are multipacting, field emission and thermal breakdown.

2.7.1 RESIDUAL LOSSES

The residual surface resistance is also temperature dependent quantity and it occurs due to impurities, adsorbed gases, trapped flux and microscopic particles. The residual surface resistance always dominates BCS resistance at lower temperatures. Typically measured values of the residual resistances are between two to fifteen nano ohms. Successive processing of the same cavity shows a difference in masurement of residual resistance. It shows that it is not a well understood phenomenon.

The other source of residual losses in SRF cavities is trapped magnetic flux due to insufficient shielding. Magnetic flux is trapped at lattice defects and in other inhomogeneities called pinning sites, and it inroduces losses [15].

An important loss mechanism is the formation of metallic hydride during the cool down of the niobium cavity. The hydrogen dissolved in bulk niobium gets precipitated on the surface as a hydride at cold tempertaure. This loss is also known as "Q disease". Q disease depends on a number of factors such as the amount of hydrogen dissolved in bulk material, rate of cool down, and the amount of other impurities. The danger of hydride formation is highest in the range of 80-150 K. The Q_0 drop is increased if the cavity is "parked" between this range for an hour or more. Q_0 reduction by a couple orders of magnitude is observed. A common way to avoid hydrogen disease is fast cool down during these temperatures, or by baking the niobium cavity at 600-900^0C for several hours.

The layer of natural niobium oxide is in the range of 10-20 nm thickness and it is dielectric, therefore responsible for residual losses due to oxide formation. While bulk dielectric losses are negligible, interface (between bulk and oxide layer) losses

can yield measurable residual resistance. A possible way to reduce these losses is to eliminate the oxide layer by heating the cavity in a vacuum furnace at temperature greater than $1000^{0}C$ [8, 12].

Thermal breakdown or "quench" is the sudden transition of the superconducting state to the normal conducting state. In an SRF cavity it happens with a sudden drop in the cavity quality factor. The normal conducting defects on the cavity surface get heated by the electrodynamic fields. When the temperature of the defects exceeds the critical temperature, the surrounding area superconductors become normal conductors. This increases the power dissipation enormously and leads to quenching of the SRF cavity. The way to reduce the thermal breakdown is by reducing the normal conducting impurites and improving the thermal conductivity of the niobium.

2.7.2 MULTIPACTING

Multipacting is a process in which an electron emitted from the cavity surface strikes it again, due to resonance condition and then the surface emit more electrons. This process builds up a large number of electrons and consumes a lot of rf power and it does not allow an increase in the cavity field by increasing the rf power. The multipacting phenomenon also depends on the shape and the surface condition of the structures. Modern day accelerators reduce the multipacting in higher beta structures by changing the shape of the cavity, however the low beta structure, spoke cavity, coupler and rf windows are still have problems of multipacting. Few multipacting barriers can be overcome by allowing multipacting to progress for several minutes, these barriers are called soft barriers, while the barriers which can not be processed are called hard barriers. Each primary electron ejects one or more electrons from the surface depending on the energy of the electron and conditions of the surface. The ratio of the number of secondary electrons ejected by the number of the primary electrons impact is called the secondary electron yield (SEY). SEY depends on the material, energy of the primary electron and surface conditions. A proper cleaning of the cavities would help the surface conditions and reduce the SEY, which would reduce the multipacting problem.

2.7.3 FIELD EMISSION

Field emission is a process where electrons tunnel out from the material in the presence of the electric field. Field emission is the main limiting factor in the SRF

cavity performance. The regions of high electric fields in the cavity start emitting electrons with excessive heating and xrays produced by bremsstrahlung. The heating due to these electrons impact on the surface lead to a drop in the quality factor and the higher electric field can not be achieved in the cavity. The original theory of field emission was provided by Fowler and Nordheim (FN) [16]. The original expression of the FN theory was later modified by the field enhancement factor β_{FN}.

The electron current density, including the enhancement factor (β_{FN}) is given by

$$J(E) = \frac{A_{FN}(\beta_{FN}E)^2}{\Phi} \exp\left(-\frac{B_{FN}\Phi^{3/2}}{\beta_{FN}E}\right), \tag{38}$$

where A_{FN} and B_{FN} are the constants and ϕ is the work function of the metal. The field enhancement factor depends on the nature and geometry of the emitter. Field emission can be avoided by maintaining the cleanest condition possible during preparation and assembly of the SRF cavity. High pressure water rinsing is the most successfull technique in avoiding the field emission phenomenon. Helium processing is also used to reduce the field emission.

2.8 CAVITY PROCESSING

The SRF cavity has to be processed before testing at a cryogenic temperature. The processing should provide an impurity free and smooth surace with no pits. It should produce a Nb surface as close to an ideal Nb surface having the least surface resistance. A typical process involves multiple steps, several of them are explained below [17, 18].

2.8.1 BUFFER CHEMICAL POLISHING (BCP)

Buffer chemical polishing (BCP) is the most commonly used chemcial etching process for SRF cavities. In BCP the cavity is filled with nitric acid (HNO_3), hydrofluoric acid (HF), and phosphoric acid(H_3PO_4) in a rato of 1:1:1 or 1:1:2. The role of nitric acid is to oxidize the niobium, while hydrofluoric acid removes the oxide. Since, the reaction is exothermic and the etch rate is too high just by using nitric acid and hydrofluoric acid, phosphoric acid is used as a buffer.

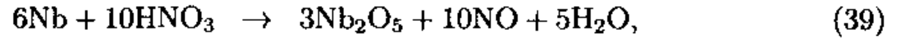

$$6\mathrm{Nb} + 10\mathrm{HNO_3} \rightarrow 3\mathrm{Nb_2O_5} + 10\mathrm{NO} + 5\mathrm{H_2O}, \quad (39)$$

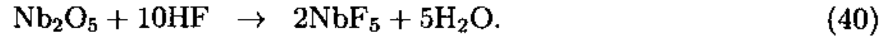

$$\mathrm{Nb_2O_5} + 10\mathrm{HF} \rightarrow 2\mathrm{NbF_5} + 5\mathrm{H_2O}. \quad (40)$$

The standard procedure with a removal rate of 1 micron per minute is called buffer chemical poliching (BCP). The etch rate depends on many factor like temperature, amount of Nb dissolved already in acid and agitation of the acid. At Jefferson Lab the procedure is done at 15^0C. The etch rate drops as Nb gets dissolved into acid, so the old acid mixture has to be replaced by a fresh acid mixture which has to be stirred continuously. Hydrofluoric acid is quite dangerous to handle, so the whole process has to be completed in an acid fume hood wearing safety clothes and following, all safety procedures. Post BCP, the cavity has to be rinsed with water to remove the acid film formed on the cavity surface.

2.8.2 ELECTRO POLISHING (EP)

An alternative method to BCP to remove Nb is electrolytic polishing or electro polishing (EP). In this procedure, material is removed by an acid mixture with the help of an electric current flow. The widely used acid mixtures is concentrated HF and concentrated sulphuric acid (H_2SO_4) in a volume ratio of 1:9. The chemical reactions are following

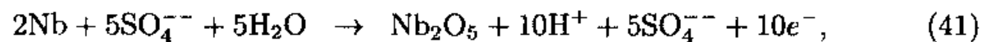

$$2\mathrm{Nb} + 5\mathrm{SO_4^{--}} + 5\mathrm{H_2O} \rightarrow \mathrm{Nb_2O_5} + 10\mathrm{H^+} + 5\mathrm{SO_4^{--}} + 10e^-, \quad (41)$$

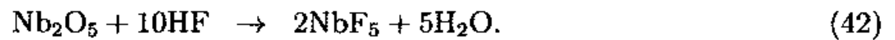

$$\mathrm{Nb_2O_5} + 10\mathrm{HF} \rightarrow 2\mathrm{NbF_5} + 5\mathrm{H_2O}. \quad (42)$$

EP makes sharp edges and burrs smoothed out and create glossy surfaces. The performance of EP cavity is better than the BCP cavity and one of the possible reason is the smoother surfaces created by EP process [19]. To avoid gas bubbles released from the acid mixture to reach the cavity surface, electro polishing is done horizontally with the half of cell empty. The horizontal EP setup is to be rotated as it is half filled with acid, and the etch rate is reduced by half. The typical etch rate during EP is 0.1-0.2 micron per minute.

2.8.3 ULTRASONIC CLEANING

Ultrasonic rinsing process is an important step in cavity surface treatment procedure. The SRF cavity is degreased by submerging in an ultrasonic bath containing ultra pure water and a soap solution for 30 minutes. The soap detergent named micro 90 helps in removing the oil grease and other contaminants. The cavity is rinsed thoroughly after degreasing with ultra pure water. All components required for the cavity assembly is also unltrasonically cleaned.

2.8.4 HIGH PRESSURE WATER RINSING (HPR)

In post chemical polishing, the cavity is cleaned by a jet of ultra pure water pressurized at 80 bar. Water is sprayed with the help of a nozzle, which moves up and down inside the cavity, which is set on a rotating table. High pressure rinsing (HPR) is a very important process in reducing the contaminants and dust particles, which helps in the reduction of field emission. All the components required for HPR must be exceptionally cleaned and the water must be ultra pure (specification 18 MV/m).

2.8.5 CAVITY ASSEMBLY AND RF TEST

The SRF cavity assembly is carried out very methodically in a class 10 clean room, to avoid the particulates from trapping inside the cavity. The assembled cavity is evacuated with the help of vacuum pumps and leak tested. The rf test is performed at crogenic temperatures by loading the cavity into vertical test cryostands. Each test cryostat is equiped with pressure sensor, temperature sensor, liquid helium sensor and rf power sensor. By measuring the rf signals the quality factor of the cavity is determined.

CHAPTER 3

BASIC PLASMA PROCESSING

Plasmas are ionized gases that consist of ions (positive and negative), electrons, excited radicals, and neutral species. Due to the presence of charged particles, they respond to electromagnetic forces. The degree of ionization (percentage of particles ionized) in the plasma can vary from 100 % to very low degree of ionization depending on the plasma used for the fusion reactor or material processing. The plasma used for material processing have the degree of ionization from 10^{-4} to 10^{-6}. In general, plasma is produced by heating the gas particles with the help of electromagnetic fields. Plasma is widely used for industrial, micro and nanofabrication purposes. The plasma often follows the quasineutrality condition, which means that the plasma as a whole carry equal amount of positive and negative charged particles. Deviations from the quasineutrality condition occur on a small scale. The plasma produced in the laboratory for fundamental studies are usually inert gases plasma like Ar, Ne, He etc. The plasma used in micro and nanofabrication usually consist of halogen gases, their compound or a mixture of inert gases with halogenated compounds. The inert gas plasma have positive ions, electrons and excited radicals, while the processing, reactive plasma carry positive ions, excited radicals, electrons and negative ions [20–25].

3.1 PLASMA PARAMETERS

There are some basic plasma parameters which exist in every type of plasma, and define the plasma characteristics. These plasma parameters indicate the properties of the plasma.

3.1.1 CHARGED PARTICLE DENSITY AND TEMPERATURE

The ions in the plasma are lost due to recombination or interaction with the wall surface. To maintain the steady state of ions these losses must be balanced by the ionization process. Typical electron/ion densities in plasmas used in laboratories are 10^9 to 10^{13} per cm^3. The concept of temperature applies to particles, which follows

the Maxwell-Boltzmann distribution. Due to extreme mass difference between the electrons and ions, the energy transfer during collision between the electrons and ions is very inefficient. This inefficiency creates a separate thermal equilibrium for electrons and ions leading to a different temperature for the electrons and ions. Usually, the electron temperature varies between (1-10 eV) in plasma used for material processing, while ion temperatures are in order of 0.1 eV. A temperature of 1 eV corresponds to approximately 11600 K. The high electron temperatures in plasmas provide an opportunity to create high temperature type reactions to form free radicals in a low temperature neutral gas invironment [20–25]. Generating the same radicals without plasma would require extreme temperature. This creates the possibility of a chemical reaction with the materials without raising the temperature of the material to the extreme limit and deforming it.

3.1.2 DEBYE LENGTH

The presence of charged particles in plasma makes plasma a conductive material, which respond to the potential fluctuations. Any potential fluctuation inside a plasma is shielded by the charges surrounding this potential. The characteristic distance by which the potential gets shielded is called the Debye length and denoted by λ_D [20–25]

$$\lambda_d = \sqrt{\epsilon_0 kT/ne^2}, \tag{43}$$

where T is the electron temperature, n is the electron/(ion) density, ϵ_0 is the permittivity, e is the electron charge and k is the Boltzmann constant.

3.1.3 PLASMA POTENTIAL

The high temperature and low mass of the electrons compared to the ions in the plasma makes the mobility of the electrons extremely high relative to ions. Due to this mobility, the electron reaches to the walls (vacuum vessel in which plasma is created) much faster and makes plasma slightly positive. This increase of positive charge makes it harder for the electron to leave the plasma and a steady state is soon developed. At this steady state, the loss to the walls is equal among ions and electrons and the potential acquired by the plasma is called the plasma potential. This potential, which is the potential of the bulk plasma, is equal to approximately several volts. The plasma potential is always several volts more positive than any

positive surface exposed to the plasma [20–25].

3.1.4 PLASMA SHEATH

A dark space or sheath is observed adjacent to all surfaces in contact with the plasma. The sheath is a region of significant voltage drop. The voltage applied to sustain the plasma is usually concentrated across the sheaths. Since plasma is a good conductor it cannot sustain much of an external field, thus the voltage drop occurs at plasma surface boundaries where charge density is low, and high fields can be sustained. The electron density is very low in the sheath region due to high mobility of electrons, which results in a lower number of excitation of neutrals leading to no glow, hence the observed dark space. Compared to the sheaths, bulk plasma has an almost uniform potential equal to the plasma potential [20–25]. Sheat thickness is up to an order of magnitude larger than the Debye radius.

3.1.5 BOHM VELOCITY

Ions enter the sheath region with the velocity defined by the ion temperature and their mass, which is called Bohm velocity [20–25]

$$u_B = \sqrt{ekT/M}, \tag{44}$$

where T is the electron temperature, M is the ion mass, e is the ion charge, and k is the Boltzmann constant. Due to current continuity principle, the Bohm velocity defines the ion current density.

3.2 TYPES OF PLASMA

There are different kinds of plasma with different characteristics depending on the frequency of electromagnetic power and the coupling method used for plasma production. There are three main types of plasma produced in the laboratory and explained further in this section: direct current (dc), radio frequency (rf), and microwave (MW) plasma. Each discharge type explained in this section requires the evacuation of the chamber well below the operating pressure and then the desired gas is fed to the chamber to be at operating pressure. The breakdown conditions vary from type to type and they are sometimes quite different than the required operating pressure for material processing.

3.2.1 DC PLASMA

DC plasma is the simplest form of electrical discharge where a high dc voltage is applied across two electrodes in a vacuum chamber. Application of high voltage to the electrodes creates an electric field, which accelerates the primary electron (somehow created by either cosmic rays, or a uv photon). These primary electrons collide with the gas atoms. Important collisions are inelastic creating excitation, dissociation and ionization. Excitation of neutral atoms and subsequent spontaneous deexcitation creates the glow, which is the reason a group of discharges is called glow discharges. The ions created in the collision process accelerate toward the cathode, while the electrons drift toward the anode. Depending on the appropriate gas density and the intensity of the electric field, the breakdown of gas occurs and the discharge can be self sustained. In the case of very low gas density, the electron might not collide with a gas molecule, while at a higher gas density, the electron might not gain enough energy from the electric field before collisions to produce ionization. In dc discharges, the breakdown voltages (V) can be plotted against ($p \cdot d$), the product of pressure and distance between the electrodes. It is called the Paschen curve and the minimum on the curve is called the Paschen minimum. This curve provides the voltage required to produce the dc plasma at a given set of electrodes and gas pressure. The potential difference applied to produce the dc plasma drops substantially within the first few milimeters from the cathode. This region is called the cathode sheath [20–26].

3.2.2 RF PLASMA

When the generating electromagnetic field is oscillating at radio frequency, the plasma is called rf plasma. RF plasma can be generated at any frequency from kHz to GHz. Due to the government communication regulations, most commercial plasma reactors operate at a frequency of 13.56 MHz. The electrode configuration to produce the rf plasma is similar to dc plasma. RF plasma allows for the use of insulating material to process, which is difficult in DC plasma. It also can be operated at much lower pressure compared to DC plasma. The behavior of rf plasma is different as electrons can follow the high frequency electromagnetic fields, while ions have larger mass and lag behind. Based on the power coupling method, rf plasma can be divided in to two types (1) capacitively coupled plasma (2) inductively coupled

plasma. In capacitively coupled plasma, two electrodes are used to produce the plasma with the help of rf power. The plasma produced by the same area electrodes is called the symmetric and the plasma produced by different area electrodes is called the asymmetric plasma. Asymmetric plasma created due to the difference between powered and grounded electrode surface area have significant influence on the sheath potential developed on the electrode surfaces. Details about the asymmetric plasma reactor and self-bias potential formation is explained later [20-26]. In inductively coupled plasma the power coupling method to plasma is magnetic and it is done through a coil.

3.2.3 MW INDUCED PLASMA

Microwave (MW) (above 300 MHz to 10 GHz) induced plasma is a general term, which comprises several different plasma types including: cavity induced plasma, free expanding plasma torches, electron cyclotron resonance plasma (ECR), and surface wave discharges. We are interested in the capacitive mirowave plasma and the ECR plasma. In capacitive mirowave induced plasma, the power generated by the magnetron is connected to the single antenna [26]. The coupling of MW power to a charged particle in a magnetic field is the basis of ECR plasma. The frequency of rotation in the magnetic field (cyclotron frequency) ω is found as

$$\omega = eB/m, \tag{45}$$

where B is the magnetic field strength, m is the electron mass, and e is the electron charge. In general, for microwave power at the frequency of 2.45 GHz, the required magnetic field for ECR coupling is 875 Gauss. The ECR plasma can also be produced for other frequencies by varying the magnetic field to suit that frequency. For commercial purposes, to use high ion density plasma, the plasma reactor is operating at the frequency of 2.45 GHz is used. In general MW plasma has higher electron density than rf plasma.

3.3 PLASMA PROCESSING

The application of plasma to modify the surface of materials is called plasma processing. Surface modification can be the deposition or growing of thin films, etching (removing of materials), plasma cleaning or ashing of the surface. Plasma

processing is the most widely used process in the microelectronics industry. Plasma processing enables modification of surfaces on materials and fabrication of structures on them in unique ways, which is not possible in any other commercially available method [24, 26, 27].

3.3.1 PLASMA CLEANING

Plasma assisted cleaning or ashing means the removal of undesired residue including organic contaminants or photoresists as applied in the semiconductor industry. Organic contaminants can be turned into volatile compounds by the plasmas of oxidizing gas like oxygen or a mixture of oxygen with inert gases like Ar or Ne.. The carbon from organic conaminants is converted to carbon monoxide and carbon dioxide. These gases with other volatile products together with water vapor are pumped out of the system with the help of vacuum pumps [22, 26]. Physical sputtering of surfaces by ions of plasma and volatile product formation of organic impurities by reactive oxygen provides ultra clean surface after plasma cleaning.

3.3.2 PLASMA ETCHING

Plasma etching is the process of material removal by forming the volatile products of material and removing them with the help of plasma generated species. Plasma species constitute atoms, radicals and ion species. These species reach the material surface either by diffusion (neutral) or driven by the electric fields (ions). The adsorption of these plasma produced species on the material depends on the chemical affinity, material temperature and plasma conditions. These species react with the molecules of the surface and form a compound, which is volatile and desorbs into the plasma phase. The volatile products formed during plasma processes are pumped out through the pumping system. In the cases of low volatility, the material carrying compounds may get redeposited on the material surface. There is a very small amount of gas used in the plasma etching process to remove the material compared to the amount of acid used in the wet etching processes. Initially, the motivation to use plasma to etch a semiconductor was driven by the need to reduce the waste of corrosive acids, and later it was preferred for pattern transfer [28]. Plasma etching is mostly developed for materials related to microelectronics industry. There is an extensive amount of research for silicon and silicon dioxide etching, but far less in the case of other materials [21, 22, 26–31].

3.3.3 ISOTROPIC AND ANISOTROPIC ETCHING

Isotropic etching means that the etch rate is the same in all directions. The isotropic etching creates a circular profile in the surface. Anisotropic etching means a directional etching leading to a vertical structure profile on the surface. Generally, chemical etching creates an isotropic etching, this is the reason that wet etchings are isotropic and a vertical structure cannot be created by chemical etching. Isotropic etching can be produced in plasma, when the etching is completely chemical and the plasma has no other role than providing etchants. Anisotropic etching in plasma is produced with the help of ions. Due to the sheath electric field, ions get directional energy and create a directional etching [21, 22, 26–31].

3.4 ETCHING MECHANISM

All known plasma etching can be grouped into four categories: (1) sputtering, (2) chemical etching, (3) ion enhanced energetic etching (reactive ion etching), and (4) ion enhanced inhibitor etching

3.4.1 SPUTTERING

Sputtering or physical etching means knocking the atoms out of the surface by lattice bond breaking impact. The ions formed in the plasma gain energy from the sheath electric field and collide with the material. In this collision, the atom from the material might get ejected from the material. The usual analogy for sputtering is given by billiard balls collisions, in which the cue ball strikes the target and sputters the target balls. Some target balls come back to the player. Depending on the ion energy, there is a number of atoms ejected from the target surface. The ratio of ejected atoms to impacting ions is called the sputter yield. Sputter yield depends upon the binding energy of the material and the ion impact energy. The high ion energy conditions for sputtering, makes low pressure plasma processes favorable because the mean free path is lower. In sputtering, the etching selectivity is very poor. Usually, sputtering is widely used in thin film deposition, where sputtered material from the target gets deposited on the substrate. In the case that there is no substrate, the sputtered material is pumped out by a vacuum pumping system [21, 22, 26–31].

3.4.2 CHEMICAL ETCHING

Chemical etching is the etching produced by radicals present in the plasma. It is sometimes called radical etching or plasma etching. There is usually a very minimal amount of contribution from ion bombardment and the etching is purely chemical. The radicals produced in the plasma get adsorbed at the target surface and form volatile compounds, usually the halides. The phenomenon of etching is close to oxide formation on the surfaces and a similar type of action creates volatile halides. The volatile compounds get pumped away by vacuum pumps. Chemical etching is isotropic as radicals reach to the target surface with uniform angular distribution. The activation energy may change depending on the flow and the type of incident particles. Chemical etching also varies with the temperature of the target. It is also the most selective kind of process because it is sensitive to the bond and chemistry of the substrate material. Generally, the target material is placed on the grounded electrode of the 13.56 MHz asymmetric rf plasma reactor for chemical etching processes [21, 22, 26–31].

3.4.3 ION ENHANCED ENERGETIC ETCHING

The ion enhanced energetic etching requires a combination of both the energetic ions and the chemical radicals. It is much more effective than either an individual chemical etching or a physical etching only. The etching process is probably chemical but is greatly enhanced by the ion bombardment. The ions gain energy from the sheath voltage that gets developed around the target and bombards it unidirectionally thereby increasing the probability of etching the target atom with chemical radicals from the plasma. The directional bombardment makes the ion assisted etching very anisotropic. This type of etching is also called reactive ion etching or plasma assisted etching. The selectivity in this type of reaction is poorer than chemical etching. This type of etching can be controlled by varying the sheath potential or temperature of the target. In the most common reactive ion etching systems, the target material is placed on the powered electrode of a 13.56 MHz asymmetric rf plasma reactor [21, 22, 26–31].

3.4.4 ION ENHANCED INHIBITOR ETCHING

In this type of etching, the discharge not only provides radicals and ions but also inhibitor precursor molecules. The utility of the precursor is to form a protective layer on the target. In the absence of the ion bombardment, this protective layer

prohibits the etching of the target, while in the presence of the ion bombardment there is no protective layer and the target material is etched. This type of etching is beneficial for highly selective and highly anisotropic etching [21, 22, 26–31].

3.5 ELECTRONEGATIVE PLASMA

The plasma involved in plasma processing of metals, insulators or semiconductors usually contains one of the halogen gases or compounds including Cl_2, CF_4, BF_3, SF_6, etc.. The plasma produced by these gases or a combination of these gases with inert gases not only produce positive ions and electrons but negative ions also. Due to the presence of negative ions, this type of plasma is called the electronegative plasma. The negative ions in these plasmas leads to depletion of electron density and change the plasma parameters like plasma potential, electron temperature, electron density and sheath thickness, which affects the processing conditions. A small percent of Cl_2 addition in argon creates this kind of electronegative plasma in which electron density, temperature and sheath thickness can be quite different than pure Ar plasma [32–35].

3.6 OBSERVABLES

The plasma etching method to remove material is mostly used in microelectronics industry for processing the semiconductor wafers. The terminology and demand from the processing methods and apparatuses are set by the semiconductor industry for silicon material. The main observables for the industry are: (1) etch rate (2) uniformity/ loading effect, and (3) selectivity.

3.6.1 ETCH RATE

The rate of material thickness removal per unit area is called the etch rate. Generally it is not too much concern for the semiconductor industry as the need to remove material is in nanometers unless it is for micromachining or deep reactive ion etching where material removed is in order of microns. When the need to remove the material is in microns, the etch rate shall not be too slow as it would require a prohibitive amount of time.

3.6.2 UNIFORMITY/ LOADING EFFECT

There is a general requirement that etching should be uniform across the wafer (processed) surface. Etching depends on a number of factors like gas flow, symmetry of gas flow and the relative position of the gas inlet and vacuum pumps. The basic requirement is that all surfaces to be etched should have a fresh and evenly distributed feedstock gas flow. The loading occurs when the reactant density is depleted due to an excessive substrate load. The etch rate decreases inversely to the area exposed to the plasma to etch. This happens due to a consumption problem and not due to a generation problem of plasma generated species [21, 22, 26–31].

3.6.3 SELECTIVITY

Selectivity is the etch rate ratio between two materials, that is required in order to have differential etching between the material and mask layer in integrated circuit manufacturing. Generally, chemical etching is the most selective as it can differentiate between various materials, while physical etching does not differentiate [21, 22, 26–31].

3.7 PROCESS PARAMETERS

The process parameters including: pressure, rf power, dc bias, temperature, gas flow rate, electrode geometry, and vacuum vessel size etc can change the plasma properties and affect the observables.

3.7.1 PRESSURE

Pressure influences the etch rate of material substantially. For the purpose of processing plasmas, low pressure means below 0.1 torr and high pressure means between 0.1 torr and 0.5 torr. The sheath thickness and voltage increases with the decrease in pressure and raises the plasma potential, resulting in higher bombardment energy on the material surface. Higher pressure leads to more neutral radicals but lower sheath thickness and lower sheath voltage. In plasma processing, the etch rate increases at lower pressure when the physical component of etching is strong, while higher pressure increases the etch rate when chemical etching is taking place. High pressure systems would involve much lower ion bombardment energy leading to less damage to the etched surface, whereas low pressure systems are more anisotropic and etch material even too hard to etch [21, 22, 26–31].

3.7.2 FREQUENCY

For plasma processing, the pressure and frequency are interchangeable parameters. Low pressure and low frequency have similar effects, it raises the flux and energy of bombarding ions. The frequency range discussed in plasma processing is between 0.5 MHz and 30 MHz. Lowering the frequency in this range increases the etch rate if etching is sputtering or is reactive ion etching. In the case of the 2.45 GHz microwave plasma, the improvement in etching is due to high density plasma production as it is much higher than the rf plasma [21, 22, 26–31].

3.7.3 RF POWER

At a given pressure, increasing power increases the density of radicals and ions. Increasing power also increases the sheath and plasma potential, changing the ion bombardment energy to the target. These changes in plasma lead to a higher etch rate. However, at very high power density, the material temperature might increase and very high bombardment energy leads to degradation of the surface [21, 22, 26–29, 31].

3.7.4 TEMPERATURE

Target temperature influences the etch rate, the surface morphology and the selectivity. Etch rates in the case of chemical etching and ion assisted etching mechanism, follow Arrhenius type dependence on the temperature.

$$\text{Etch rate} \propto e^{-E_a/kT}, \tag{46}$$

where E_a is the effective activation energy and T is the temperature of the target. The effective activation energy is material dependent. The chemical etch rate can be increased up to the ion assisted etch rate by increasing the temperature, but it reduces the anisotropy. Depending on the material, the surface morphology, like roughness, can be decreased by increasing or decreasing the temperature.

3.7.5 GAS FLOW RATE

In general, the flow rate should be large enough to avoid depletion of radicals during etching. The flow rate effect to etching is related through residence time. The residence time is given by

$$\tau = Vp/760F, \tag{47}$$

where V is the reactor volume in cm^3, p is the pressure in torr, and F is the flow rate in sccm. Gas flow rates are in general between 5 sccm and 200 sccm, depending on the pumping speed of the vacuum pump and desired pressure [21, 22, 26–31].

3.7.6 DC BIAS

The dc bias applied either to the substrate or target change the sheath potential around the material. The change in the sheath potential leads to a change in the ion bombardment energy and change in plasma etching conditions [21, 22, 26–31].

3.7.7 ELECTRODE GEOMETRY AND MATERIAL

The changes in the nature of the electrode (area, material, shape) leads to the variation of plasma properties. The change in area or shape affects the sheath voltage potential substantially at the powered electrode in an asymmteric rf plasma reactor, which alters the plasma processing conditions. However, the change in the material of the electrodes could alter the plasma environment if it produces the involatile product. These products get deposited on the wall or substrate affecting the purity of the final surfaces [21, 22, 27–31].

3.8 PLASMA DIAGNOSTICS

To measure and monitor the plasma processes, two types of diagnostic methods are usually applied. One is an active method based on electrical measurement, where a conductive object is inserted into the plasma and electrical properties are measured. The other is a passive method, where radiation emitted from the plasma is observed by a spectrometer placed outside the plasma vessel. For the first method a langmuir probe is the most popular technique, and for second an optical emission spectroscopy is the popular one [21, 28, 32].

3.8.1 LANGMUIR PROBE

The Langmuir probe is one of the simplest and earliest plasma diagnostic method developed by Dr. Irvin Langmuir. It measures the localized values of the electron density(n_e) and electron temperature (T_e). Langmuir probe is a conductor inserted into plasma and electrically biased with varying voltages with respect to the vacuum vessel wall. The current collected by this conductor is measured, and the current voltage variation is analyzed. At sufficiently negative voltage at the probe, all electrons are repelled and the resulting current is called ion saturation current. As the voltage increases the higher energy electrons start striking the probe and the electron current increases. The floating potential (V_f) is achieved when electron and ion current becomes equal and the total current disappears. As the voltage increases, the current becomes exponentially dependent on the voltage following Child Langmuir law. The electron temperature is evaluated from the logarithmic slope of the current-voltage characteristic. As the voltage rises further it reaches the potential level, called plasma potential V_p, after which the current loses the exponential dependence on the voltage and there is only a slight increase with the voltage. There are a few drawbacks of using the Langmuir probe for plasma parameter measurement. One, the use of the Langmuir probe requires inserting a conductor directly into the plasma, which if not sufficiently small compared to the vacuum vessel size, might change the plasma properties itself. Second, the Langmuir probe exposed to the processing plasmas might get etched and impurities would also affect the target material etching [21, 28, 32].

3.8.2 OPTICAL EMISSION SPECTROSCOPY

Optical emission spectroscopy is the oldest of the plasma diagnostics since early researchers realized that the color of the plasma depends on the nature of the gas filled in the system. Low pressure plasmas emit a unique spectra characteristic to the chemical composition of the gas. The ability to relate the optical intensity of emitted or absorbed light to the number density of the active species makes spectroscopy very valuable. The relation of the electron density to the optical density is simple: the higher the electron density and temperature at a given point the higher, the chances of these electrons to excite the gas atoms / molecules and the higher the optical intensity radiated. Even a mere look at the photographs of the discharge may suggest the

plasma structure formation. Spectral lines are the results of the electrons transitions from the higher energy excited states to the lower energy excited states. The energy emitted or absorbed can be determined by caculating the difference between the final and initial state of energy by Planck's relation.

$$\nu = (1/hc)E_f - E_i, \tag{48}$$

where E_f is the final state energy and E_i is the initial state energy. The energy levels of atoms are different from each other, leading us to a unique spectral pattern observed for each species. However, the molecular spectra is more complex compared to the atomic spectra, as internal motions of the nuclei in polyatomic molecules are quite complicated. In a diatomic molecule, two nuclei can vibrate along the axis and rotate around the center of the mass of the molecule. These motions lead to different vibrational and rotational energy level creating vibrational and rotational spectra. As there are sometimes thousand of spectral lines in the molecular spectrum, it appears continuous over quite a large wavelength range. In order to quantitatively analyze the emission spectra in most of the plasmas, the problem is often reduced to finding the relation between the emission intensity and the density of the ground states. The spectral line intensity can be written as

$$I = g_2 A_{21} n_2 h\nu_{12}, \tag{49}$$

where A_{21} is the Einstein atomic transition probability for spontaneous emission, n_2 is the density of the emitting state, g_2 is the state multiplicity, equal to (2J+1) and ν is the frequency of the emitted light. By measuring the absolute emission intensity and knowing the atomic transition probability, the excited state density can be calculated, assuming the Boltazmann distribution total density of the states can be computed. Generally, a kinetic model is developed between the total density and the density of the excited state. The usual assumption is that these excitations are the result of the electron impact in a single step from the ground state.

CHAPTER 4

RF PLASMA

During my work on plasma processing of SRF cavities, I have contemplated using three discharge types: dc, rf, and microwave discharge. In the case of plasma etching or sputter deposition of insulating materials, where material has to cover the electrode, dc discharges proves inefficient. Insulating materials acquire the floating potential in dc discharges, which is not convenient for many plasma processes to occur. This problem can be solved by using ac discharges, which are very similar in nature to dc discharges except the sheath structure and voltage are varying with time. In AC/RF discharges, the plasma is switching on and off at twice the driving frequency. The driving frequency should be high enough so that the charged particle created in one cycle should not be lost when current is passing through zero. Thus the frequency needed is above 50 KHz for continuous plasma production. Due to government communication regulation, most commercial plasma reactors operate at 13.56 MHz. Otherwise, plasma can be produced as higher frequency up to the gigahertz range, as in microwave discharges. Sometimes higher-order harmonics of 13.56 MHz frequency, like 27.12 MHz or 40.68 MHz, are used either alone or in combination with 13.56 MHz to produce plasma for specific applications. Due to the oscillatory nature of the applied field, the net energy transfer to electrons is more efficient in rf discharges compared to dc discharges. This additional energy deposition to the electron population results in a higher level of ionization in rf discharges. There are two type of rf discharges depending on the coupling scheme of the rf power. These are the capacitively coupled rf plasma, when the discharge is driven through the voltage applied between the two electrodes, and the inductively coupled plasma, where rf power is inductively coupled to discharge with the help of a coil. In the inductively coupled plasma, the sheath potential is not coupled to the rf power density, while in the capacitively coupled plasma sheath potential is directly coupled to the rf power density. Separate control of ion flux and ion energy is not possible in capacitively coupled plasma, while it can be achieved in inductively coupled plasma. However, application of the inductively coupled plasma in the cavity processing is too complex and we opted for the capacitive setup. Therefore, in this chapter, we will only

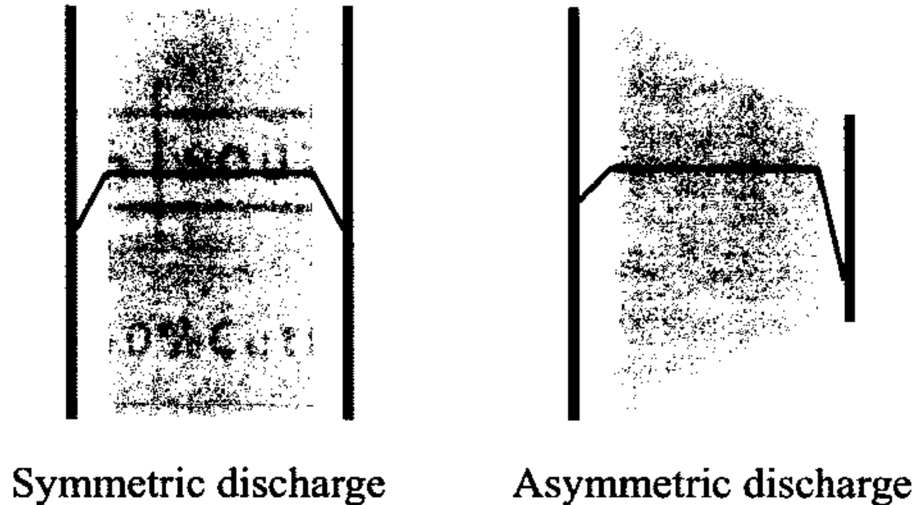

FIG. 1: Scheme of plasma sheath potential distribution in symmetric and asymmetric discharge.

discuss the capacitively coupled plasma. There are two types of plasma reactors in capacitively coupled rf plasma depending on the geometry of the electrode involved in plasma production. The plasma characteristics like sheath potential and plasma potential vary depending on the type of plasma reactors. The two types of plasma are called symmetric rf plasma and asymmetric rf plasma [20, 22–25, 36]. The sheath voltage diagram in Fig. 1 provides an example of the sheath voltage difference in symmetric and asymmetric discharges.

4.1 SYMMETRIC PLASMA

In the capacitive coupled rf plasma, when the driven (powered) electrode area and grounded electrode area is the same, the plasma produced is called symmetric plasma. In general, in low pressure plasma systems, the grounded vessel wall also starts to act as a part of the grounded electrode and the symmetric area electrode creates asymmetrical plasma. To study the symmetrical system the electrodes are usualy confined to a glass chamber. In the symmetric system, the plasma potential V_p must exceed the rf potential of the driven and grounded electrode at a certain time in one rf period. This makes plasma potential approximately half of the rf potential applied. The symmetry of the system imposes that the sheath voltage is

just as large at the grounded electrode as it is on the powered electrode. This is an important feature of the symmetric discharges as the ion bombardment energy, which is proportional to the sheath voltage, which is high on both the electrodes [20, 22–24].

4.2 ASYMMETRIC PLASMA

Due to the presence of a blocking capacitor in the matching network of rf power supply, when the surface area of the powered electrode is smaller compared to the grounded electrode area, the plasma produced is called the asymmetric plasma. The sheath potential in asymmetric plasma differs at the two electrodes. The grounded electrode has lower sheath potential compared to the powered electrode sheath potential. The ratio between these two sheath voltages depends on the area ratio of the electrodes. The classical treatment of the asymmetric discharge was introduced by Koenig and Maissel in 1970 [37]. If the areas of the electrodes are A_1 and A_2 , the sheath voltages and thicknesses developed due to the rf discharge are V_1 and V_2, D_1 and D_2 respectively. In a space charge limited model the current density can be expressed by

$$J_i = KV^{3/2}/m_i^{1/2}D^2, \tag{50}$$

where K is the constant, V is the voltage, D is the sheath thickness and m_i is the mass of the ion.

As the current density of positive ions at both the electrodes are equal, we can write

$$V_1^{3/2}/D_1^2 = V_2^{3/2}/D_2^2. \tag{51}$$

The capacitance across the sheath area around the electrodes is proportional to the surface area and inversely proportional to thickness

$$C \propto A/D. \tag{52}$$

Due to capacitive division of sheath voltages,

$$V_1/V_2 = A_2D_1/D_2A_1. \tag{53}$$

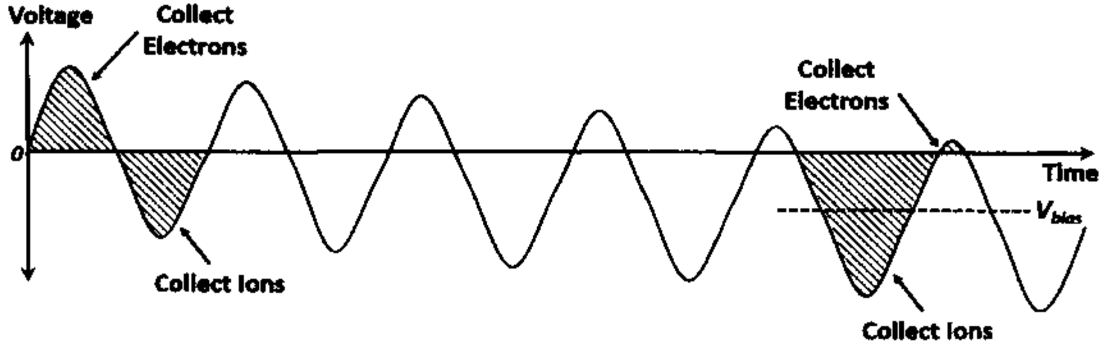

FIG. 2: Illustration of formation of self-bias potential

Substituting this into equation, we would get

$$V_1^{3/2}/V_2^{3/2} = D_1^2/D_2^2 = (A_1V_1/A_2V_2)^2, \tag{54}$$

which leads to

$$V_1/V_2 = (A_2/A_1)^4. \tag{55}$$

This simple result suggests that the larger sheath voltage drop happens at the smaller electrode and by varying the area of the electrodes, the sheath voltage can be changed for the same power rf plasma. This sheath voltage provides the ion energy which helps in the etching process. However, this is a very simplistic formula assuming collisionless plasma [20, 22] and more accurate scaling models are available.

4.2.1 SELF-BIAS POTENTIAL

In the rf plasma, due to the smaller mass, electrons respond freely to an applied electric field as ions are too heavy to respond to the field at higher rf frequency. As the electrode gets positively powered it collects electrons, while the grounded electrode attract ions which move slowly. This attraction of a large number of electrons leads to the reduction of applied potential or equivalently added negative bias. In a number of rf cycles, the electrode reaches a sufficiently negative voltage so that when the positive peak of the applied voltage exceeds 0 V, enough electrons are collected to balance the number of slower ions [20, 22]. The average negative dc bias developed at the powered electrode usually reaches one half of the applied peak to peak rf voltage.

This negative bias potential as shown in Fig. 2 is called self-bias potential and it varies with pressure, rf power, gas composition and electrode geometry. It becomes a very important parameter in rf plasma processing as ions bombard the material placed on the powered electrode with the energy of this bias potential plus plasma potential. Plasma potential is always the highest potential in plasma. It is slightly more positive than the most positive potential in the plasma. The plasma potential is quite different for symmetric and asymmetric cases. In the symmetric case, the plasma potential is quite high, while in the asymmetric case the average plasma potential is quite low, just a few tens of volts. The sheath at the lower area electrode has almost all the rf voltage dropped as a self-bias dc potential and the positive ions would bombard the lower area electrode with this energy. However, the larger area or grounded electrode would have less energetic bombardment of ions as sheath potential at larger area electrode is low. The self-biasing affects the etch rate characteristics in planar geometry [38] as it helps in increasing the ion bombardment energy. The addition of halogen (electronegative) changes the plasma dynamics particularly the sheath electric field [39, 40], which leads to the change in the self-bias potential and etch characteristics of rf plasma. In the plasma of electronegative gases (Cl_2, BCl_3, O_2, etc..) mixed with electropositive gases (He, Ne, Ar, N_2, etc..), the electron to negative ion density varies with the pressure, power, frequency and the feedstock composition. The plasma sheath thickness in electronegative gases is smaller than the electrpositive gases due to smaller Debye radius. The change in Debye radius and electron temperatures are due to the formation of negative ions, which changes the negative charge density and the energy lost in dissociation of electronegative molecules leads to change in the elctron temperature. The power deposition in these type of plasma is not very clear, thus a study of self-bias potential variation with the pressure, rf power and geometry parameters is necessary.

4.2.2 A LINEAR MODEL FOR SELF-BIAS POTENTIAL

In the rf power supply, due to design of generator and matching network that includes the blocking capacitor, the loaded electrode has a self-bias potential, unless it is not grounded through inductance or purposefully changed otherwise. The whole process can be explained with the simple electrical engineering model [32, 41]. In this model, sheaths are characterized with capacitances C_1, C_2 and the plasma between them is considered to be an ideal conductor and the floating potential is neglected.

This type of theoretical treatment is given in detail [41]. The two sheath capacitors C_1, C_2 and the blocking capacitor C are in series, with a generator producing sine shaped potential. The potential at the powered electrode may be written as

$$V(t) = V_{dc} + V_a \sin \omega t, \tag{56}$$

while the plasma potential relative to the grounded electrode may be written as

$$V_p(t) = \overline{V_p} + \triangle V_p \sin \omega t. \tag{57}$$

Since equal currents pass through C_1 and C_2,

$$\omega C_1 (V_a - \triangle V_p) = \omega C_2 \triangle V_p, \tag{58}$$

hence

$$\triangle V_p = \frac{C_1}{C_1 + C_2} V_a \tag{59}$$

describes temporal behavior of the plasma. We assume that at certain moment the plasma comes in contact with the electrode and the electron flux is compensated by the ion flux, since there is no direct current through the circuit. However, the plasma potential can never drop below the electrode potential, since the plasma is separated from the electrode through positive space charge sheath. When plasma touches the electrode, its potential becomes equal to the electrode potential. Therefore, the minimum plasma potential

$$V_{p(min)} = \overline{V}_p - \triangle V_P = 0\,, \tag{60}$$

at

$$\omega t = 3\pi/2\,, hence, \triangle V_p = \overline{V}_p\,. \tag{61}$$

However, when the plasma touches the loaded electrode at

$$\omega t = \pi/2\,, \tag{62}$$

its potential is

$$V_{p(max)} = \overline{V}_p + \triangle V_p = 2\overline{V}_p\,, \tag{63}$$

which is equal to the powered electrode potential at that moment,

$$V_{max} = V_{dc} + V_a. \tag{64}$$

This yields the well known formula

$$\overline{V}_p = \frac{V_{dc} + V_a}{2} = \triangle V_p, \tag{65}$$

which defines self bias potential and average voltage fall

$$V_{dc} = \frac{C_1 - C_2}{C_1 + C_2} V_a, \tag{66}$$

and

$$\overline{V}_p = \frac{C_1}{C_1 + C_2}, \tag{67}$$

and

$$\overline{V}_1 = \frac{C_2}{C_1 + C_2}. \tag{68}$$

Since the sheath capacitance grows with surface area, these equations show that when the smaller surface area electrode is powered, the self-bias potential is negative and $\overline{V_p}$ is lower than $V_a/2$. In symmetric system, where $C_1 = C_2$, the self-bias potential V_{dc} is zero and average plasma potential $\overline{V_p} = \mathrm{V}_a/2$. If larger area electrode is powered, self-bias potential is positive and $\overline{V_p}$ is closer to V_a. Though these formulae describe much of the experimental work, Garscadden and Emeleus [42] derived a refined expression for V_{dc} developed across a sheath by the application of an rf voltage V_0

$$\triangle V_{dc} = \frac{kT_e}{e} \ln \left[I_0 \left(\frac{eV_0}{kT_e} \right) \right], \tag{69}$$

where I_0 is the zeroth-order modified Bessel function of the firs kind and T_e is the electron temperaturein the discharge. If

$$\frac{eV_0}{kT_e} \gg 1, \tag{70}$$

this expression can be written as

$$\triangle V_{dc} = -V_0 + \frac{kT_e}{2e} \ln \left[\frac{2\pi e V_0}{kT_e} \right]. \tag{71}$$

This gives the dc bias required between the surface and plasma to maintain the equal ion and electron fluxes, when an rf voltage V_0 is applied.

4.2.3 ANALYTICAL SOLUTION BY LIEBERMAN

A number of different model of rf sheath have been proposed, compared with other models Liebermans models have both low and high pressure version and also both collisionless and collisional rf sheaths are treated [25, 43–47]. The rf+dc case is also described. Since ion flux is conserved assuming collisionless plasma sheath, the particle and energy conservations equations are

$$n_i u_i = n_0 u_B, \tag{72}$$

$$\frac{1}{2}Mu_i^2 = \frac{1}{2}Mu_B^2 - e\overline{\phi}, \tag{73}$$

where n_0 is the plasma density at $x = 0$ and $\overline{\phi}$ is time average potential in the sheath, n_i is the ion density, and u_i is the ion speed at x, u_B is the Bohm velocity. The instantaneous electric field $E(x,t)$ in the sheath is

$$\frac{\partial E}{\partial x} = \frac{e}{\epsilon_0} n_i(x)\,, s(t) < x \tag{74}$$

$$= 0\,, s(t) > x. \tag{75}$$

Here $s(t)$ is the distance from the ion sheath boundary at $x = 0$ to the electron sheath edge; the electron sheath thickness is $s_m - s(t)$. the instantaneous potential $\phi(x,t)$ is detrmined by equation

$$\frac{\partial \phi}{\partial x} = -E. \tag{76}$$

By time averaging over an rf cycle, the equations about average electric field $\overline{E}(x)$ and potential $\overline{\phi}(x)$ can be obtained

$$\frac{\mathrm{d}\overline{E}}{\mathrm{d}x} = \frac{e}{\epsilon_0}(n_i(x) - \overline{n}_e(x)), \tag{77}$$

$$\frac{\mathrm{d}\overline{\phi}}{\mathrm{d}x} = -E, \tag{78}$$

where $\overline{n}_e(x)$ is the time avergae electron density and $\overline{E}$ and $\overline{\phi}$ are also time averages. The rf current density can be written as

$$J_{RF}(t) = -\overline{J}_0 \sin(\omega t). \tag{79}$$

Equating this to conduction current at the sheath yields

$$-en_i(s)\frac{\mathrm{d}s}{\mathrm{d}t} = -\overline{J}_0 \sin \omega t. \tag{80}$$

These are the basic equations for Liebermans model. The integration of the Eqs. (73) and (79) provides us

$$E = \frac{e}{\epsilon_0}\int_s^x n_i(\zeta)d\zeta \; s(t) < x \tag{81}$$

$$= 0; s(t) > x, \tag{82}$$

and

$$\frac{e}{\epsilon_0}\int_0^s n_i(\zeta)d\zeta = \frac{\overline{J}_0}{\epsilon_0\omega}(1 - \cos\omega t). \tag{83}$$

From these two equations we obtain

$$E(x, \omega t) = \frac{e}{\epsilon_0}\int_0^x n_i(\zeta)d\zeta - (1 - \cos\omega t)\,, s(t) < x \tag{84}$$

$$0, s(t) > x. \tag{85}$$

The next several steps are pure mathematical treatments, which details can be found in Ref. [45]. After some mathematical mainpulations the total dc voltage across the sheath can be related to the ion current and ion sheath thickness by equation

$$J_i = K\epsilon_0 \left(\frac{2e}{M}\right)^{1/2} \frac{\overline{V}^{3/2}}{s_m^2}, \tag{86}$$

where K value is equal to 0.82. Using similar formula for spherical shell model we obtain sheath law [46].

$$J = \frac{500}{243\pi}^{1/2} \epsilon_0 \left(\frac{2e}{M}\right)^{1/2} \frac{V^{3/2}\lambda_i^{1/2}}{s_m^{5/2}}. \tag{87}$$

The sheath properties are critical in detrmining the self -bias voltage at the powered electrode. The current continuity defines the scaling law of the electrode bias voltages in asymmetric discharges. Assuming that the sheaths are capacitive and

rf voltage V_{rf} across each sheath is equal to the dc glow to the electrode voltage V across the sheath. Due to conituity of rf currents

$$\frac{V_a A_a}{s_a} = \frac{V_b A_b}{s_b}. \tag{88}$$

Using $J_a = en_a u_B$ and $J_b = en_b u_B$ in sheath formula, we can obtain

$$\frac{n_a s_a^{5/2}}{V_a^{3/2}} = \frac{n_b s_b^{5/2}}{V_b^{3/2}}. \tag{89}$$

By eliminating s between above two equations, we can obtain

$$\frac{n_a}{n_b} = \frac{V_b}{V_a}\left(\frac{A_b}{A_a}\right)^{5/2}. \tag{90}$$

Depending on how we assume the ratio n_a/n_b, we can find out the scaling law. For a homogeneous density n_a/n_b=1, we obtain

$$\frac{V_a}{V_b} = \left(\frac{A_b}{A_a}\right)^{5/2}. \tag{91}$$

For all other values of n_a/n_b

$$\frac{V_a}{V_b} = \left(\frac{A_b}{A_a}\right)^{q}, \tag{92}$$

where the area ratio scaling exponent varies depending on the sheath law. For Child law it is 3.42 for collisional diffusion and 4 for homogeneous density, for Cobine law it is 2.71 for collisional diffusion and 3 for homogeneous density [25, 43–47]. The experimental values for these scaling exponent show the deviation from the theoretical values. The more detailed expression about bias voltage in cylindrical coaxial discharges are provided in Ref.[44].

4.3 SUMMARY

The asymmetric plasma is widely used in semiconductor industry due to advantage of high self bias potential on smaller powered electrode. The wafer is placed on the powered electrode for reactive ion etching. The formation of self-bias potential and asymmetric plasma for planar geometry is studied theoreticaly [25, 43–46, 48], experimentaly and computationaly [49–54]. The addition of electronegative gases changes the plasma parameters and in turn changes the asymmetry in the plasma

also [33, 34, 55–57] . The addition of dc voltage changes both the plasma parameters and plasma density and plasma potential [58, 59].

CHAPTER 5

EXPERIMENTAL SET UP FOR NIOBIUM SAMPLES

The two primary requirements for the plasma etching of the SRF cavities are the removal of the 100-150 micron of material from the inner surfaces of the SRF cavity, and to create as smooth and impurity free surface as possible. Plasma etching of niobium (Nb) has been mostly done in the context of developing the Josephson junction, where Nb thin film is usually etched for tunnel junction application. Various gases have been used for this purpose including CF_4 and SF_6 in an rf plasma environment [60–65]. The plasma etching and charecterization of other metals of planar nature is also been reported in Ref.[66–71] . Our first attempt to etch the bulk Nb was made with the help of BF_3 [72]. Generally, a halogen gas or a halogenated compound in a mixture with inert gases is used to plasma etch metal or a semiconductor. The choice of the gases used in the etching processes are dictated by their ability to form a volatile product. The other conditions are safety and environmental effects. The plasma surface treatment, where etching is not involved the gases used can be nitrogen or oxygen diluted in inert gas as reported in Ref. [73, 74]. The gas mixture chosen during our current experiments are chlorine diluted in argon at various mixing ratios. The objective of an etching process in an rf discharge is to remove layers of impurities,bulk material, oxides and surface contaminants that were accumulated during cavity pre-fabrication. These power-dissipating materials should be removed with the gas flow in the form of volatile compounds. The surface of pure Nb achieved with the etching should have roughness at the level that is comparable to the wet chemical etching methods. The environmental concerns related to exhaust for chlorine (Cl_2) gas are minimal. Argon (Ar) is used as the gas carrier for Cl_2, since it is inexpensive. The use of Ar/Cl_2 combination for plasma etching for other material is reported in Ref. [75–80]. The development of the plasma processing of the SRF cavity was performed in several stages, In the first two stages Nb samples were involved. The first stage was the flat sample experiment. The second stage, which presented the beginning of the three-dimensional etching process, was the ring sample experiment. The two experiments will be addressed separately.

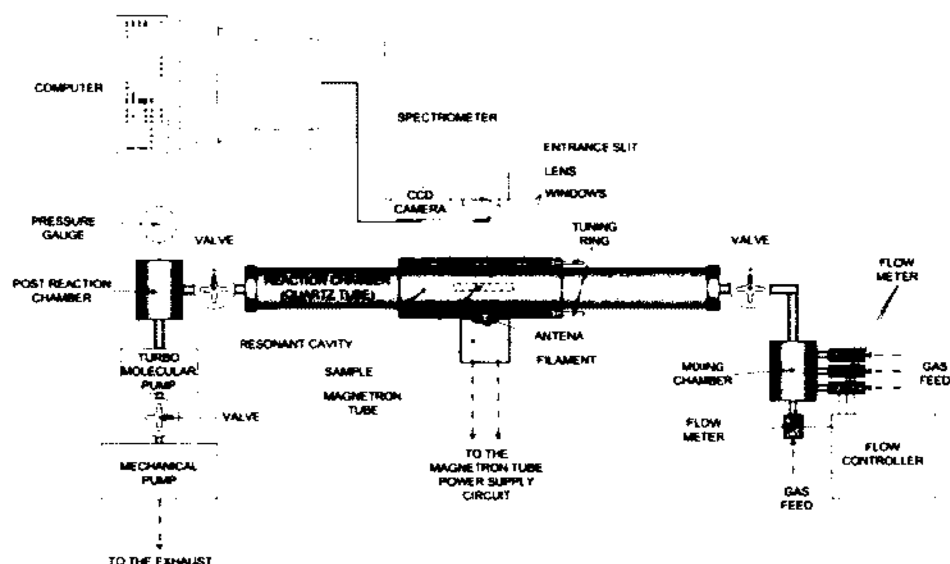

FIG. 3: Scheme of the experimental setup for the flat Nb sample etching

5.1 FLAT SAMPLE EXPERIMENT

The experiment was conducted in a barrel type reactor using an Ar/Cl_2 mixture, where the Cl_2 concentration was 3% and Ar concentration was 97%. The frequency of the power supply used for plasma generation was a microwave frequency of 2.45 GHz. The disk type Nb sample was placed on the top of the MW antenna inside the glass tube. The experimental setup for the flat sample experiment is shown in Fig. 3. The combination of a rotary and turbo pump was used to produce the vacuum. The Nb etch rate dependence was measured as a function of pressure, MW power and chlorine concentration. Preliminary optical emission spectroscopy was done with the help of a spectrometer. The etch rate measurement and it variation with pressure, power and chlorine concentraion was reported in Ref [81].

The experiment on the flat sample proved the feasibility of etching bulk Nb in an Ar/Cl_2 plasma environment. The surface analysis of the plasma etched sample was done with the help of atomic force microscopy, optical microscopy and scanning electron microscopy. The surface analysis of the plasma etched Nb in the flat sample experiment indicates that the surface roughness of the plasma etched niobium is better or equivalent to BCP etched or electropolished niobium as shown in Fig. 4 and Fig. 5. The detailed results of the surface analysis were reported in Ref. [82].

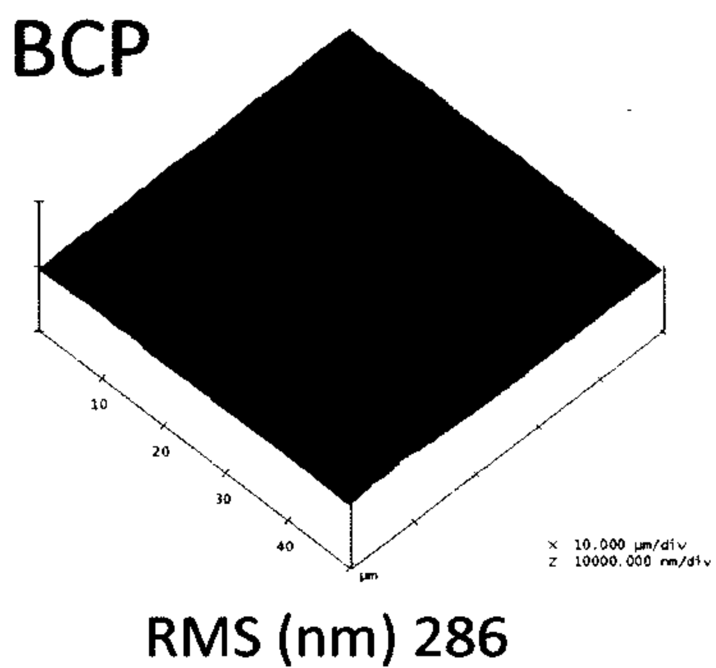

FIG. 4: Atomic force micrograph of a sample processed with BCP technique. Surface roughness was 286 nm.

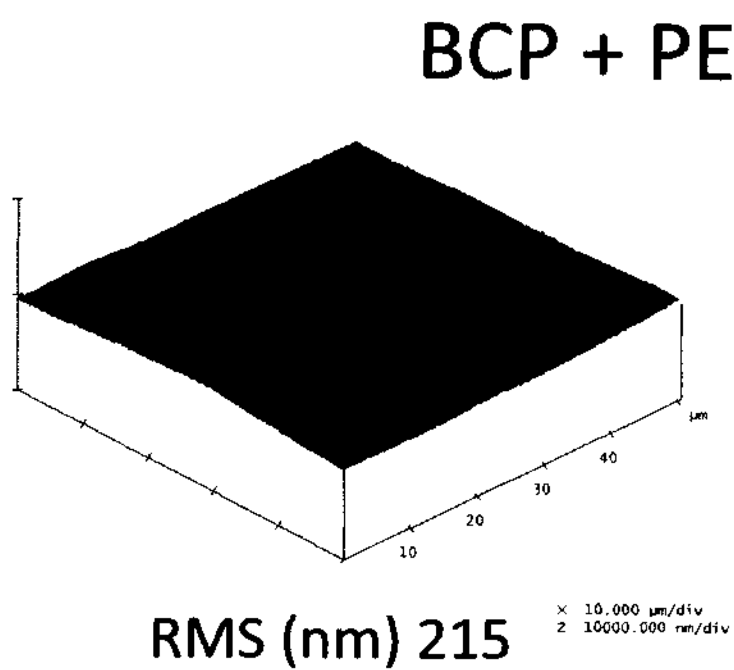

FIG. 5: Atomic force micrograph of a plasma etched BCP sample. Surface roughness was 215 nm.

5.2 RING SAMPLE EXPERIMENT

The transition from flat samples to the SRF cavity involves three major challanges: 1) the plasma has to etch the curved niobium surface with cylindrical symmetry, 2) the surface area from where the Nb has to be etched is large, 3) the cavity shape is a variable diameter cylindrical structure with beam tube diameter much smaller than the cell.

The SRF cavity presents a particular challenge for the rf plasma processing of its inner wall as it has a curved cylindrical symmetry and, therefore, the processed surface has a larger area than the surface of the inner electrode. By contrast, the technology that has been in the mature stage of development, such as semiconductor wafer processing, is based on essentially planar geometry. Moreover, the wafer to be etched is placed on the smaller-area electrode in order to take advantage of the asymmetry in the plasma sheath voltage. In the present case, the cavity which is to be etched is grounded and has a large surface area, so in the absence of positive d.c. voltage on the inner electrode, the sheath potential is substantially lower on the cavity surface than the sheath potential of the inner electrode.

5.2.1 CYLINDRICAL CAVITY

To transit from a flat sample to a fully etch SRF cavity, we have built a cylindrical cavity experiment, where ring shaped Nb sample were used. The aim of this experiment was to study the effect of the diameter variation of the inner electrode on the plasma and its effect on processing. In the experiments described here, the coaxial plasma is generated using an electrode running coaxial with the material cylinder to be etched. The coaxial plasma is excited with an rf waveform of 13.56 MHz. This frequency was chosen because its corresponding wavelength (22 m) is much larger than the characteristic size of the sample being polished. It is expected to give a more uniform polish and it is the industrial standard. The microwave (2.45 GHz) has a wavelength of approximately 12 cm which is almost equal to the cavity length. We have developed an experiment with a simple cylindrical cavity of 2.86 inch (7.2 cm) internal diameter and 6 inch (15 cm) length. This cylindrical cavity has 8 mini conflat ports, some intended for holding Nb samples and some had view ports for diagnostic purposes. The cavity is shown in Fig. 6.

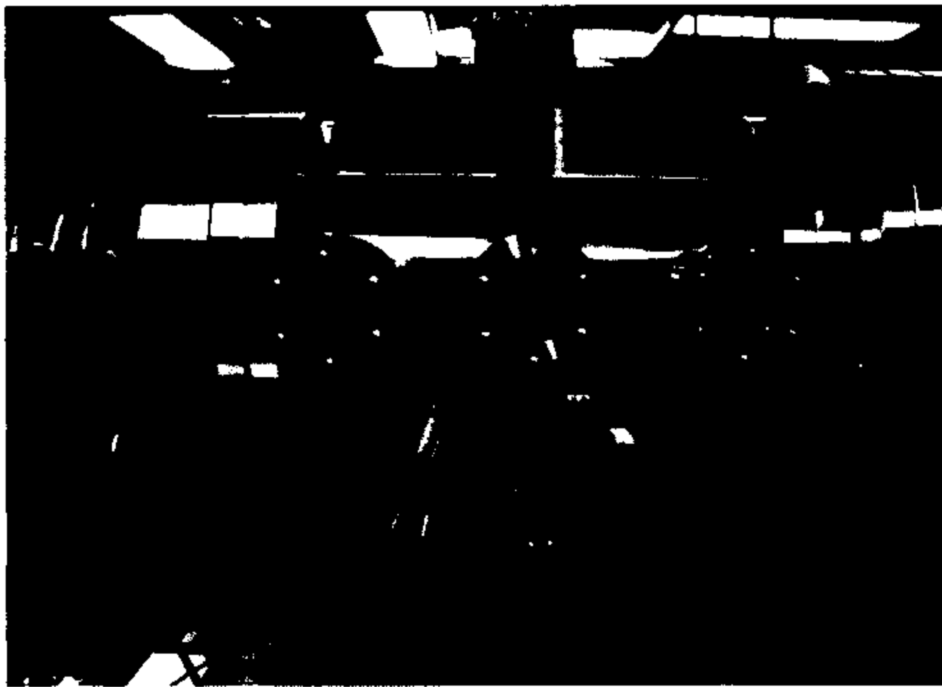

FIG. 6: Photo of the cylindrical processing cavity.

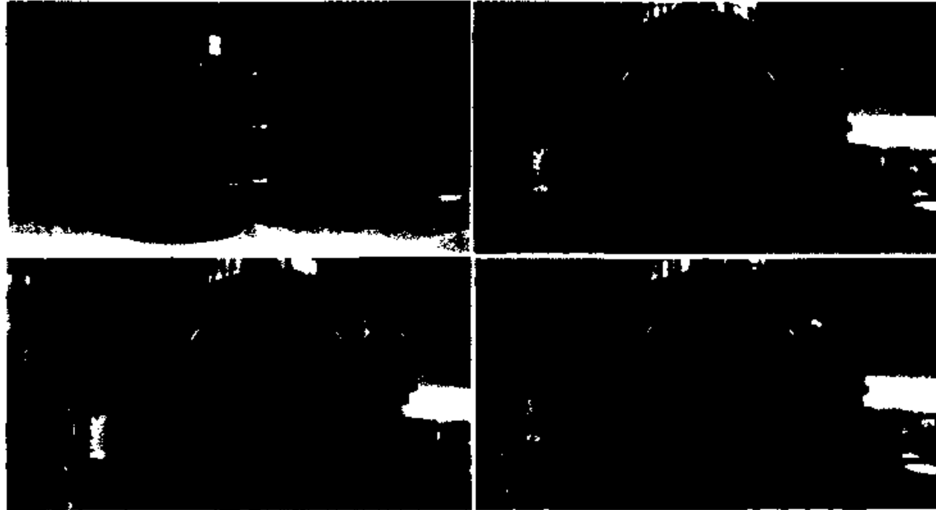

FIG. 7: Cylindrical cavity and inner electrodes with varying diameter. In clockwise direction: the disassembled arrangement and three end on views of the assembled electrode configuration, starting with the lowest diameter of the electrode.

5.2.2 VARIABLE ELECTRODE

The main goal of this preliminary experiment was to study the etching process of the outer electrode surface. For this purpose we opted for a variable-diameter inner electrode with the aim to study the influence of the surface area of the inner electrode upon the plasma properties. A set of variable diameter electrodes with the experimental cylindrical cavity is shown in Fig. 7. The three electrodes are 2.5 cm, 3.8 cm, and 5.0 cm in diameter.

5.2.3 EXPERIMENTAL SETUP

The experimental setup for the cylindrical cavity processing is shown in Fig. 9. The cylindrical chamber is evacuated with the help of a combination of roughing and turbo vacuum pumps. Pumping chlorinated gases can be very harmful to the vacuum pumps [83]. The rough pump uses synthetic oil, inlet sorption filter and an oil circulator as shown in Fig. 8 to increase its life cycle. The turbo pump used was a corrosive resistant turbo pump.

The gas flow and rf power are applied in the opposite direction, which is shown in Fig. 9. The red arrow is indicating the gas flow direction and the blue arrow is

FIG. 8: Pumping system for corrosive gases.

showing the power coupling direction. The gas was mixed in a three-branch manifold, each branch containing mass flow meters. The first gas line is attached to the premixed gas cylinder of 15% Cl_2 diluted in Ar and the second gas line is connected to a pure Ar cylinder. The third gas line was a re serve and not used for the present work.

The mix was dominated by Ar as a buffer gas, and Cl_2 as the key provider of chemical radicals. We are using an rf power supply with an attached automatic matching network and an option to connect a dc power supply in series with the rf generator with the purpose to modify the dc bias of the inner electrode. To measure the etch rate of Nb, we opted for two types of samples. One type was a flat sample attached to mini conflat flanges, shown in Fig. 9, the other was a ring type sample. Those samples were prepared for the AFM, SEM EDX surface analysis, whereby an appropriate statistical analysis can be initiated.

The next step in developing cavity etching technology is to use a sample, which is a ring rather than a flat coupon. The ring sample has proven to allow controlled studies of the etching rate variations in cylindrical geometry of a coaxial asymmetric

FIG. 9: Photo of experimental setup for cylindrical plasma processing.

FIG. 10: Photos of etching samples: (a) Flat sample (b) Ring samples.

discharge. In all experiments, one or more ring samples were positioned to fit tightly on the inner surface of the outer electrode, to ensure uniform electric and thermal contact. The ring type samples as shown in Fig. 10, were attached in the full circle to the inside wall of the outer electrode. The ring sample is made of a Nb ribbon with 2.5 cm width. The radius of the ring is 7.2 cm, which is approximately the beam tube diameter of the single cell SRF cavity. It was expected that the ring sample would exhibit a more precise rate of etching performance, closer to the SRF cell configuration, as it covered a wide curved surface area, which is a couple order of magnitudes larger than the flat sample surface area.

As the plasma properties and, in turn, the surface processing effects vary substantially with the frequency, pressure, chlorine concentration, temperature and power levels inside the reactor, we have to optimize these parameters for the most efficient and uniform surface material removal from the samples placed on the cavity perimeter.

5.2.4 EXPERIMENTAL SETUP FOR TEMPERATURE VARIATION

The temperature control of the ring-type sample is achieved by wrapping heating tapes around the outer wall of the outer cylinder as shown in Fig. 11. The current in the heating tape is controlled with a variable autotransformer and the temperature was measured by a thermocouple attached to a Fluke multimeter.

5.2.5 ATMOSPHERIC PRESSURE RF POWER FEEDTHROUGH

An atmospheric pressure coaxial rf power feedthrough was developed to couple the rf power and to ensure that the discharge is confined within the cylindrical cavity to be processed. Its schematic is shown in Fig. 12. This rf power feedthrough helps in preventing the discharge inception in front of the cylindrical cavity to be processed. The inner tube of this coaxial feedthrough is 0.64 cm in diameter and is made of copper. The outer tube is 1.5 cm in diameter and is made of stainless steel. The ratio of the inner and outer tube is approximately 2.3 to minimize the rf impedance. One end of the feedthrough is connected to an HN type coupler and the other end is connected to an electrical vacuum feedthrough with a mini conflat flange. The space between the tubes in the coaxial feedthrough was kept at atmospheric pressure to prevent plasma formation inside the coaxial structure. The vacuum electrical feedthrough is threaded at the end, and is coupled to the powered electrode. The

FIG. 11: Photo of experimental set-up for temperature variation during etching cylindrical cavity.

threaded section is covered by the powered electrode to avoid damage by the Ar/Cl_2 plasma.

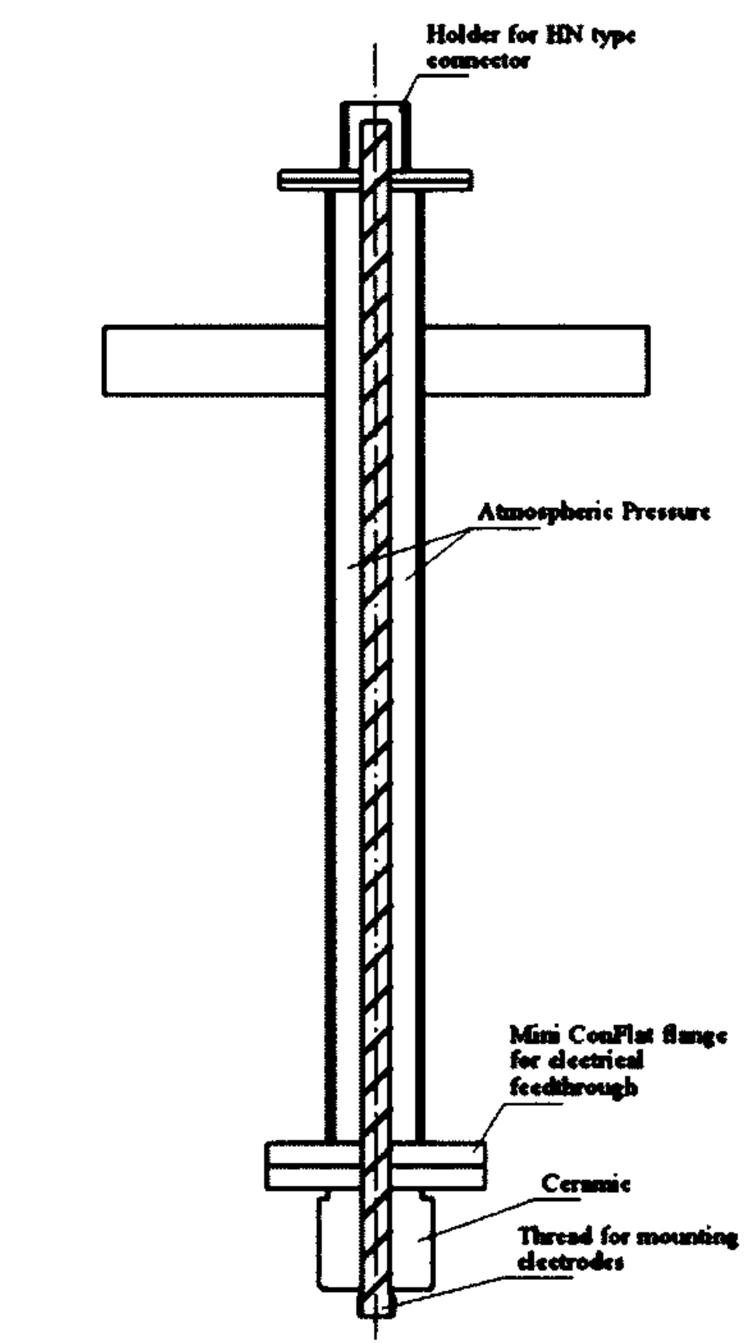

FIG. 12: Schematic diagram of atmospheric pressure rf power feedthrough.

CHAPTER 6

EXPERIMENTAL RESULTS FOR RING SAMPLES

The properties of the asymmetric discharges were extensively studied in the context of the development of planar semiconductor processing technology starting as early as the 1970s [25, 37]. Koenig and Maissel, used simple arguments, such as constant ion density near both electrodes, Child's law and absence of collisions in the sheaths, to arrive at the conclusion that the inverse scaling of the electrodes sheath voltage and surface area follows a power law with a scaling exponent of four, as shown in Chapter 4. A number of later experimental work implied a much lower exponent [41, 84–86]. We are presently interested in the cylindrical geometry in particular, where some experiments and models do exist [44, 86]. Although chemical radicals (excited neutral chlorine atoms, molecules and ions) are produced by the plasma to carry on the required reactions for material removal from the niobium surface, some form of ion-assisted etching is always present. This means that a certain potential is needed for the ions to be accelerated prior to hitting the surface, but a chemical radical is also needed in order to etch bulk Nb. Therefore, the experimental procedure in this experiment had to include a series connection of a dc power supply to the inner electrode in series with the rf power supply. Etching of the electrically grounded Nb surface requires bringing the driven (inner) electrode to a positive dc potential in series with rf power, in order to lift the plasma potential above a certain value, so that the potential difference between the plasma and the grounded surface allows the ions to gain the necessary energy for etching niobium.

Before attempting to etch the niobium sample, we tested the cylindrical cavity for full volume plasma production, to determine if plasma is spreading in all the portions of the cavity or not. Depending on the diameter of the driven electrode, there is a certain pressure (above 20 mTorr) where the plasma is completely filling the cavity. When operated below the critical pressure, the plasma is spread only over a certain section of the cavity. This effect is illustrated by observation at various pressures, shown in Fig. 13.

Although much care was taken to sustain the plasma spreading in the full cavity, the attempt to etch a niobium sample on the outer wall without applying the positive

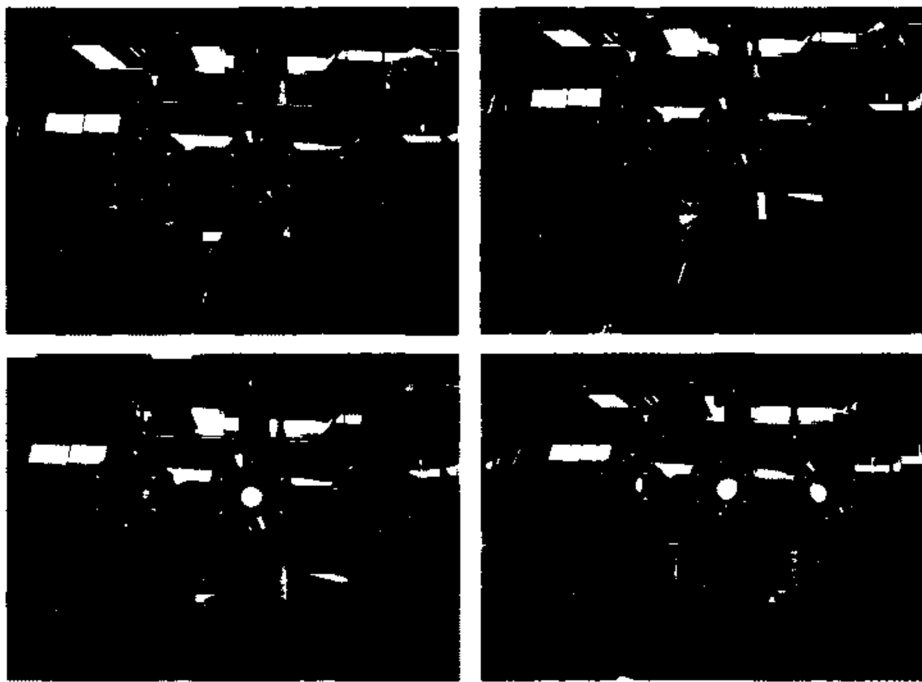

FIG. 13: Spreading of plasma inside the cylindrical cavity at different conditions: top left, lower pressure; top right, medium pressure; bottom left, higher pressure at low power; and bottom right, higher pressure and higher power.

dc bias on the driven electrode was not successful. We tried all possible pressure and power ranges in the given setup, but there was no appreciable material removal to be measured.

6.1 DEPENDENCE OF THE ETCH RATE ON THE PROCESS PARAMETERS

We are presenting the first results of the three dimensional (3D) plasma etching of the inner surface of bulk niobium cavities. The successful completion of this technology will enable the processing of inner surfaces of any three dimensional structure, not only SRF cavities. The variation of the etching rate with the inner electrode diameter and with pressure at a fixed electrode diameter, constant power, and constant chlorine concentration is presented in figures. The gas mass flow rates to achieve indicated pressures were 0.25, 0.39, 0.55 and 0.69 l/m, respectively. All measurements were made at the grounded electrode temperature of 422 K. The error in Cl_2 concentration was 2%, in power 3 W, and in pressure 4 mTorr, in temperature 2 K and in dc bias 2 V respectively. The etch rate was measured by measuring the mass difference before and after the plasma exposeure of the ring sample and dividing it by the surface area, by Nb density, and by the processing time. Each experimental run was carried out for more than 90 minutes and in some cases for 100 minutes to avoid the fluctuation in etch rate measurements due to lag time in starting the etching process [70]. New samples are cut from the same Nb sheet for each run to rule out any difference in the material properties. The removed layer thickness was 2 to 9 microns. The calculated estimated error in measurement of mass and area leads to an error in etch rate of 0.82 nm/min, but when the error in pressure, power, concentration, temperature and dc bias is included, we estimated the error to be about 10% in etch rate measurement.

6.1.1 DEPENDENCE OF THE ETCHING RATE AND SELF-BIAS VOLTAGE ON THE DIAMETER OF THE DRIVEN ELECTRODE

As stated before, when the diameter of the driven electrode is varied, the electrode surface area ratio is changed and, as a consequence, the negative self-bias potential developed across the inner electrode sheath varies. We are, however, interested in the etching rate variation on the grounded electrode. Constant dc bias on the driven electrode does not lift the plasma potential around the grounded electrode by the

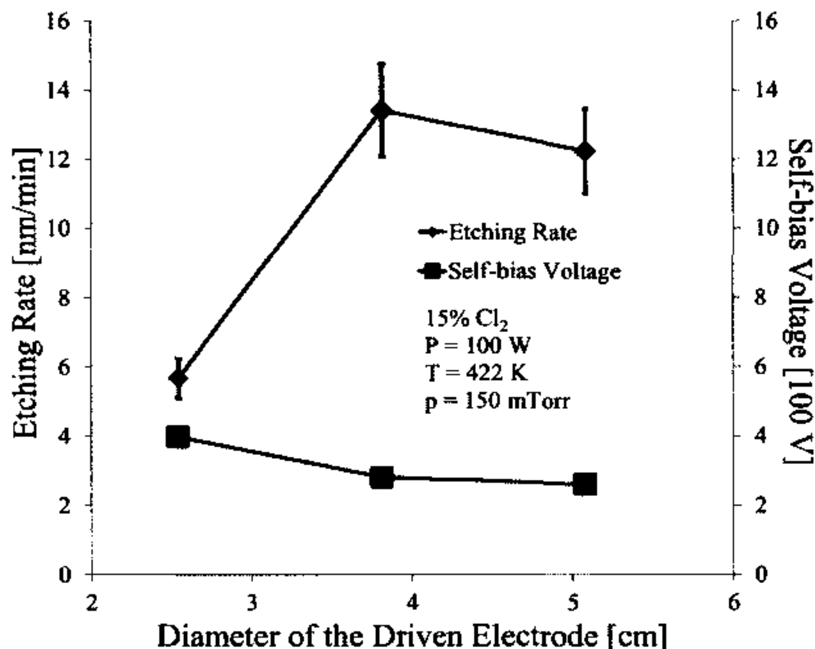

FIG. 14: Etching rate and self-bias dependence on the diameter of the driven electrode. Solid lines are visual guidelines.

same value for different area inner electrodes, due to its substantially different self bias potential.

We have measured the variation of the etching rate with the diameter because the etch rate also depends on the volume of the produced plasma, which increases when we decrease the diameter of the driven electrode and it can affect the etch rate although the plasma potential is lower. All etch rate data are taken at constant dc bias of +290 V applied on the inner electrode. The negative self-bias potential in the absence of the dc bias is measured at the same pressure, power and gas concentration. The measured etching rate and self-bias potential dependence on the inner electrode diameter are given in Fig. 14.

6.1.2 DEPENDENCE OF THE ETCHING RATE ON PRESSURE

There are three competing effects associated with the variation of pressure in the system. Increased pressure means increased concentration of radicals, which are in this case the excited neutral chlorine atoms, molecules, and reactive ions of the chlorine. Concentration of molecules is directly proportional to the pressure, but the

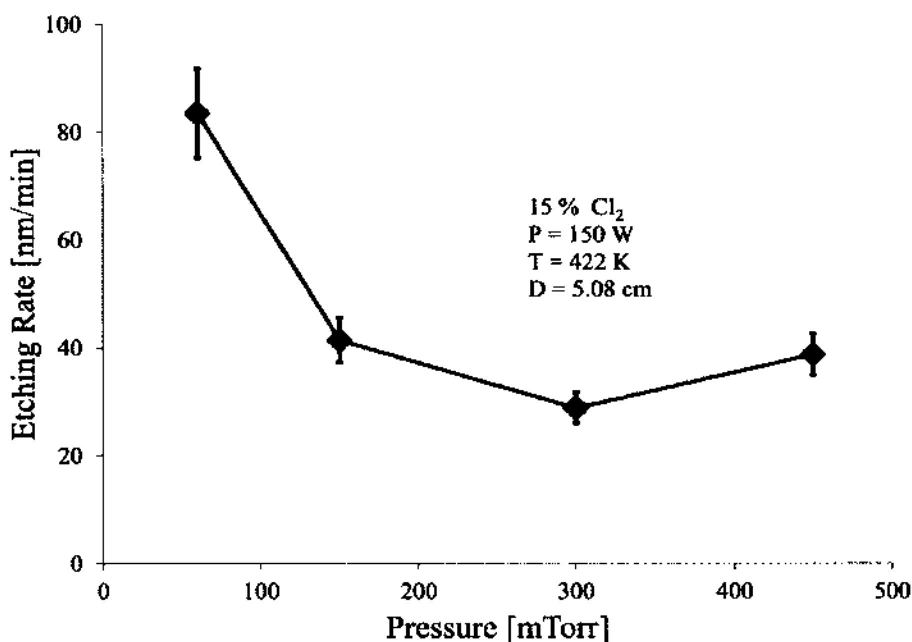

FIG. 15: Etching rate dependence on the gas pressure. Solid line is visual guideline.

concentration of reactive ions depends on the rf power and the electronegativity of the discharge. Therefore, at constant rf power, a larger etch rate at higher pressure is indicative of chemical etching, and a smaller etch rate on higher pressure and its weaker dependence on pressure suggests the reactive ion etching mechanism. In addition, pressure increase leads to lower residence time and an increase in collision rates among gas molecules which lead to depletion of radicals. Those affect the etching rate as the increase of pressure was obtained by increasing the gas flow rate. The etch rate dependence is shown in the Fig. 15.

This diagram shows that operating at low pressure is more favorable. The maximum etching rate measured was obtained at about 60 mTorr. It then decreased or showed saturation behavior with increasing pressure. This result indicated that reactive ion etching was the probable mechanism for material removal.

6.1.3 DEPENDENCE OF THE ETCHING RATE ON THE RF POWER

The variation of the etching rate with rf power when all other parameters were kept constant is shown in Fig. 16. It follows the general property of reactive rf

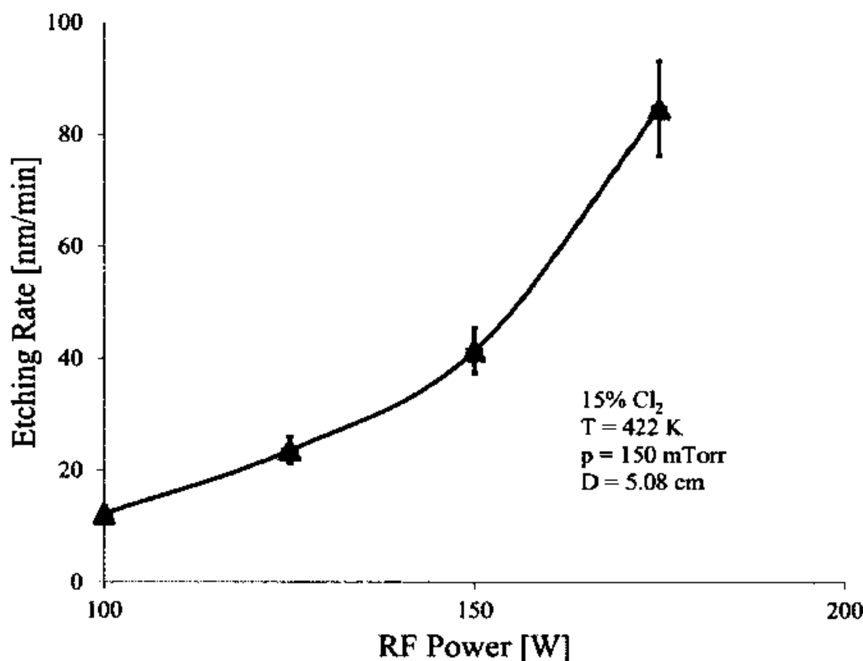

FIG. 16: Etching rate dependence on rf power. Solid line is the exponential fit.

discharges that the increase in power increases the amount of radicals and ions at a given pressure, which in turn increases the etching rate. In this case the trend did not saturate within the limited power range. There is a difference between the present case and the general trend in planar technology as used in the semiconductor etching industry. In planar geometry, increasing power also increases the self-bias of a driven electrode which in turn helps in increasing the etch rate. In our case, the bias is constant and pressure, chlorine concentration and temperature remain constant.The only variable parameter was rf power. The rf power per unit volume could not be calculated as volume of the plasma varies with the rf power.

Our data indicate that there are two regimes of the etching rate increase with power. Between 100 W and 150 W, the etching rate increases according to the power law with exponent of three. Above 150 W, the increase becomes steeper. This is consistent with the transition depending on the power as reported in [65, 87].

6.1.4 DEPENDENCE OF THE ETCHING RATE ON THE CHLORINE CONCENTRATION

In Fig. 17, we present the dependence of the average etching rate on Cl_2 concentration diluted in Ar. The concentration of chlorine was changed by mixing gases from two cylinders, one 15% Cl_2 diluted in Ar and the other pure Ar. The lower percentage concentration of chlorine 10% and 5% was achieved by reducing the flow of the Cl_2/Ar mixture to 0.26 l/m and 0.13 l/m respectively and by increasing the flow of pure Ar to achieve the same pressure. In this process, the gas pressure in the experiment was kept constant. Other parameters, such as rf power, dc bias, and temperature of the substrate remained constant during the experiment. There are several possible explanations for the saturation effect at relatively low chlorine concentration (see Fig. 17). First, additional chlorine may not have been consumed completely on the surface reactions, which has been observed in the Ar/Cl_2 discharges [88]. Second, chlorine residence time was not long enough to enable the surface reactions. Further study will elucidate the role of these two effects in the process. We note also that at low power, the discharge is capacitively coupled and electronegative [87], where the electron density is reduced due to the increase of negatively charged chlorine ion population. This saturation effect may be related to relative electron density reduction due to the increased electronegativity of the discharge. However, positive chlorine ion density, which may be important for the reactive ion etching, should not be affected by the build-up of electronegativity. Consequently, the assumed mechanism of saturation based on the increased electronegativity is not completely certain and has to be studied in more detail. It seems that the increase of chlorine concentration above 5% does not provide any substantial benefit to the process.

6.2 DETERMINATION OF THE ETCH RATE MECHANISM AND DEPENDENCE OF ETCH RATE UNIFORMITY ALONG THE GAS FLOW DIRECTION ON PROCESS PARAMETERS

To develop the plasma etching method for bulk micro machining of long cylindrical structures made of Nb, an understanding of the etch mechanism of Nb in Ar/Cl_2 plasma is required. It is also important to know the nature of the etch mechanism responsible for material removal in order to determine if it is purely physical etching (sputtering), purely chemical etching, or a mixture of both. The understanding of etch mechanism would help in creating smoother surfaces, which can be created

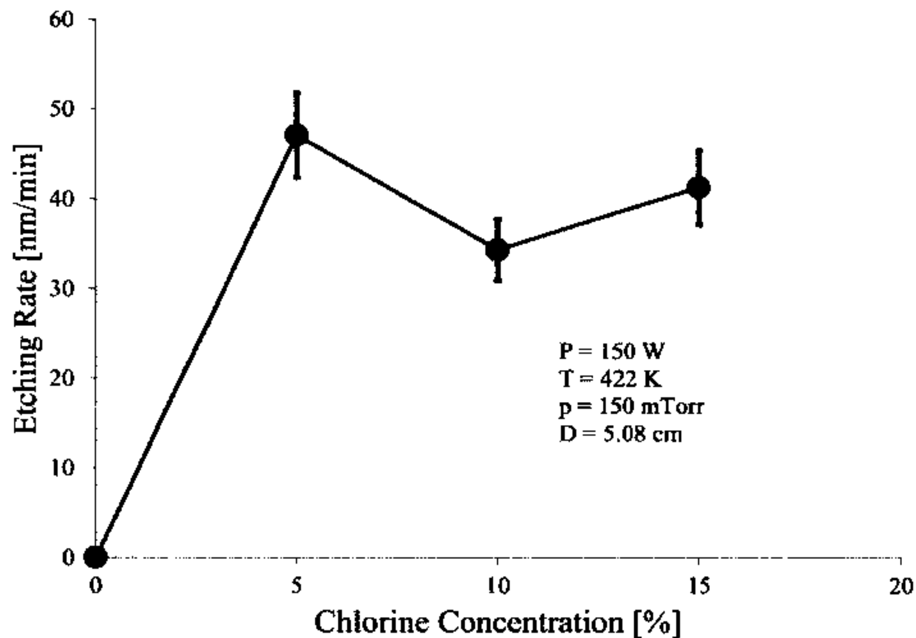

FIG. 17: Etching rate dependence on concentration of chlorine (% Vol) diluted in argon. Solid line is visual guideline.

by variation of physical and chemical nature of etching [89]. Another factor in developing this process is the uniformity of the etch rate across the cylinder, because the non-uniformity in surface quality along the cavity profile may affect the field distribution. Our results show that the etching rate follows the Arrhenius form of dependence on the temperature and which shows some analogy to the etching of Si with Cl_2 [25, 90]. Further, by changing the sheath potential at the outer surface of the coaxial discharge using the bias on the inner electrode, the ion bombardment energy on the etched surface is changed and the dependence of the etch rate on the bias potential is measured. This study would lead to the additional clarification of the etching mechanism. Sputtering or physical etching is achieved by bombarding the surface with energetic ions and mechanically removing the material, while chemical etching involves the conversion of the material to a volatile product by chemical reactions between the material and neutral etchant radicals produced in plasma. Energetic ion assisted etching or reactive ion etching remove material by making the gaseous product in the presence of energetic ions, which would not be possible by involving the neutral plasma species [78, 91–94].

Another factor in developing this process is the uniformity of the etch rate across the cylinder because the non-uniformity in surface quality along the cavity profile may affect the field distribution. Etch rate uniformity along the cylinder axis is estimated by comparison of the effect on two Nb rings positioned at different places inside the outer cylinder. The effect of the gas flow rate was also probed by operating with different pumping speeds and maintaining the same pressure in the processing chamber.

As earlier explained, in our coaxial rf plasma reactor, the inner electrode has a smaller surface area than the outer cylinder, whose inner surface has to be etched. Due to the presence of a blocking capacitor in the rf power supply, the smaller surface area electrode will have a self-bias potential. The surfaces exposed to plasma are bombarded by the ions with energy gain proprtional to potential difference between bulk plasma and the surface. Time averaged plasma potential V_p and the average ion energy E_{ion} in a collisionless sheath are related [58].

$$\epsilon_{ion} = q(V_p - V_{bias}) \text{ (for inner electrode)} \tag{93}$$

$$\epsilon_{ion} = q(V_p) \text{ (for outer electrode)} \tag{94}$$

where q is the ion charge. The plasma potential can be changed by applying a positive dc bias to the inner electrode [41, 58, 84], which will change the sheath potential on the outer cylinder. The incident ion energy on the inner surface of the outer cylinder varies due to the change in sheath potential as illustrated in Fig. 18.

In order to investigate the physical nature of the etching mechanism, we have studied the variation of the etch rate with the sheath potential by raising the dc bias on the inner electrode. To study the chemical nature of the etch mechanism, the temperature of the outer cylinder was varied and the activation energy was evaluated using the Arrhenius equation. The temperature dependence of the etch rate has been studied for a number of materials [69, 76, 77, 95] at various plasma conditions. Heating effects on the etch rate for Nb was studied in a CF_4/O_2 gas mixture [65] but there was no study for the Ar/Cl_2 mixture.

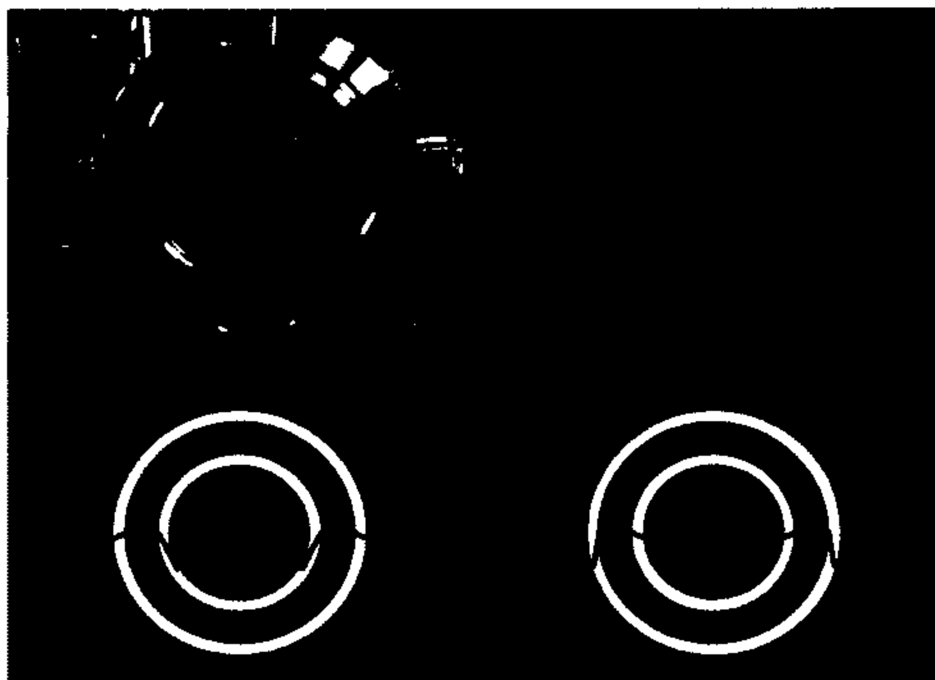

FIG. 18: Cross-sectional images and schematic of coaxial rf electrode, plasma, and sheath potentials: (a) Image of coaxial electrodes (b) Image of coaxial plasma (c) Plasma sheath potential distribution in coaxial rf plasma (d) Plasma sheath potential distribution in coaxial rf plasma with positive dc bias on the inner electrode.

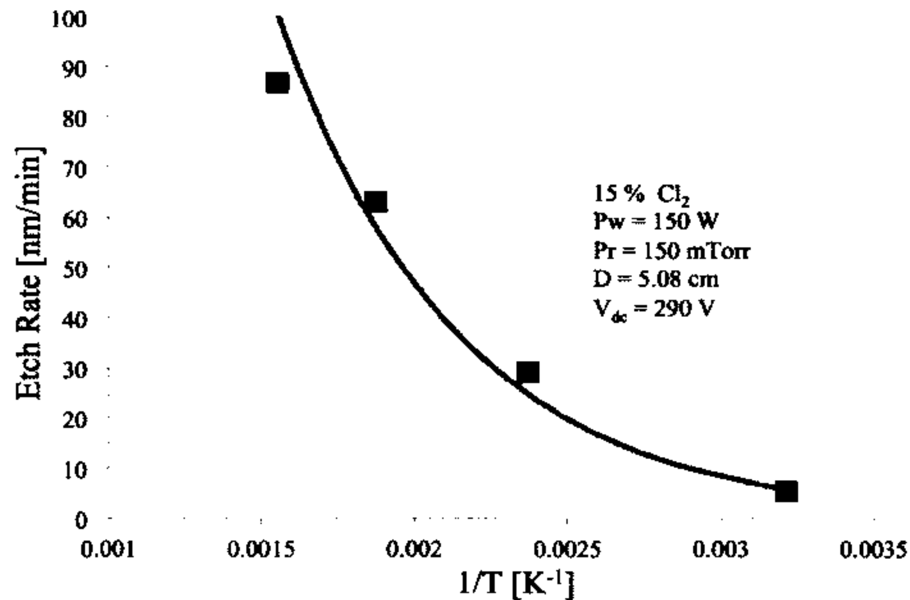

FIG. 19: Etching rate dependence on the Nb temperature. Solid line represents exponential fit.

6.2.1 ETCHING RATE DEPENDENCE ON TEMPERATURE AND EVALUATION OF ACTIVATION ENERGY

The temperature of the substrate plays an important role in determining the chemical reaction rates, adsorption of the reactant species to the substrate and desorption of the reaction products from the substrate [65, 67, 69–71, 76, 77, 95–97]. It also gives us an indication about the nature of the etch mechanism, as chemical etching mechanisms normally exhibit the Arrhenius type dependence on the temperature [65, 78]. To determine the temperature dependence on the etch rate, temperature is varied from 311 K (38 °C) to 644 K (381 °C) with all other etch conditions shown. Dependence of etch rate on the inverse temperature, $1/T$, is shown in Fig. 19.

Figure 19 shows a strong temperature dependence of the etch rate, which indicates that the mechanism of Nb etching in Ar/Cl_2 plasma has a strong chemical component. Under the condition presented in Fig. 19, the effective activation energy estimated from the exponential fit of the plot for Nb etched in Ar/Cl_2 plasma is 0.15 eV for the given experimental conditions. As higher temperature improves the morphology of the surface [76], particularly at higher temperature with an increased

power level [95], increasing the temperature of the SRF cavity for faster etching and smoother surface is a viable option.

6.2.2 ETCHING RATE DEPENDENCE ON THE DC BIAS

Due to high mobility of the electron, in plasma processes, an ion sheath is formed in front of any material exposed to plasma due to high mobility of the electrons. Through this sheath, positive ions gain kinetic energy and hit the surface of the material [85, 98]. In our coaxial rf plasma reactor, when no dc power supply is attached, the inner electrode acquires a negative self-bias potential (on the order of hundred volts for moderate power of 100 Watt), which varies with power, pressure and gas composition. A negative bias on the inner electrode does not influence the plasma potential, but a positive bias on the electrode will cause the plasma potential to increase. While all grounded surfaces are bombarded with positive ions with energies characteristic of the plasma potential, by positively biasing the inner electrode, the incident ion energy on the grounded surface can be increased [84]. The variation of the dc bias on the inner electrode and the measured etch rate are shown in Fig. 20.

Figure 20 shows a strong dependence of the etching rate on the bias potential (V), and the positive side of the graph shows a very good fit to $V^{0.57}$ which is very close to the square root functional dependence reported in other works [31, 77]. The etch rate dependence on the dc bias is widely reported [38, 71, 99] . The knee in the curve might indicate two thresholds for the ion etching, one related to (Ar^+ and Cl^+) and the other threshold for ($Cl_2{}^+$) as suggested in Ref. [31, 77]. This also shows that below a certain bias potential there is no etching possible on the grounded Nb surface, which tells us that a critical amount of plasma potential is required to start the Nb etching process.

6.2.3 ETCHING RATE DEPENDENCE ON THE TYPE OF GAS AND OTHER ETCHING PARAMETERS

The etch rate dependence on the temperature indicates a strong chemical component, while strong dependence of the etch rate on ion energy suggests a physical form of etching. To clarify these results, a new set of measurements was conducted using pure Ar gas to separate the physical component of the etching process. There

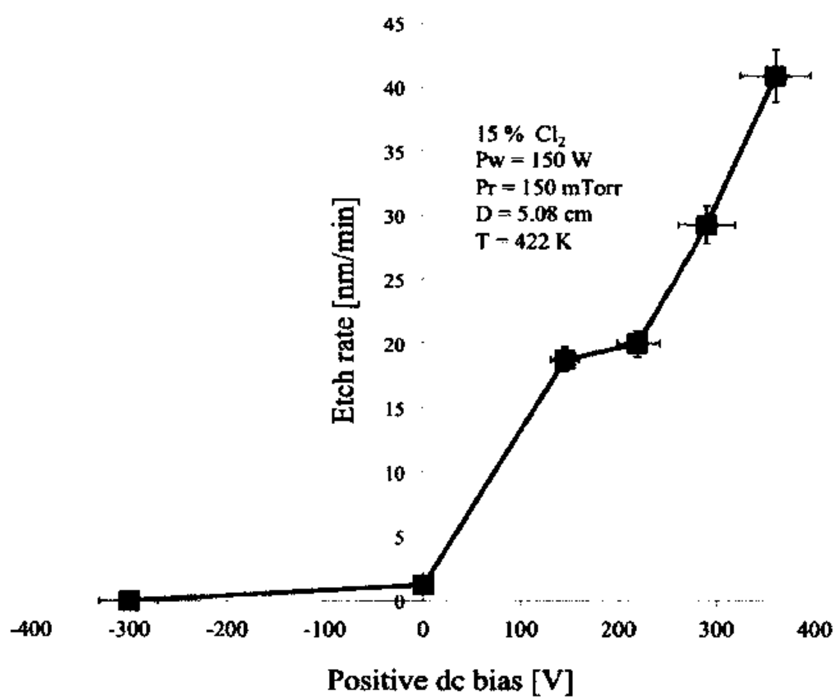

FIG. 20: Etching rate dependence on the dc bias at the inner electrode. Solid line is a visual guideline.

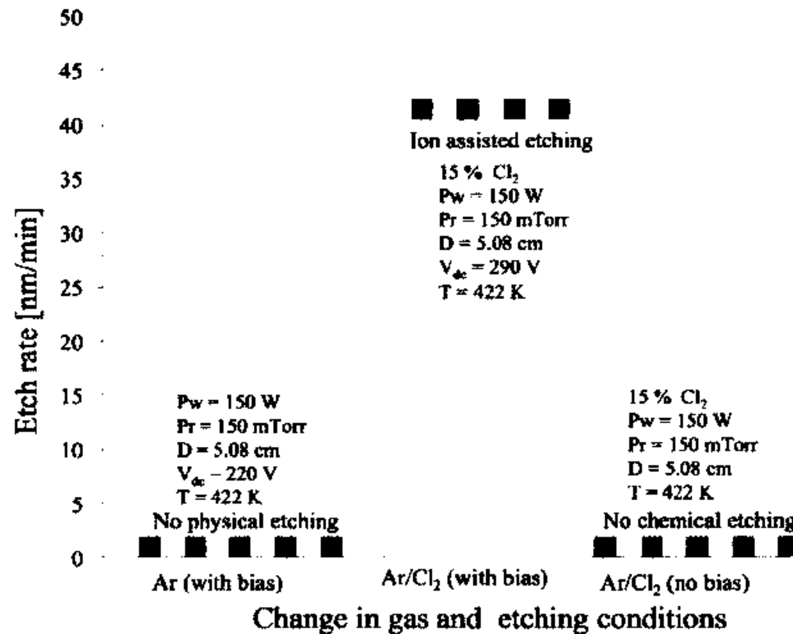

FIG. 21: Etching rate dependence on gas composition and indicated etching parameters.

was no significant mass removal by pure Ar gas. To separate the chemical component of the etching, the experiment was conducted with an Ar/Cl_2 mixture with no positive bias on the inner electrode. There was no significant mass removal observed. Therefore, pure chemical etching of Nb samples on the outer electrode is also not possible. There is appreciable etching only in the case when there is sufficient ion energy available to hit the surface and the mixture of the gas contains some amount of Cl_2. Fig. 21 shows this in graphical format. The Nb (placed on the grounded outer wall) etching is possible only in the condition when Ar/Cl_2 was used as a gas mixture and positive bias is applied to the inner electrode.

Figure 21 shows the behavior very similar to that of Fig. 2 in the paper by Coburn and Winters [93]. It is safe to say that Nb etching in Ar/Cl_2 plasma is indeed reactive ion assisted etching. The Arrhenius type dependence of the etch rate on the temperature shown in Fig. 19 indicates a strong chemical component of the ion-assisted etching mechanism with strong dependence of the etch rate on the sheath potential, that is the ion energy shown in Fig. 20 also suggests the presence of the

TABLE 1: Etch rate variation at fixed pressure and different flow rates achieved using the gate valve.

Pressure (mTorr)	Flow rate (l/min)	Etch rate (nm/min)
60	0.25	84
60	0.13	47

physical aspect of ion assisted etching. The temperature, bias, and gas variation shows that the Nb etching mechanism is neither purely physical etching nor purely chemical. Therefore we identify it as ion assisted etching, or reactive ion etching.

6.2.4 ETCHING RATE DEPENDENCE ON THE GAS FLOW RATE

The dependence of etching on the flow rate of gases is defined in the semiconductor industry by a parameter called residence time. The residence time in a plasma reactor is proportional to pV/F, where p is the pressure, V is the volume of the chamber and F is the gas flow rate, which has an important role in etching characteristics [100]. Determining the effect of the gas flow rate on the etch rate is a challenging task since the etch rate also depends on the pressure. We investigated the effect of flow rate on the etch rate at the same pressure by variation of the pumping speed, employing a partially closed gate valve or by operating only with a roughing pump.The same level of pressure for a reduced flow rate is achieved by a gate valve between the vacuum pumping system and the reaction chamber. It is also achieved by stopping the turbo pump and getting the same pressure by just using the roughing pump. The effect of the gas flow rate on the etch rate is a thoroughly studied for other materials [66, 67, 69, 80, 101]. Two sets of measurements were performed to elucidate this effect. In the first experiment at low pressure range, the flow rate was reduced to one half of the maximum and the same pressure was maintained constant with the help of a gate valve to control the pumping speed. The results are given in Table 1.

Table 1 shows that increasing the flow rate contributes to increasing the etch rate. The lower etch rate in a reduced flow rate can be attributed to lower availability of radicals. In the second experiment, we shut down the turbo molecular pump and the same pressure was achieved with the roughing pump. Achieving the same pressure with the roughing pump only, requires a lower gas flow rate. The etch rate data for both pumps with corresponding flow rates are shown in Table 2.

TABLE 2: Etch rate variation at a given pressure and different flow rates achieved with and without turbo molecular pump.

Pressure (mTorr)	Flow rate (turbo on) (l/min)	Etch rate (turbo on) (nm/min)	Flow rate (turbo off) (l/min)	Etch rate (turbo off) (nm/min)
300	0.55	29	0.10	15
450	0.69	39	0.21	31

Table 2 shows that the reduction in flow rate decreases the etch rate even at relatively high pressure, which means that at this pressure and power the etch rate is still determined by the availability of the radicals. Therefore, Table 1 and Table 2 both show that the etch rate at lower and higher pressure are constrained by the radical production rate. The impact of the gas flow rate on the etch rate is significant.

6.2.5 ETCH RATE NON-UNIFORMITY DEPENDENCE ON VARIOUS PROCESS PARAMETERS

The dependence of etch rate on the surface area of the material exposed to etching is referred to as a loading effect [88]. In parallel plate planar discharges, this effect leads to an etch rate decrease and non-uniformity in the etch rate for large area wafer surfaces [88, 102]. This non-uniform etch rate effect in a coaxial type plasma reactor has never been studied up to present work. It is much more severe and complex in the case of coaxial discharge because of unidirectional flow of the gases. In planar discharges, used in the semiconductor industry, the gas is flown through a shower head. In that case, all produced radicals are uniformly exposed to the full surface of the material to be etched. In the present design of gas flow in the coaxial discharge, the flow pattern is inhomogeneous, and the materials closer to the flow plume get exposed to the fresh radicals first and only the unconsumed radicals can move further. The influence of this effect on Nb etch rate uniformity in coaxial structures has yet to be determined. To determine the etch rate variation at different distances from the Cl_2 source, we placed two Nb ring-type samples at one inch distance from each other and exposed them to power and gas flow with opposite directions as shown in Fig. 22(c). The ring-type samples are one inch wide and each have a surface area of approximately 59 cm^2 as shown in Fig. 22(a).

Figure 22(c) illustrates the sample configuration and position for the study of the

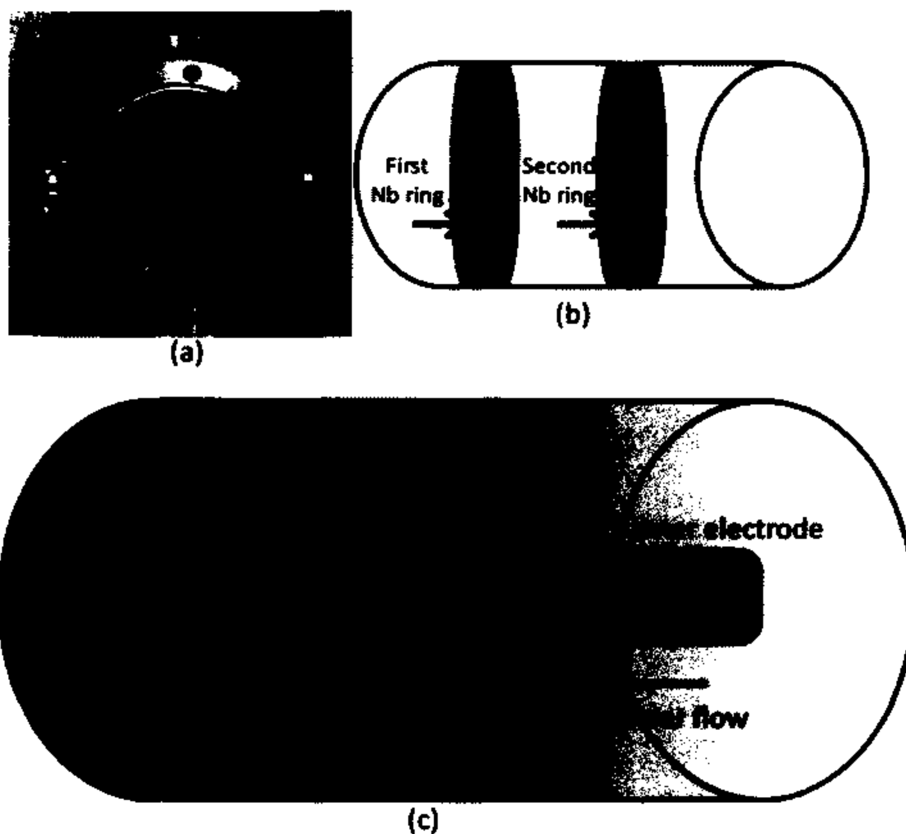

FIG. 22: Schematic and image of the Nb ring sample placed on inner surface of the outer cylinder: (a) Cross sectional view of two ring samples placed on the inner surface of the outer cylinder indicated with arrows (b) Schematic of axial view of the two ring samples (c) Schematic of loading effect with inner electrode and two ring samples when plasma is on. Arrows show the direction of the gas and rf power flow.

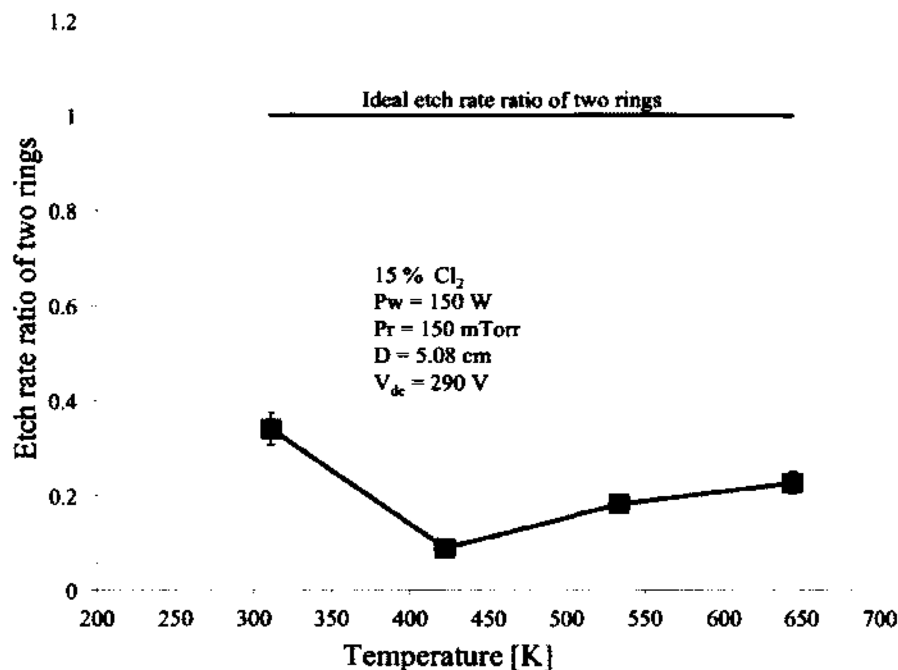

FIG. 23: Etch rate ratio of two rings versus temperature of the substrate. Solid line is a visual guideline.

etch rate non-uniformity effect with the presence of the inner electrode and plasma. The change in color represents the depletion of radicals due to consumption by the Nb ring positioned close to the gas flow source.

The etch rate non-uniformity is caused by the depletion of the reactants [102]. In the present experiment, two ring samples were placed at about 2.5 cm apart and the etch rates were measured at both rings with varied plasma conditions. The ring placed the closest to the gas flow source was etched more than the ring placed further downstream. The diagrams shown below describe the ratio of the etching rates on the downstream and upstream rings as a function of the process parameters, and are indicative of the effect of an individual etching parameter on the uniformity of the etching rate. For a perfectly uniform etching, as plotted on the graphs, the ratio should be equal to 1 (ideal etch rate). In Fig. 23 the variation of this ratio with temperature of the Nb sample is shown.

Figure 23 shows that the increasing temperature does not significantly improve the uniformity of the etch rate. It is slightly better at lower temperature. However,

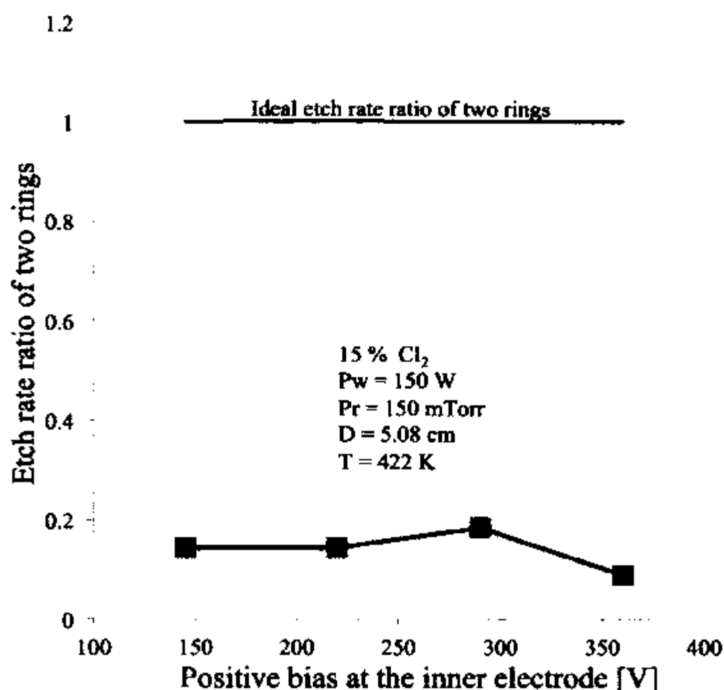

FIG. 24: Etch rate ratio of two rings versus the positive bias on the inner electrode. Solid line is a visual guideline.

at lower temperatures the overall etch rate is also low as shown in Fig. 19. Therefore, we conclude that the sample temperature cannot be a very effective control parameter for better uniformity. In Fig. 24 the variation of the etch rate between Nb rings versus the positive bias on the inner electrode is shown. It shows that the etch rate ratio is nominally increasing, but on a high positively biased inner electrode, when the etch rate is usually higher, the ratio decreased.

In Fig. 25 we present the data for the etch rate ratio and the rf power applied between the electrodes.

Figure 25 clearly shows that increasing the rf power reduces the etch rate ratio, which means at higher power, when the etch rate is high due to an increase of the radical and ion production [103], the consumption ratio by the first ring also increases. All parameters (temperature, dc bias at the inner electrode, and rf power) make the reaction probability high for making a volatile product. This causes the etch rate to go high, but simultaneously the probability of the radicals to get consumed by the first ring also increases which makes the etch rate uniformity remain approximately

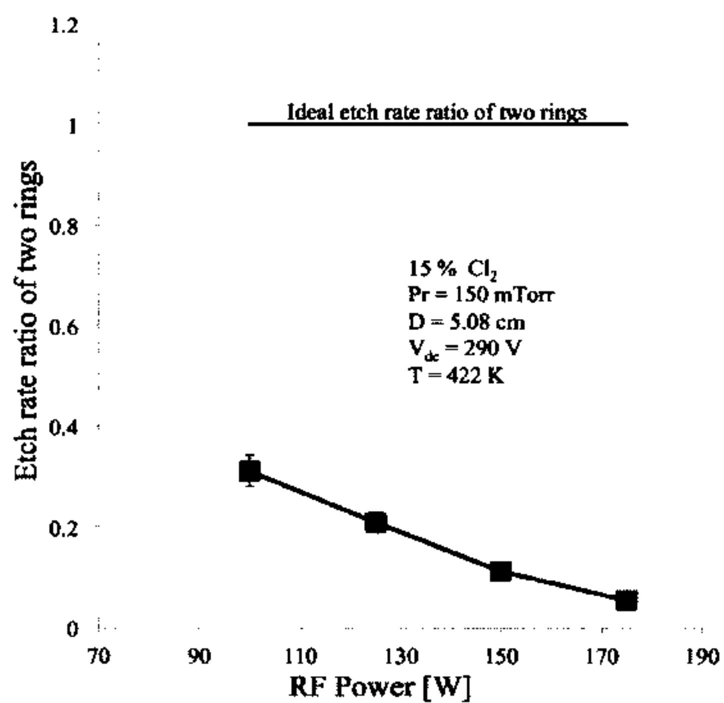

FIG. 25: Etch rate ratio of two rings versus rf power in the system. Solid line is a visual guideline.

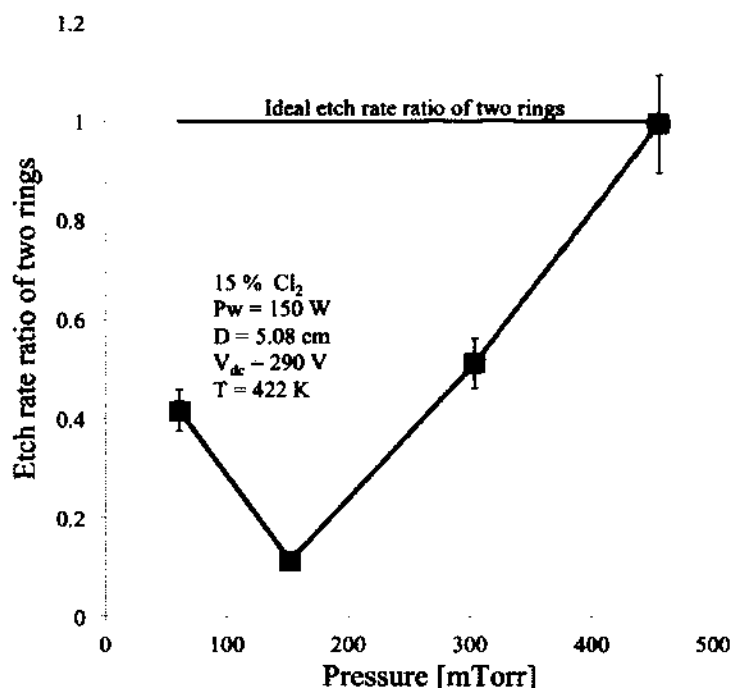

FIG. 26: Etch rate ratio of two rings versus pressure of the system. Solid line is a visual guideline.

constant as shown in Fig. 23 and Fig. 24 or decrease, as shown in Fig. 25. The measured etch rate uniformity data for the pressure variation are presented in Fig. 26.

Figure 26 shows that radical density increases with increasing pressure, which in this case is done by increasing the flow rate of the gas, the radical density increases. This leads to a better etch rate uniformity. Although the etch rate in the system decreases with increasing pressure [103], it does provide an etch rate uniformity very close to ideal. The data for the etch rate uniformity versus the percentage of chlorine in gas mixture is presented in Fig. 27.

The data in Fig. 27 show that the etch rate uniformity increases with the increase of chlorine content in the Ar/Cl_2 gas mixture. This suggests that the etch rate uniformity is constrained by the radical amount in the plasma. We conducted an experiment to increase the radical production by changing the diameter of the inner electrode. By decreasing the diameter of the inner electrode we increased the volume of the plasma. The data for the etch rate uniformity versus diameters of the

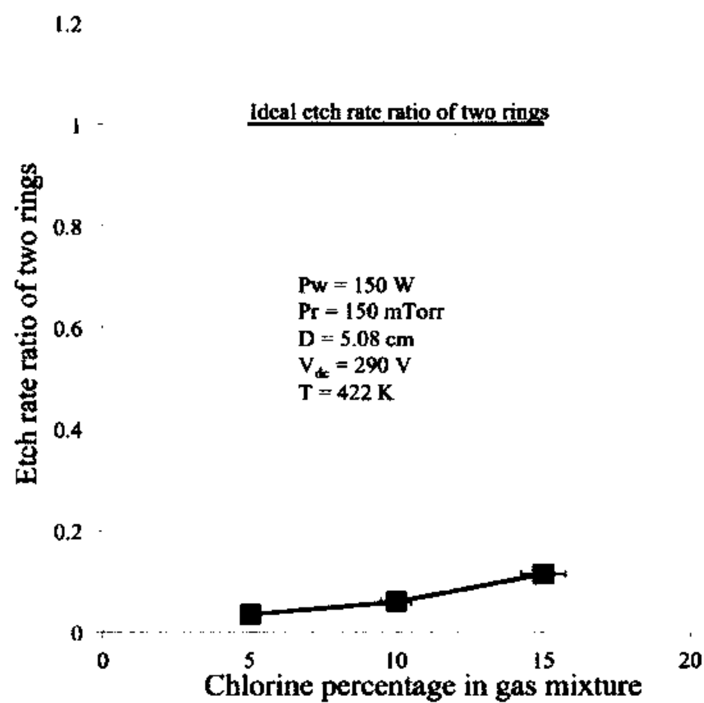

FIG. 27: Etch rate ratio of two rings versus Chlorine percentage in Ar/Cl_2 gas mixture. Solid line is a visual guideline.

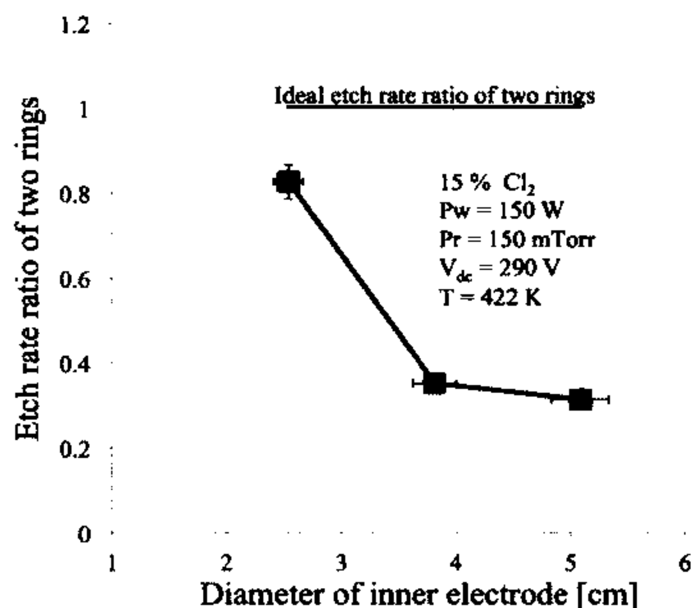

FIG. 28: Etch rate ratio of two rings versus diameter of the inner electrode in the system. Solid line is a visual guideline.

inner electrode is presented in Fig. 28.

Figure 28 shows that by decreasing the diameter of the inner electrode we can increase the volume of the plasma production region. This increases the chances of radicals to diffuse further downstream instead of reacting at the first ring only, which makes the etch rate uniformity better. However, the uncontrolled reduction of the diameter would lead to low etch rates [103]. Fig. 26, Fig. 27, and Fig. 28 show that the parameters which are responsible for the higher radical production (pressure, chlorine concentration, and volume production of the radical) also control the etch rate uniformity. The non-uniformity of the etch rate in a coaxial plasma reactor is severely constrained by the radical consumption by the material closest to the gas flow source. To verify this effect, we removed the first ring and measured the etch rate of the second ring. The results are shown in Table 3.

The table shows that the etch rate of the second Nb ring increases substantially when we remove the first Nb ring. This result confirms that the decrease in the second ring etch rate is due to the consumption of radicals by the first Nb ring. The experiment for the etch rate non-uniformity effect shows that the parameters involved in increasing the number of radicals at the surface tend to improve the etch

TABLE 3: Etch rate variation of the second ring with/ without the first Nb ring. Etching conditions are the same.

No. of Nb ring Present	First ring etch rate	Second ring etch rate
Two Nb ring present	31(nm/min)	11 (nm/min)
One Nb ring present		37 (nm/min)

rate uniformity. To uniformly etch a cylindrical structure the pressure, the gas flow rate, and chlorine concentration have to be high, while the diameters of the inner electrode, rf power, temperature, and dc bias have to be low or moderate.

6.3 VARIATION OF THE SELF BIAS POTENTIAL WITH PROCESS PARAMETERS AND OTHER ASYMMETRY MEASUREMENTS

The understanding of the asymmetry in sheath voltage distribution in coaxial plasma is important for the modification of the inner surfaces of three dimensional objects. A dc self-bias potential is established across the inner electrode sheath due to the surface area difference between the inner and outer electrodes of the coaxial plasma. The self-bias potential measurement was used as an indication of the plasma sheath voltage asymmetry. The plasma sheath voltages were tailored to process the outer wall by providing an additional dc current to the inner electrode with the help of an external dc power supply. The dc self-bias potential dependence on the process parameters such as gas pressure, rf power and percentage of chlorine in the Ar/Cl_2 gas mixture is studied experimentally. The dc current needed to reduce the self-bias potential to zero is measured for the same process parameters.

Here, a generic discharge geometry would be a coaxial system of two cylindrical electrodes shown schematically in Fig. 29, and a radio frequency discharge with two coaxial sheaths generated between them. We are developing a method to modify the inner surface of SRF cavities made of Niobium (Nb) by using a coaxial capacitively coupled rf plasma of an argon/chlorine (Ar/Cl_2) gas mixture. The removal of Nb can be achieved with the ion-assisted etching of the inner surface of the outer electrode. Although SRF cavities exhibit a variable diameter cylindrical structure, as a first step we have adopted a constant diameter cylinder configuration, where the cavity is represented by the outer cylinder and an auxiliary, powered electrode is the inner cylinder. The surface area asymmetry between the inner and outer electrodes due

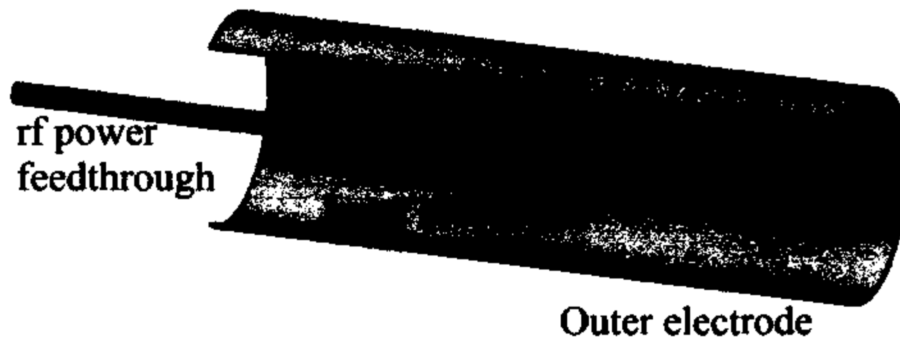

FIG. 29: Schematic layout of two coaxial cylindrical electrodes.

to the coaxial geometry creates a negative self-bias potential on the plasma sheath at the inner electrode. While the self-bias formation in planar geometry can be advantageous for semiconductor wafer processing (as it is placed on the electrode having the self-bias potential), it is detrimental in the case of processing the inner surface of cylindrical structures. The negative dc self-bias potential provides much higher energy of ions impinging the inner (powered) electrode as compared to the ion energy to the outer (grounded) electrode. Since the ion energy gained in the outer electrode sheath is very low, it is not feasible to etch the outer electrode without applying a positive dc bias to the inner electrode by an external dc power supply. This power supply drives an additional dc current through the inner electrode in order to bias it positively and change the plasma potential of the bulk plasma, thus increasing the voltage drop in the outer electrode sheath, which leads to an increase of ion energy impinging the outer wall.

Variation of plasma potential and, in turn, the change of ion energy by applying a dc voltage for a planar asymmetric rf plasma is reported in [41, 58, 59, 84]. Due to extensive use in the semiconductor industry, planar asymmetric plasma reactors are relatively well understood. The theoretical model for the sheath voltage ratio between two electrodes for these discharges and its dependence on the corresponding surface area is provided in [43, 44, 104] and the combined operation of dc and rf plasma is described in [47]. Early work on the geometrically asymmetric capacitively coupled rf discharges was focused on a planar powered electrode and a large area

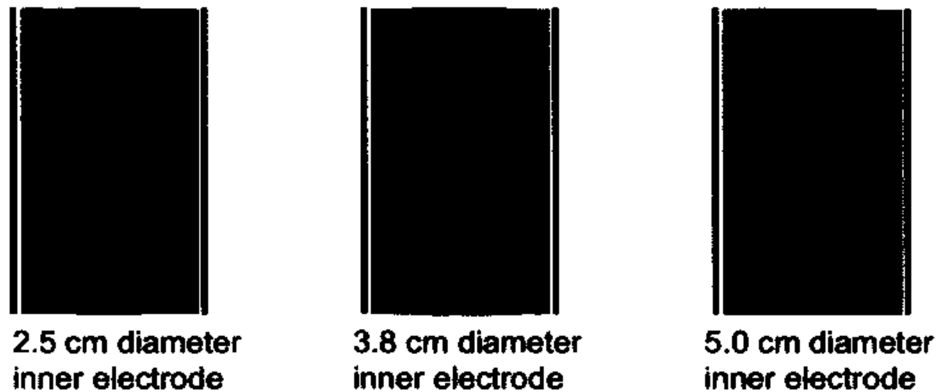

FIG. 30: Schematic layout of coaxial cylindrical dischrages with different diameter inner electrodes.

grounded enclosure that sometimes had the cylindrical form [41, 44, 84, 86], mimicking the reactor walls. In the models of planar parallel plate discharge, the enclosure was applied to fully confine the discharge. In the generic case of the cylindrical asymmetry, which is used in the present research (see Fig. 30), the two electrodes are coaxial cylinders. The inner (powered) cylinder has a smaller surface area and the outer cylinder is the grounded electrode. We are unaware of any other detailed description of the experimental configuration in the open literature that could be reduced to the generic coaxial cylinder geometry, in spite of its apparent simplicity. In the case of constant diameter cylinder surfaces, the discharge is also asymmetric, because the surface area of the two electrodes is substantially different. We have partially compensated this asymmetry by employing an inner electrode with variable diameters and also by introducing a dc voltage to alter the sheath voltage on the outer cylinder for ion-assisted etching of its wall. The additional dc current is needed to bring the negative self-bias potential at the inner electrode to zero or to a positive value. This dc current can also be considered as an indication of plasma electron density. The self-bias dependence on gas pressure and rf power for planar asymmetric plasma is also reported in [105]. however, its behavior for Ar/Cl_2 plasma in coaxial type asymmetry is not known. The quantitative measurement of the self-bias potential for different diameter electrodes and its variation with process parameters is important because it provides guideline information for any kind of surface modification to the inner surface of three dimensional structures.

We are applying the cylindrical rf discharge in a mixture of Ar and Cl_2, which

implies that the discharge is electronegative, with a number of consequences to its properties. The main subject of this section is to inspect the effects of the Ar/Cl_2 discharge properties on the asymmetry, compared to the pure Ar plasma. To evaluate the asymmetry in a coaxial type rf plasma reactor, we are using a 7.1 cm diameter and 15 cm long cylindrical tube as an outer electrode, which is part of the vacuum vessel. The inner electrode is of varied diameters (2.5, 3.8 and 5.0 cm) and fixed length of 15 cm. An rf (13.56 MHz) power supply is used to produce the plasma. It is connected to an automatic impedance matching network, which also measures the self-bias potential developed on the inner electrode sheath. The matching network has an additional option to connect a dc power supply in order to vary the dc bias on the inner electrode. The setup includes a dc power supply to provide the current required in each condition to reduce the dc self-bias to 0 V. The gases used were pure argon or chlorine diluted to 15% by adding argon.

An increase in the negative bias at the inner electrode leaves the plasma potential unchanged, but it can be changed significantly if a positive dc bias is applied [41, 58, 59, 84]. The dc coupling allowed a dc current to flow to the powered electrode and to expand the plasma structure to the whole chamber. In the case of low rf power without dc bias, the plasma is confined to the inner electrode and no etching is achieved. The plasma confinement is also observed in planar geometry [59]. In our experiments, the etch rate data for different diameters of the inner electrode indicate that the variation in plasma potential was smaller in the case of the smaller diameter electrode and the etch rate of Nb (inner wall of the outer electrode) was reduced. The negative self-bias potential developed across the inner electrode sheath for all three inner electrode diameters was measured at different gas pressures, variable rf power and two gas compositions. The required dc current to bring this potential to zero or positively biased at a certain value was also recorded.

The self-bias potential for pure Ar and the Ar/Cl_2 mixture, for constant diameter electrode, is meausred for different gas pressure and rf power. The dc current required to increase the self-bias potential to zero is plotted for the Ar and Ar/Cl_2 plasma for the same electrode diameter with different gas pressure and rf power. The uncertainty in our measurements of Cl_2 concentration was 2%, in rf power, 3 W; in pressure, 4 mTorr; in dc bias, 2 V; and in dc current, 5 mA. The cylindrical discharge was not confined and the plasma expanded longitudinally with power. However, the measurements of the self-bias proved useful since the results helped to determine

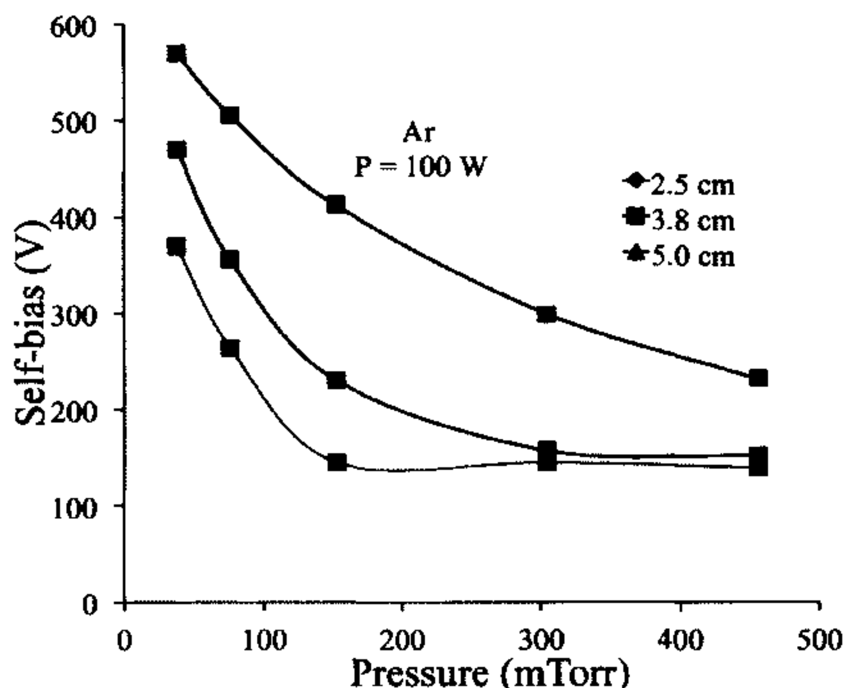

FIG. 31: Self-bias potential dependence in the Ar plasma on the pressure for different diameter inner electrodes. Solid lines are visual guideline.

conditions for high etch rates of Nb in the cylindrical configuration. In the following section we will discuss the self bias potential behavior in pure Ar, and in Ar/Cl_2 plasma separately.

6.3.1 SELF-BIAS POTENTIAL DEPENDENCE ON PRESSURE AND RF POWER FOR DIFFERENT ELECTRODE DIAMETERS IN AR PLASMA

The self-bias dependence on pressure was measured at rf powers of 25, 50, 100 and 200 W. The variation of self-bias potential with the pressure for Ar plasma using the three diameter electrodes is shown in Fig. 31 at a rf power of 100 W. The trends of the curves for the other measured rf powers are similar.

The self-bias displayed in Fig. 31 shows two distinct pressure regimes, one below 150 mTorr and the other above 150 mTorr. Though the self-bias potential is negative, it is plotted on the positive axis for convenience. The increase of the self-bias at low pressures can be explained by the expansion of the plasma volume to the grounded

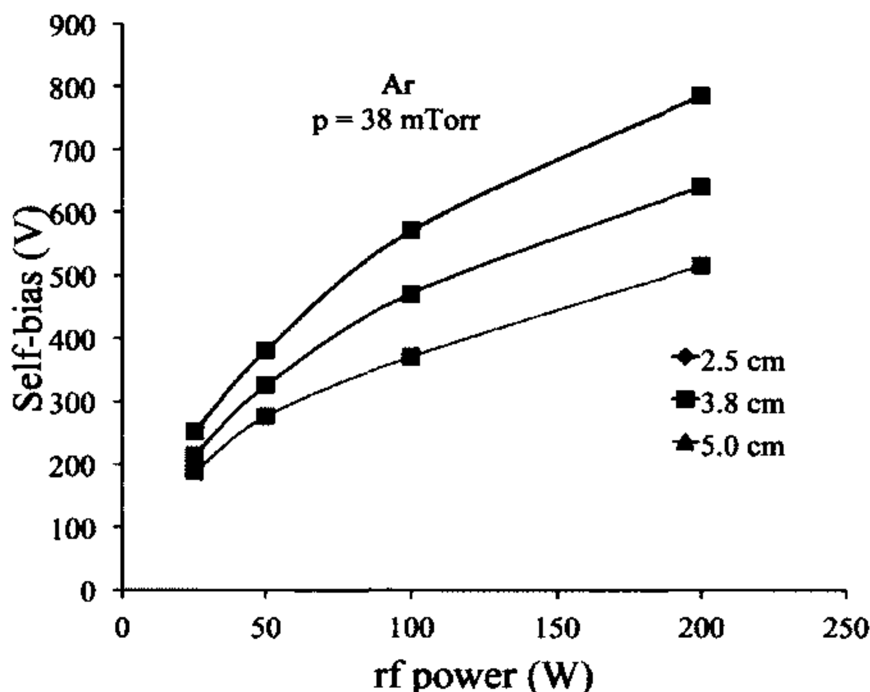

FIG. 32: Self-bias potential dependence in the Ar plasma on the rf power for different diameters inner electrodes. Solid lines are visual guideline.

area as also seen in the planar configuration [105]. The rf power dependence of self-bias for different diameter electrodes is shown in Fig. 32.

The increase in the self-bias with the absorbed rf power is not only due to the expansion of the plasma, but also due to the rf voltage increase. The fit to these curves shows almost square root dependence on the rf power indicating that all the rf voltage is dropping on the inner electrode sheath as a negative dc bias, which was also observed in the planar geometry [34].

6.3.2 THE SELF- BIAS POTENTIAL DEPENDENCE ON THE GAS COMPOSITION

The self-bias voltage is different for pure Ar discharge and for the Ar/Cl_2 discharge. Fig. 33 shows the variation of self-bias voltage with rf power for the inner electrode diameters of 2.5 and 3.8 cm. The addition of chlorine in argon changes the plasma parameters [33, 34, 55, 106]. The self-bias voltage for the Ar/Cl_2 gas mixture is smaller than for pure Ar at lower rf power but larger at higher rf power.

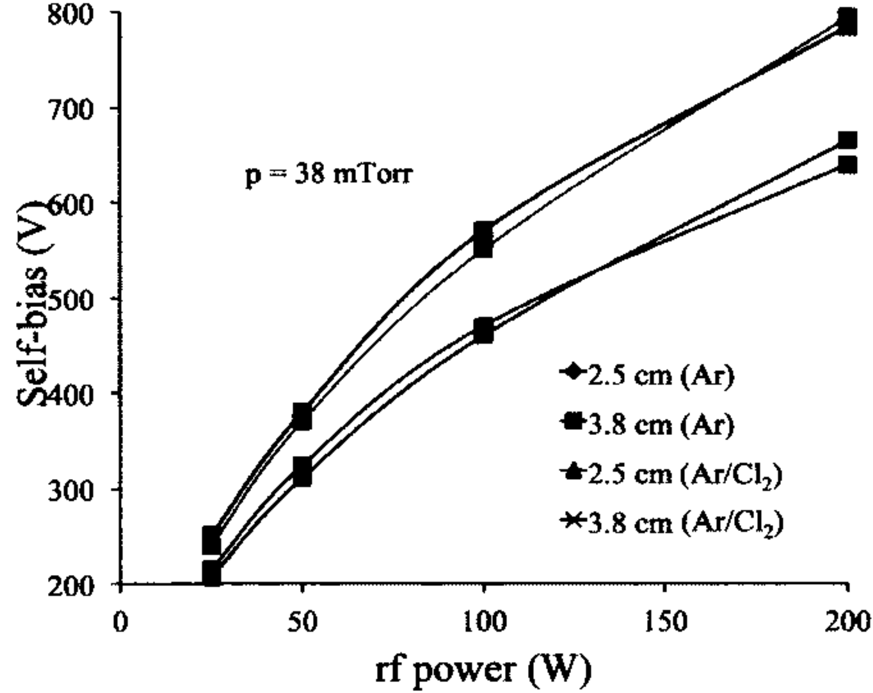

FIG. 33: Self-bias potentail dependence on the rf power for different diameter inner electrodes in Ar and Ar/Cl_2 plasma. Solid lines are visual guideline.

Though the uncertainty in self-bias measurements is 2 V, the differences between the Ar and Ar/Cl_2 plasma self-bias potential at higher power densities are in the order of 20-30 V, which is much above the measurement error. This behavior can be partially explained with the relative electron density decrease at lower power in the Ar/Cl_2 plasma, compared to the positive ion density due to large plasma electronegativity. The electron density is almost equal to the positive ion density at higher rf power density as reported in [87]. This property of chlorine plasma is reflected in the self-bias voltage variation at higher rf power.

In the case of the inner electrode diameter of 5.0 cm, the plasma volume is smaller and equal density of electrons and positive ions is reached earlier similar to the result reported in [87]. However, the electron temperature is higher in the Ar/Cl_2 plasma compared to the Ar plasma, consequently the self-bias potential in the Ar/Cl_2 plasma is higher than the pure Ar plasma, which is shown in Fig. 34.

The variation of the self-bias with pressure, at a fixed rf power for the pure Ar and Ar/Cl_2 plasma for inner electrode diameter of 5.0 cm is shown in Fig. 35.

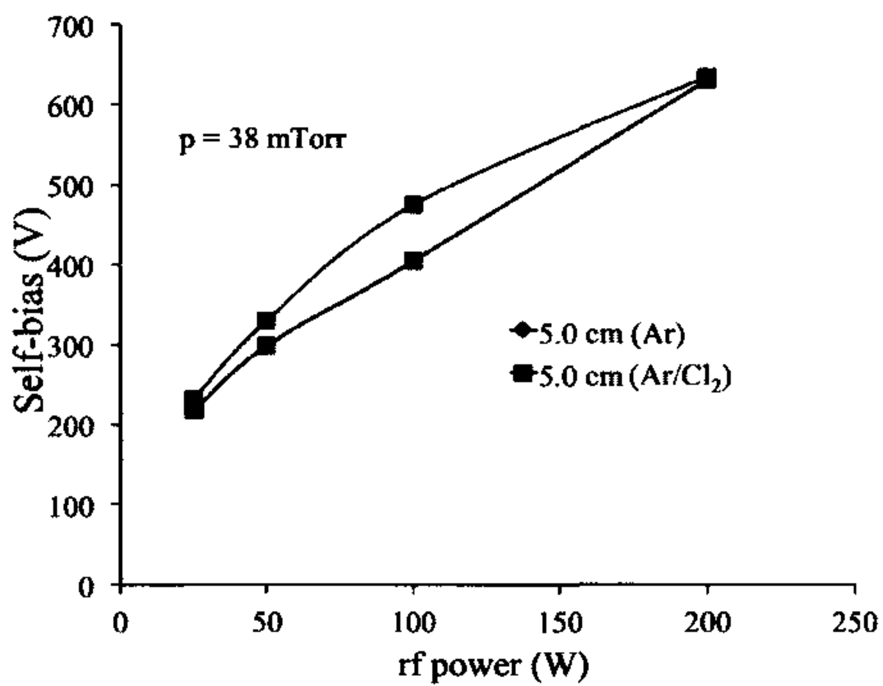

FIG. 34: Self-bias potential dependence on the rf power for electrode diameter of 5.0 cm for pure Ar and Ar/Cl_2 mixture. Solid lines are visual guideline.

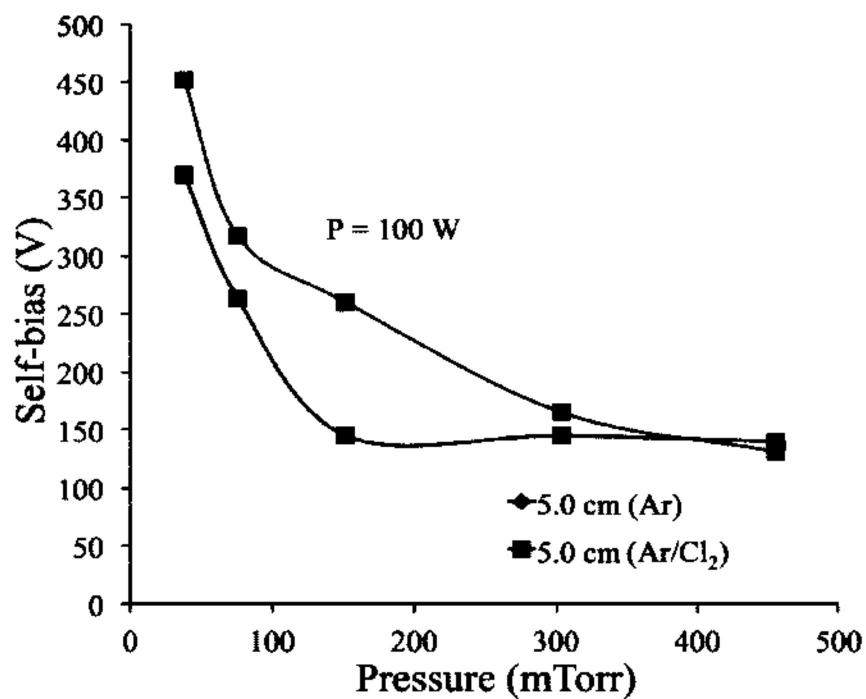

FIG. 35: Self-bias dependence on the gas pressure for electrode diameter of 5.0 cm for pure Ar and Ar/Cl_2 mixture. Solid line is a visual guideline.

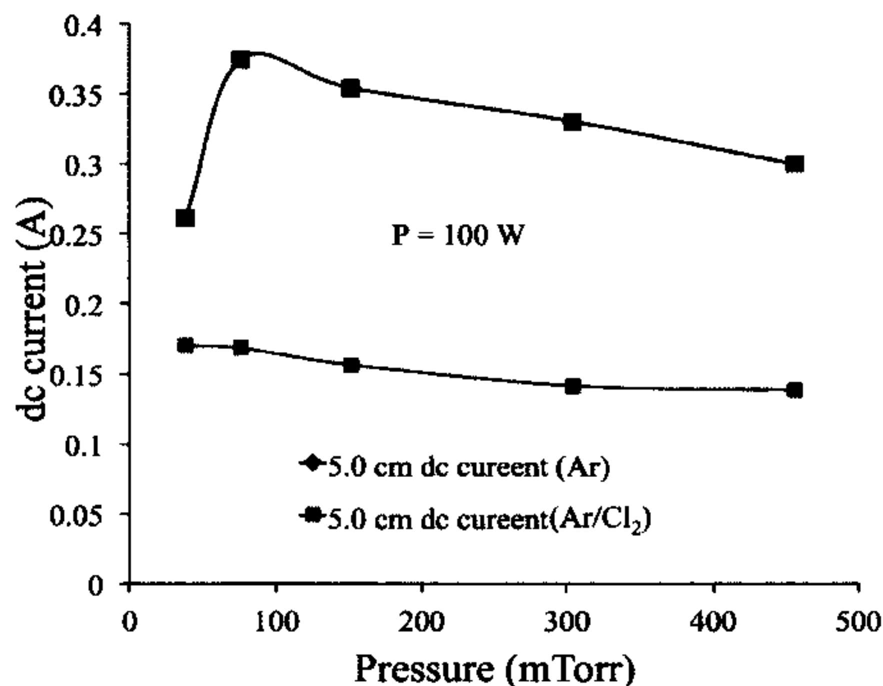

FIG. 36: The dc current variation with pressure for 5.0 cm diameter electrode for Ar and Ar/Cl_2 plasma. Solid line is a visual guideline.

Figure 35 shows that, due to lower electron density and higher electron temperature in the Ar/Cl_2 plasma, the self-bias voltage is higher compared to the pure Ar plasma. This higher self-bias voltage shows that the addition of electronegative gases such as Cl_2 increases the asymmetry in rf plasma reactors.

6.3.3 THE DC CURRENT DEPENDENCE ON THE GAS COMPOSITION.

Additional dc current has to be provided with the help of an external power supply to bring the dc bias to zero or a positive value in order to increase the plasma potential for all three inner electrodes. The current, needed to increase the negative dc self-bias to 0 V, can be treated as an indicator of electron density in the plasma. The dc current required to increase the self-bias voltage to zero for the pure Ar and Ar/Cl_2 plasmas is plotted in Fig. 36.

Figure 36 shows that much less current has to be provided in the case of the

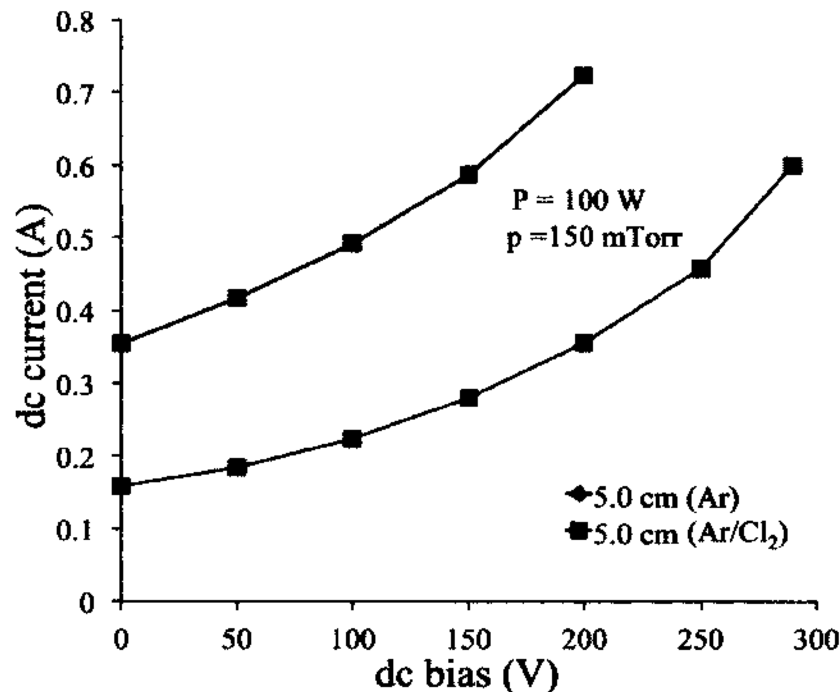

FIG. 37: The dc current variation on the dc bias voltage at fixed pressure and fixed rf power for Ar and Ar/Cl_2 plasma. Solid line is a visual guideline.

Ar/Cl_2 plasma, as the electron density is approximately an order of magnitude lower in Cl_2 plasmas compared to the Ar plasma, which was reported earlier in [34]. A similar trend is recorded for the other two diameter electrodes for all the pressure and power conditions. The addition of Cl_2 decreases the electron density in the plasma. The increase in dc bias voltage increases the current provided by the dc power supply. The dc current variation with dc bias voltage is shown in Fig. 37.

The increase in dc current with bias voltage indicates that positive dc biasing not only increases the plasma potential but also the plasma density, as also shown in the case of planar geometry [105]. The self-bias data show a difference between the Ar and Ar/Cl_2 plasma for about 20 V (See Fig. 34). An explanation for this difference is based on the fact that the number density of electrons is highly reduced in the electronegative Ar/Cl_2 discharge. The study of self-bias voltage in coaxial cylindrical electrode geometry is important, because cylindrical geometry has been rarely studied in its generic form, in spite of its simplicity and adaptability to practical use, such as surface processing of concave structures. This study also presents the variation in

dc current required for bringing the self-bias potential to zero or positive for the Ar and Ar/Cl_2 plasma and the role of plasma density in this variation. These results also lead to the observation that positive dc bias at the inner electrode increases the plasma density together with the sheath potential at the outer electrode, which is beneficial in etching the inner surface of the outer cylindrical wall of a cavity.

6.4 OPTIMIZATION OF THE ELECTRODE SHAPE TO REVERSE THE ASYMMETRY IN PLASMA

When the surface areas of two electrodes in an rf discharge are not equal, it creates an asymmetry in plasma sheath voltages, measured as a negative dc voltage on a smaller surface area electrode. The dependence of the sheath voltages on the surface area of the electrodes is explained theoretically for planar geometry in [43, 44, 104] and a model for a coaxial plasma is described in [44]. The change in plasma potential, and in turn the change in ion energy by applying dc voltage to an electrode in rf plasma for planar geometry, is reported [41, 58, 59, 84]. In order to modify the inner surface of the grounded outer wall, the inherent asymmetry of the coaxial capacitively-coupled plasma (CCP) is compensated for and tailored in part by an external dc power supply, which has to provide an external dc current to the inner electrode in order to change its dc bias. The SRF cavities present a unique challenge as they represent a cylindrical structure with variable diameter. The beam tubes in SRF cavities have a much smaller diameter compared to the maximum cavity diameter, particularly in the lower frequency elliptical SRF cavities. This poses a bottle-neck problem, where the maximum inner electrode diameter is restricted by the beam tube diameter. To overcome this problem, it is possible to increase the inner electrode surface area without increasing its diameter. Four differently structured inner electrodes were constructed and their effect on the self-bias potential was measured. Therefore, favorable processing conditions for the grounded concave electrode can be achieved by a combination of geometric and electrical corrections of the asymmetry. The self-bias dependence on the pressure and power for rf plasma is shown in [105] for planar geometry. Its behavior for coaxial geometry, particularly in the Ar/Cl_2 plasma was described in section 6.3. Here we are presenting the effect of the inner electrode surface area enhancement on the self-bias potential. The corrugated structures built on the inner electrode transform the asymmetry of the plasma by changing polarity from negative to positive self-bias potential. Its effect

on the etching of the ring type samples placed on the outer electrode was remarkably beneficial. Although the effect of the size and bias of the electrode [107] and the structure of the electrode on plasma behavior [108] are studied for planar geometry processes, to the best of our knowledge, changing the polarity of the asymmetry by geometrical modification of an electrode in coaxial configuration is shown for the first time in the present work.

To understand the effect of the structure formation on the inner electrode to the asymmetry in a plasma, a coaxial type rf (13.56 MHz) plasma reactor was used with a 7.1 cm diameter and 15 cm long cylindrical vessel as the outer electrode and with a variable structured inner electrode as shown Fig. 38. The inner electrode is the powered electrode and the outer electrode is grounded. The matching network attached to the rf power supply not only measures the self-bias potential, but has an option to attach an external dc power supply to provide a dc bias. The gases used are pure argon (Ar) and 15% chlorine (Cl_2) diluted in Ar. The details about the experimental results with flat cylindrical electrodes were shown in section 6.3.

Variously structured inner electrodes are illustrated in Fig. 39, where (a) is a 5.0 cm diameter strait tube, (b) is a standard large pitch bellows with 3.8 cm inner diameter and 4.8 cm outer diameter, and (c) is the discloaded corrugated structured (DLCS) electrode with a 2.5 cm inner diameter tube welded with multiple disc rings with a 5.0 cm outer diameter and 2.5 cm inner diameter. The distance between two disc rings was 3.0 mm and their thickness was 1.00 mm. Standard small pitch bellows, not shown in the Fig. 39, but indicated in Fig. 38 were also used in the experiment (with an outer diameter of 4.8 cm) were also used in the experiment. The similar diameter of all four electrodes kept the plasma volume approximately constant and the surface area change of the inner electrode was the only parameter affecting the self-bias potential. Negative self-bias potential developed across the sheaths of all these four differently shaped inner electrodes sheaths was measured at variable gas pressure, rf power and at two gas compositions. The incident ion energy on the grounded wall depends on the plasma potential. The more asymmetric the plasma is, the harder it is to modify and increase its potential to be favorable to etch the outer electrode. In the case of coaxial rf plasma, the etch rate is observed to decrease with the inner electrode diameter [103]. In the development of the plasma etching technology for the inner surfaces of concave 3D structures, generation of a less asymmetric plasma would be beneficial, particularly for a lower frequency SRF

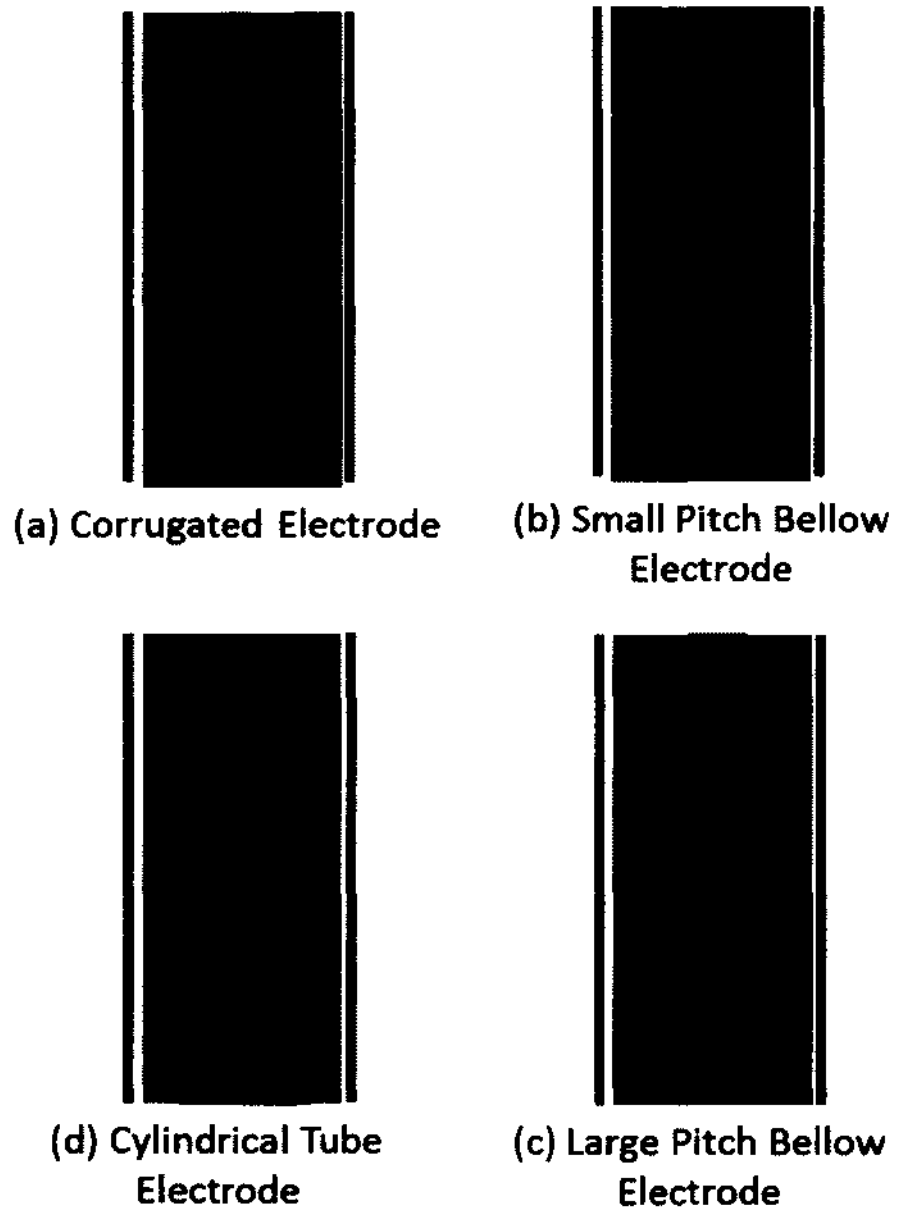

FIG. 38: Illustration of various structured inner electrodes in coaxial plasma: (a) disc loaded corrugated structure (DLCS), (b) small pitch bellows, (c) large pitch bellows, and (d) straight cylindrical tube.

cavity, which has a very large diameter ellipsoid profile compared to the beam tube diameter. The ion-assisted etch rate of Nb (placed on the outer wall) for same positive dc bias is measured for various inner electrode shapes.

The self-bias potential of all four structures was measured at constant external discharge parameters, and the results are given below. The uncertainty of Cl_2 concentration was 2%, in rf power, 3 W; in pressure, 4 mTorr; in dc bias, 2 V; and in dc current, 5 mA. In all diagrams, except in Fig. 45, the absolute value of the self-bias potential was used, although it was actually negative at the inner, powered electrode. The dc current required to make this potential zero or a positive value was recorded. The etch rate for the Nb samples placed on the outer wall for the different electrodes was also measured. The etch rate experiment was carried out for more than 90 minutes to avoid the fluctuation in etch rate measurements due to the lag time in starting the etching process [70]. The self-bias potential is plotted as a function of the gas pressure and rf power in pure Ar discharge for different structure electrodes and it is shown as a function of gas pressure and rf power for the Ar/Cl_2 plasma. The self-bias potential variation with rf power is shown at higher pressure when the external dc power supply is attached. The etch rate of Nb for various structures of the inner electrode shows the highest etch rate for a corrugated structure electrode.

6.4.1 SELF-BIAS POTENTIAL DEPENDENCE ON THE PRESSURE AND RF POWER IN AR PLASMA FOR VARIOUS STRUCTURED INNER ELECTRODES

The self-bias potential dependence on the pressure was measured at a constant rf power of 100 W. The variation of the self-bias potential with pressure for an Ar plasma using the four differently structured electrodes is shown in Fig. 40.

Figure 40 shows that the geometrical enhancement of the inner electrode surface area reduces the negative self-bias potential compared to the straight tube electrode. It also shows that the corrugated structures are the most effective for the asymmetry reduction. Two pressure regimes were described also earlier in work [105]. These clearly displayed regimes are indicated in the present work. At low pressure regime (below 150 mTorr) all results show similar behavior. However, at high pressure regime the tube electrode self-bias potential is constant but the corrugated structure and small pitched bellows show a decrease. The decrease in the self-bias potential at higher pressure could be explained by the change of the sheath thickness. As the

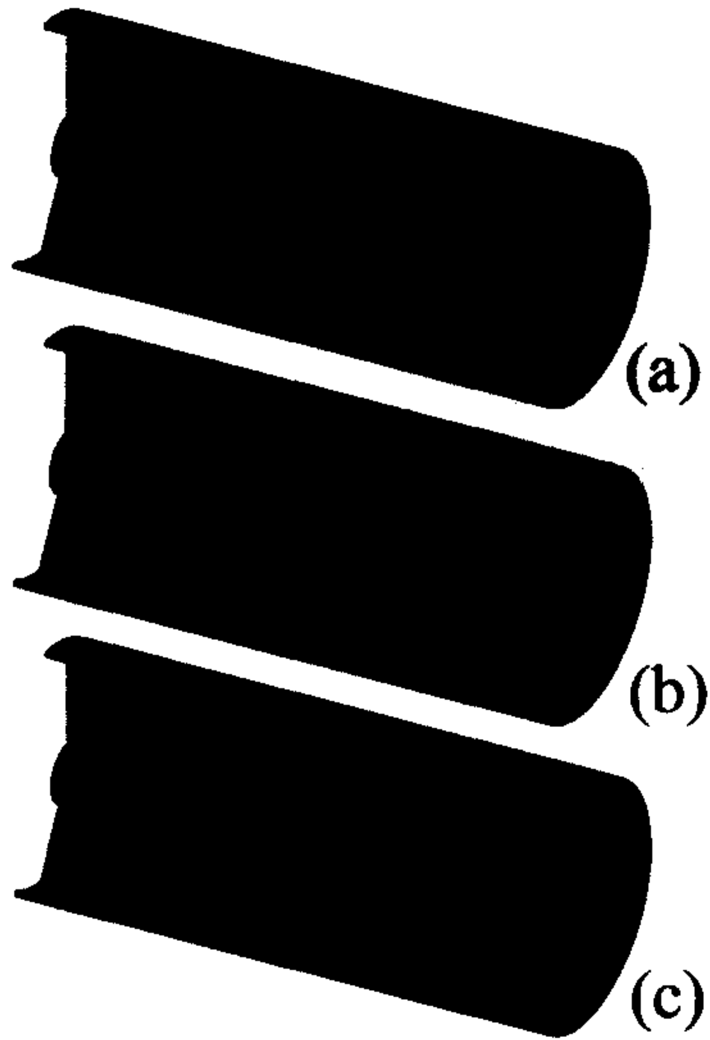

FIG. 39: Illustration of various structured inner electrodes in coaxial plasma: (a) strait tube, (b) large pitch bellows, and (c) disc-loaded corrugated structure (DLCS).

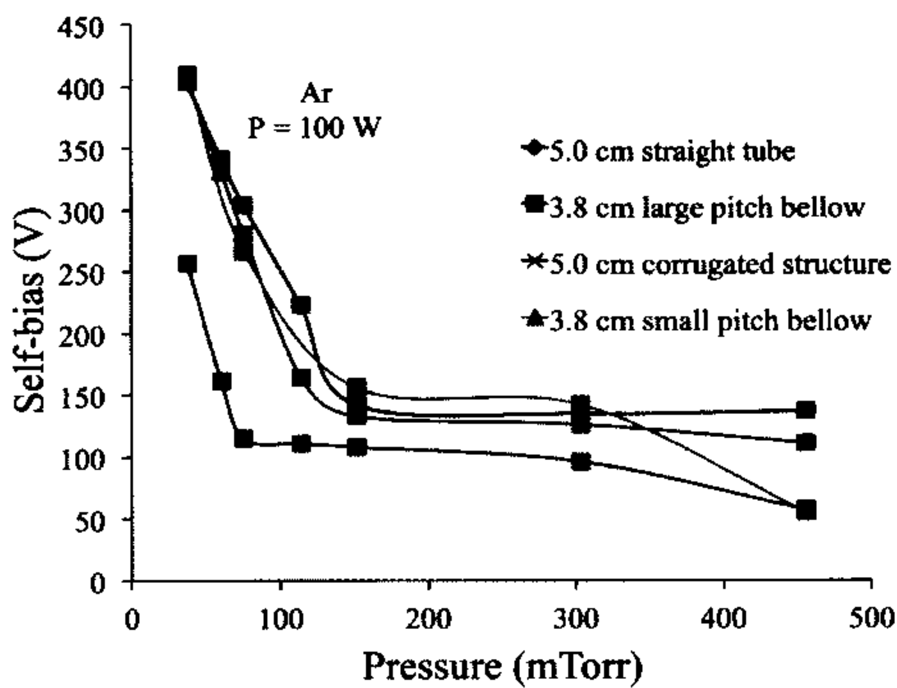

FIG. 40: Self-bias potential dependence on the pressure for various structured electrodes in the Ar plasma. Solid lines are visual guidelines.

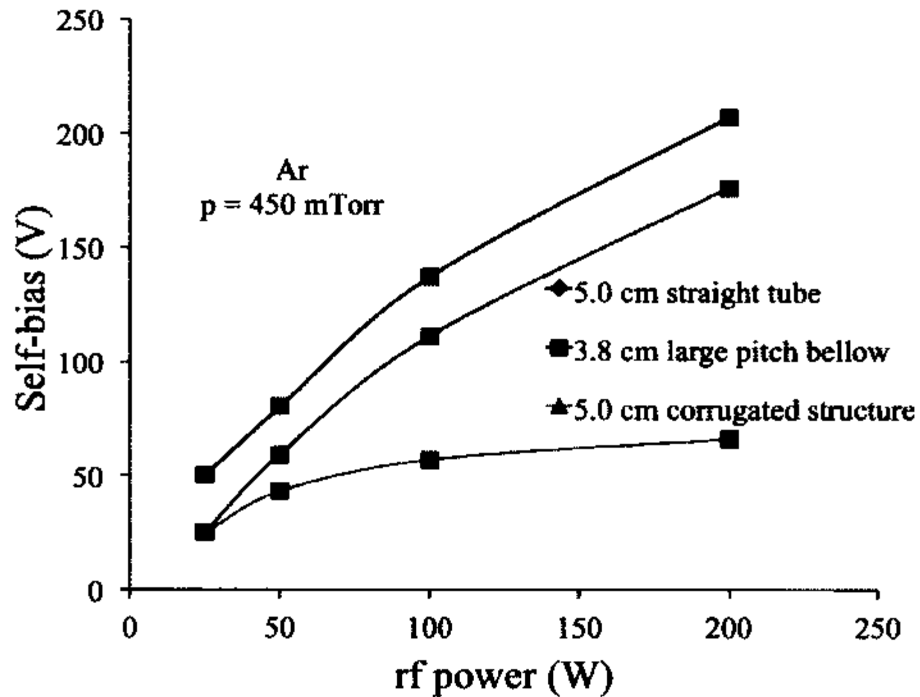

FIG. 41: Self-bias potential dependence in the Ar plasma on the rf power for various structured electrodes in the Ar plasma. Solid lines are visual guidelines.

sheath thickness decreases with pressure, it follows more closely the shape of the structure and the effective surface area of the inner electrode becomes larger. To explore this observation further, the rf power is varied at higher pressure for the Ar plasma and the variation of the self-bias potential with the rf power for three different structures are shown in Fig. 41.

Figure 41 shows that the rf power does not affect considerably the self-bias potential for the corrugated structure, but has a substantial effect when the straight tube and the large pitch bellows shaped electrode was used. Using the corrugated structure, not only we are increasing the effective surface area to reduce the self-bias potential, but the plasma density is increased also, as described in [108], for planar geometry.

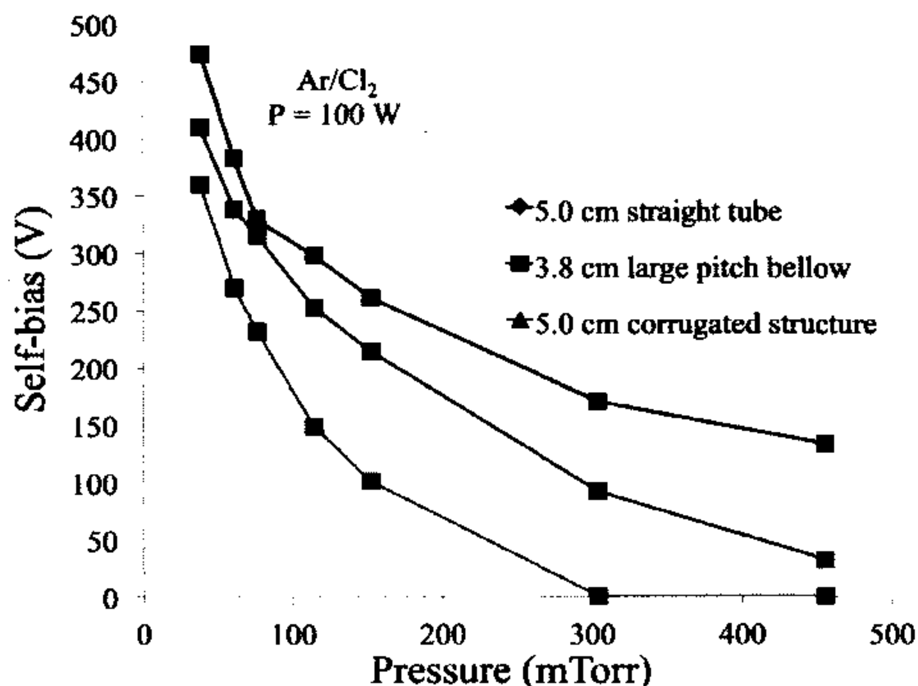

FIG. 42: Self-bias potential dependence on pressure in the Ar/Cl_2 plasma for various structured electrodes. Solid lines are visual guidelines.

6.4.2 SELF- BIAS POTENTIAL DEPENDENCE ON THE PRESSURE AND RF POWER IN AR/CL_2 PLASMA FOR VARIOUS STRUCTURED INNER ELECTRODES

The addition of Cl_2 alters the electron density and the electron temperature compared to a pure Ar plasma [33, 34, 87]. The change in plasma parameters, particularly at a higher pressure and rf power, leads to a decrease in the self-bias potential in the coaxial geometry [109]. Fig. 42 shows the pressure dependence of the self-bias potential for rf power of 100 W in Ar/Cl_2 plasma for three differently structured electrodes.

Figure 42 shows that the self-bias potential for the corrugated structured electrodes decreased to zero at higher pressure. It increased to a positive voltage as will be shown later. The matching network attached to the rf power supply could not read the positive bias voltage, and it reads zero as the lowest voltage even when it is positive as confirmed by voltage data measured at the dc bias supply. The increase

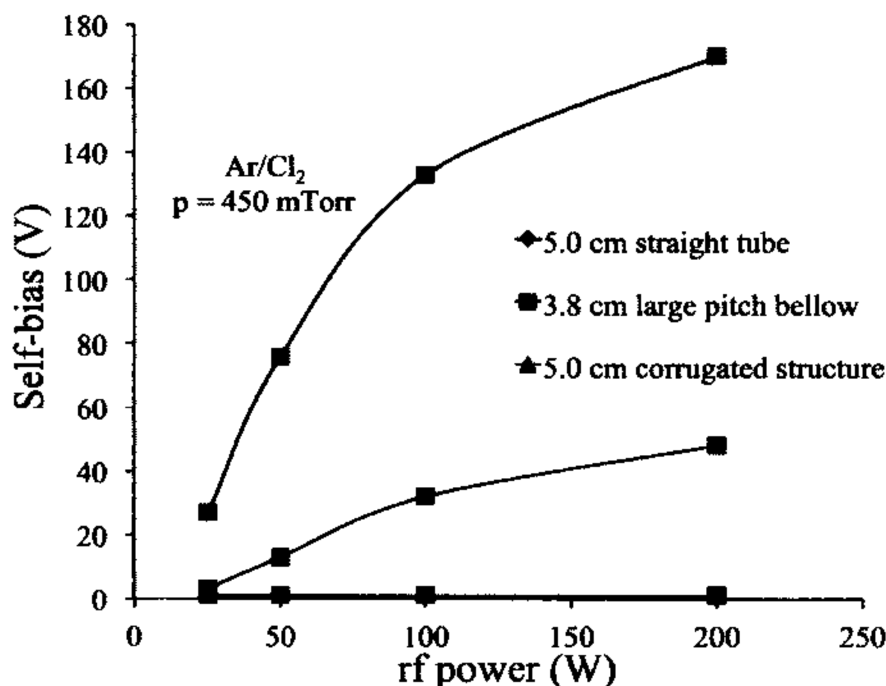

FIG. 43: Self-bias potential dependence in the Ar/Cl_2 plasma on the rf power for various structured electrodes. Solid lines are visual guidelines.

in the rf power does not change the self-bias potential measurement in the matching network as shown in Fig. 43, where the self-bias potential variation with rf power at 450 mTorr pressure in Ar/Cl_2 plasma is given.

Figure 43 shows that there is no self-bias potential developed across a corrugated structure for a high pressure Ar/Cl_2 plasma. It is to be noted that the increasing power does not change the situation, instead the self-bias potential turns positive and increases in the positive direction as shown in Fig. 45.

6.4.3 VARIATION OF DC CURRENT AND BIAS POTENTIAL FOR VARIOUS STRUCTURED INNER ELECTRODES

Self-bias potential can be brought to zero or a positive value by providing additional dc current to the inner electrodes. The dc current required to bring the self-bias potential to zero is plotted in Fig. 44 as a function of rf power at a constant pressure of 450 mTorr.

Figure 44 shows that there is no current needed for Ar/Cl_2 plasma at higher

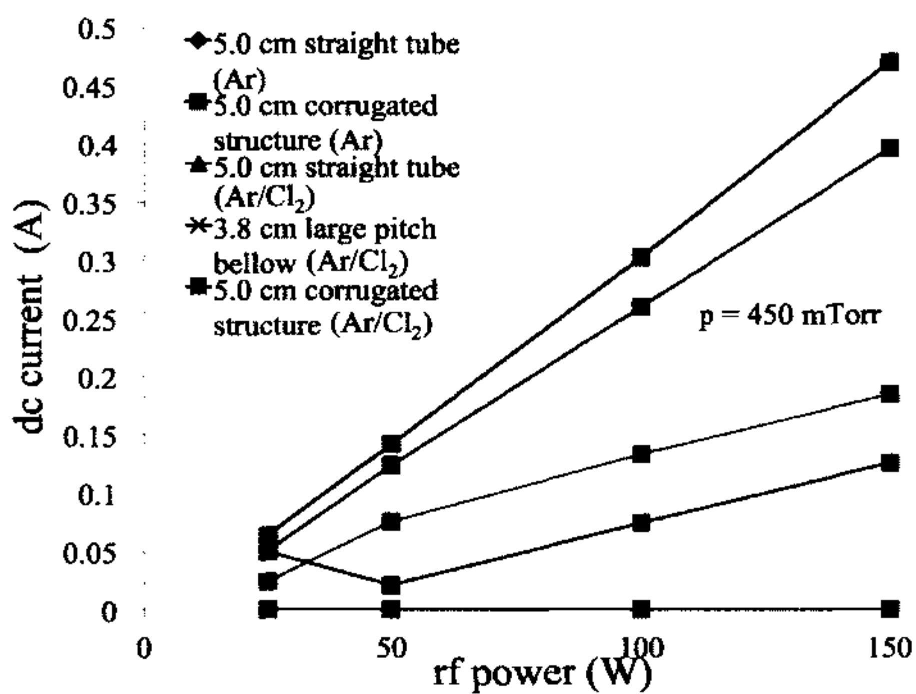

FIG. 44: The dc current variation with rf power for various structured electrodes and two different gas compositions. Solid lines are visual guidelines.

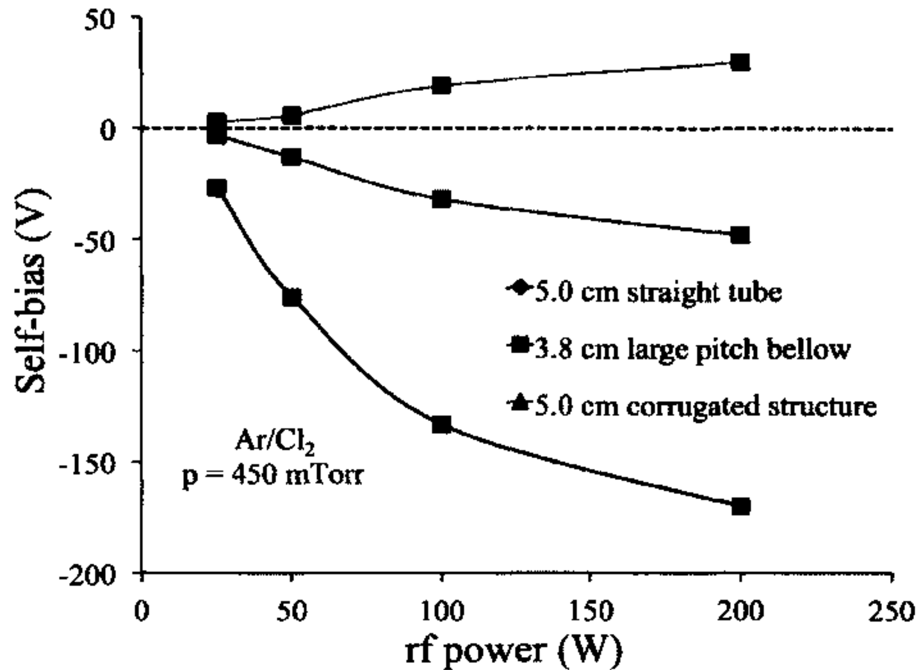

FIG. 45: Self-bias potential dependence on the rf power in the Ar/Cl_2 plasma for various structured electrodes. Solid lines are visual guidelines.

pressure for the corrugated structure, although for the other structure, the current needed to make self-bias zero for Ar plasma is high compared to the Ar/Cl_2 plasma due to its lower electron density. The increase in rf power does not change this situation although the increase in rf power shows a dc voltage increase on the dc power supply. The tube electrode and large pitch bellows electrode show an increase in the dc current requirement with the increase in rf power, and show no change in the dc voltage reading, which is zero. This positive dc voltage in the case of a corrugated structure electrode, can be described as a positive dc self-bias voltage. Considering this, we plotted the dc bias voltage for the structured electrodes in Fig. 45, where the dc self-bias voltage is plotted negative so that the reversal of the self-bias potential can be shown in the plot.

Figure 45 shows that in the Ar/Cl_2 plasma at higher pressure, the use of a corrugated structure electrode leads to the reversal of the asymmetry in the plasma. Instead of the negative dc self-bias potential, it acquires the positive dc self-bias potential, which increases with rf power.

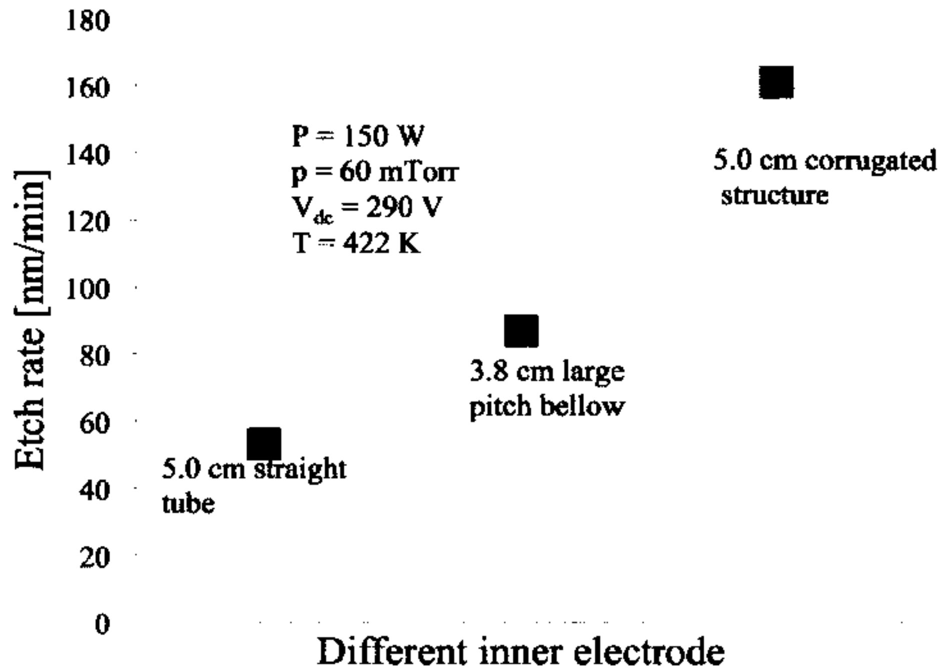

FIG. 46: The etch rate variation with differently structured electrodes for the same plasma conditions.

6.4.4 ETCH RATE DEPENDENCE ON THE STRUCTURE OF THE INNER ELECTRODE

Maintaining similar plasma conditions, the etch rate of Nb placed on the outer wall was measured while only the electrode shape was varied. The graph of the etch rate versus the different structure electrodes is shown in Fig. 46. The Nb etch rate increased fourfold, compared to the straight tube, when the corrugated structure was applied.

Consequently, during optimization of the electrode shape, we explored the effect of geometrical enhancement of the surface area of the inner electrode and investigated the possibility to reduce the asymmetry in a coaxial CCP reactor. The geometrical modification of the inner electrode surface area to change the asymmetry of the coaxial cylindrical discharge is a novel concept. It is a cylindrical analogue to planar asymmetry corrections, which were studied in detail in [108]. The effect of differently shaped inner electrodes on the self-bias potential at various pressures and rf power

is measured, and the corrugated structure is found to be optimal for reducing and reversing the asymmetry. The addition of Cl_2 makes the asymmetry significantly smaller at higher pressure and rf power. It is shown that for the DLCS inner electrode, there is no need to provide additional current to zero the self-bias potential. At higher pressure, in the Ar/Cl_2 plasma, the dc self-bias potential, which is negative with a powered inner electrode, reacts to the reversal of the asymmetry in the plasma by becoming positive. The etch rate was measured for the same positive dc bias at lower pressure for various structured inner electrodes. The etch rate is higher for the DLCS electrode due to the reduction in plasma asymmetry. The computational modeling of these structures in electronegative discharges is in progress. Based on these models we can design the optimum pitch and depth of the corrugated structure for given pressure and power condition.

CHAPTER 7

EXPERIMENTAL SET UP FOR SINGLE CELL SRF CAVITY

Elliptical SRF cavity represents a structure with varying diameter, where the beam tube diameter is much smaller compared to the elliptical section. Before plasma etching of a single cell SRF cavity, we designed a single cell pill-box cavity made of stainless steel with similar axial dimensions as the single-cell Nb srf cavity of 1497 MHz, with multiple mini conflat (CF) flanges welded to it for diagnostic purposes. The pill-box cavity was filled with ring and disk Nb samples on the inner surface. The purpose was to study the etch rate behavior of Nb on all the available surfaces before etching an actual single cell SRF cavity. The smaller beam tube diameter compared to the cell diameter imposes some restrictions on the diameter of the inner electrode. In order to create less asymmetric plasma without increasing the diameter of the inner electrode, the shape of the inner electrode was changed and its effect of the self-bias potential was measured and the results are given in Section 6. Based on the self-bias potential and etch rate measurement [109, 110], an electrode with a corrugated structure was chosen. The length of the inner electrode was made shorter due to variation of asymmetry in the pill-box cavity. Our approach was to set up the experiment so that the etching effect could be studied for every specific section of the inner surface of the elliptical cavity as a function of each processing parameter. An excessive non-uniformity in the Nb etch rate is observed along the gas flow direction due to depletion of the active radicals [111]. The uniform surface processing across a constant or a varying diameter structure is a complex task even without the depletion of radicals, as observed in [112, 113].Therefore, a linear, synchronous translation of the inner electrode and the gas flow inlet was opted to overcome the etch rate non-uniformity. The processing was accomplished by moving axially the inner electrode and the gas flow inlet in a step-wise way to establish sequential segmented plasma columns with almost identical conditions. The test structure was a pill-box cavity made of steel of similar dimension as the standard elliptical SRF cavity. This was adopted to experimentally verify the effect of plasma surface reaction on cylindrical

structures with variable diameter using the segmented plasma generation approach. The pill-box cavity is filled with niobium ring- and disk type samples and the etch rate of these samples was measured.

7.1 SINGLE CELL PILL-BOX CAVITY EXPERIMENT

The schematic diagram of the experiment is shown in Fig. 47. This setup has potentially universal applications to any concave 3D geometry, but we are focussed on describing the method of cavity wall reactive ion etching to remove the bulk Nb, transient metal impurities and oxides from the bulk Nb in the surface layer and to improve its superconductive properties. The pill-box cavity is representative of the 3D geometrical structure, and it is used to establish plasma etching parameters before the elliptical cell is processed. Work with the pill-box cavity proved useful in defining the process parameters for the reactive ion etching, but the same setup can be applied to any metal surface preparation including thin film deposition and plasma cleaning. Multiple ring samples inside the pill-box cavities were used to determine regions of radical reactions with the surface and to enable their spread over the whole cavity wall. Further, the experiments with various sizes of the inner electrode helped to establish conditions for uniform electrode surface area ratio and to determine the sectional step-wise processing procedure. The coaxial rf power feedthrough, filled with atmospheric pressure gas to avoid unnecessary plasma formation, was moved axially together with the inner electrode by a specially designed manipulator.

The apparatus, shown in Fig. 47, consists of the rf power supply, which is equipped with a matching network and connected in series with a dc power supply that provides positive dc bias on the inner electrode. The rf power is coupled to the inner (driven) electrode with a coaxial vacuum feedthrough. The feedthrough and the inner electrode are attached to a controllable axially moving manipulator. The cavity, acting as a vacuum vessel, is connected through the antechamber to the pumping system, which consists of a turbo molecular vacuum pump and a roughing pump with vacuum valves and diagnostic gauges. The exhaust gases are collected and processed in a homemade scrubber that is filled with sodium hydroxide solution in water. Gas is fed to the system through a mixing manifold and a specially designed gas inlet, which disperses the gas mixture. The gas inlet is connected to a second controllable axially moving manipulator, which is synchronized with the first manipulator. Diagnostic tools are connected through five ports to the pill-box cavity, thus localized observation

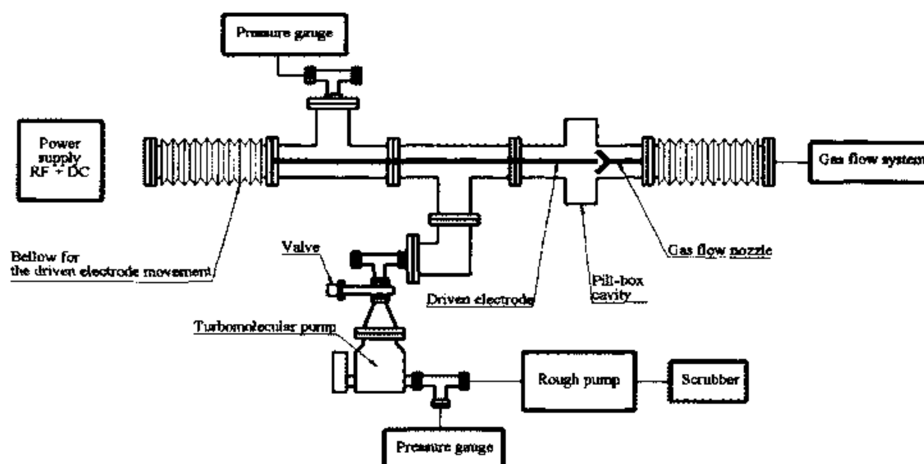

FIG. 47: Schematic diagram of the single cell pill-box cavity experiment.

of the process was enabled. However, in the case of the SRF elliptical cavity, the only observation direction available is through a quartz window at the end of the vacuum assembly so any diagnostics is limited. The cavity wall is electrically grounded and serves as the outer electrode of the cylindrical rf discharge. The surface temperature is controlled during the etching process by an external heating tape.

7.1.1 SINGLE CELL PILL-BOX CAVITY

To understand the plasma surface modification on a variable-diameter cylindrical structure, we used a single cell pill-box cavity, shown in Fig. 48. The formerly used accelerator pill-box cavity consisted of an array of cylindrical structures separated by conductive or superconductive walls. In the present case, the pill-box cavity acts as the outer concave grounded electrode. The objective was to study the plasma-surface interaction of all available surfaces on the varied diameter structures.

The test pill-box cavity is made of three cylindrical structures made of stainless steel. The two smaller cylinders are a 7.1 cm in inner diameter and 10 cm in length. The large cylinder is a 15 cm in inner diameter and 10 cm in length. The smaller and the larger cylinders mimicked the beam tube and the single cell 1497 MHz SRF cavity. All three cylinders have four holes at 90 degrees each with a mini conflate flange (CF) welded to it for diagnostic and sample holding purposes. These cylindrical structures were joined by transition flanges.

FIG. 48: Cylindrical single cell pill-box cavity

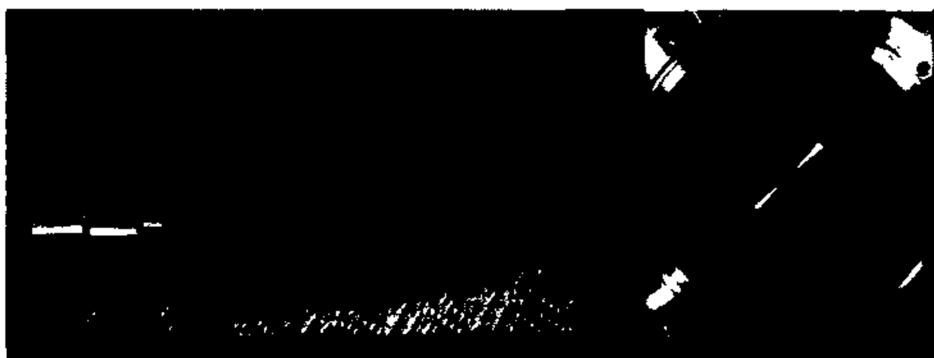

FIG. 49: Photos of variable diameter Nb ring samples to be placed in the pill-box cavity (left) and Nb ring samples inside the pill-box cavity (right).

The inner surface was completely filled with the ring and disk samples to make it a single cell Nb pill-box cavity. In this configuration, each part of the inner structure can be studied separately. The side image of the Nb ring type samples is shown in Fig. 49. The width of each ring sample is 2.5 cm and its ring diameter is equal to the cylindrical steel cavity diameter (15 cm outer diameter and 7.5 cm inner diameter). The disk type samples are used to cover the sidewall of the test cavity to examine the lateral effect of the plasma on Nb.

7.1.2 ELECTRODE GEOMETRY

The inner electrode was coupled to an rf and dc powered source. Its length is chosen considering the complexity in plasma asymmetry due to the varied diameter structure of the SRF cavity. In Fig. 50, three options considered for the inner electrode are shown. The shorter electrode option was chosen to avoid the problem of multiple asymmetries. The plasma sheath potential asymmetry depends on the inner and outer electrodes surface area ratio. In this work, the voltage asymmetry effect was compensated for by applying a positive dc bias to the inner electrode. The concern about the applicability of options (a) and (b) was that the separate sections exhibit different asymmetry that could not be compensated for by a uniform positive bias, which would lead to etching non-uniformity. Therefore, option (c) was chosen and the inner electrode was cut short to 9.0 cm so that it could be confined to a single-diameter cylindrical cavity. In addition, we designed a disc-loaded, corrugated structure to increase the surface area and reduce asymmetry between the inner and outer electrode surfaces [110].

7.1.3 SEGMENTED PLASMA GENERATION

The Nb ring samples placed nearer to the gas entry point get much more exposure to fresh radicals compared to the samples placed further downstream from the gas entry point. The depletion of active radicals along the gas flow direction due to the consumption creates extreme non-uniformity in the etch rate between samples. To overcome this problem, we opted for segmented plasma production by movement of the inner electrode. The inner electrode is moved, while the plasma is confined to its length in order to establish the plasma surface interaction on a more compact and better controlled surface section.

The samples placed inside the beam tube diameter cavity are shown in Fig. 51.

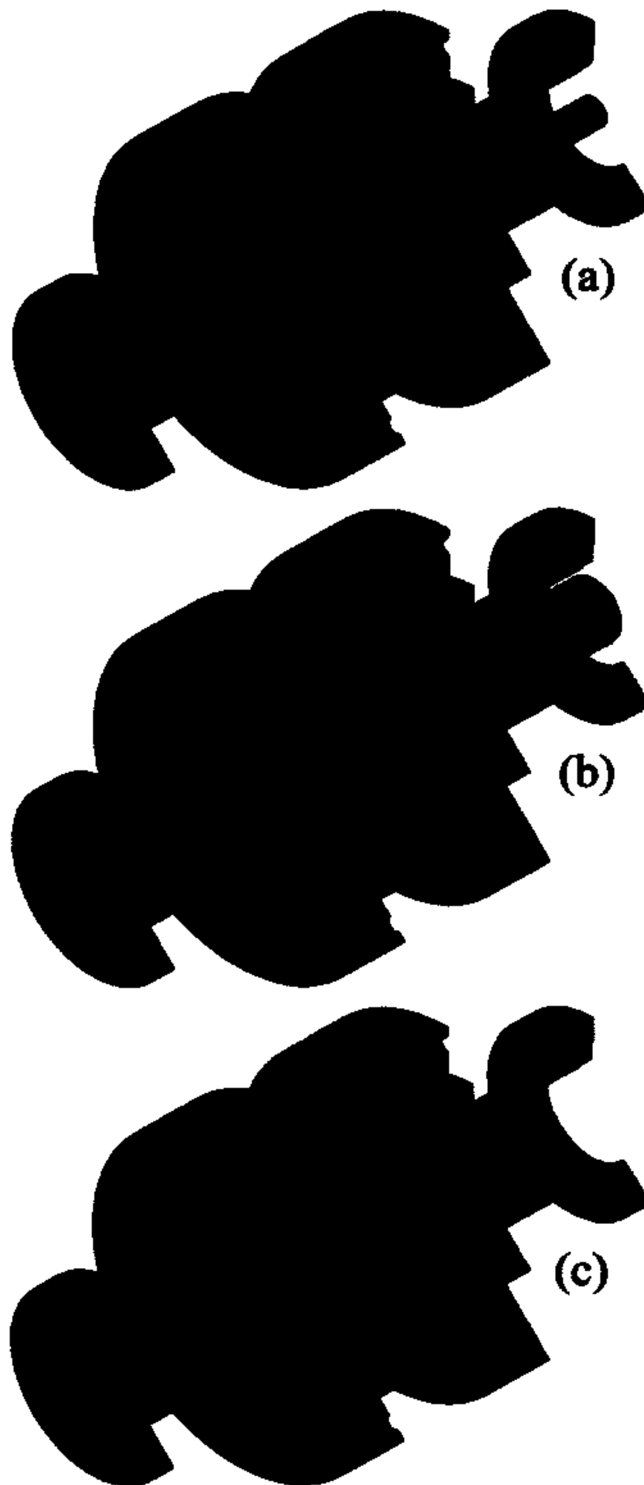

FIG. 50: Arrangements of the inner electrode length in the pill-box cavity (a) variable shape electrode for full length cavity (b) full length electrode (c) shortened electrode in the pill-box cavity.

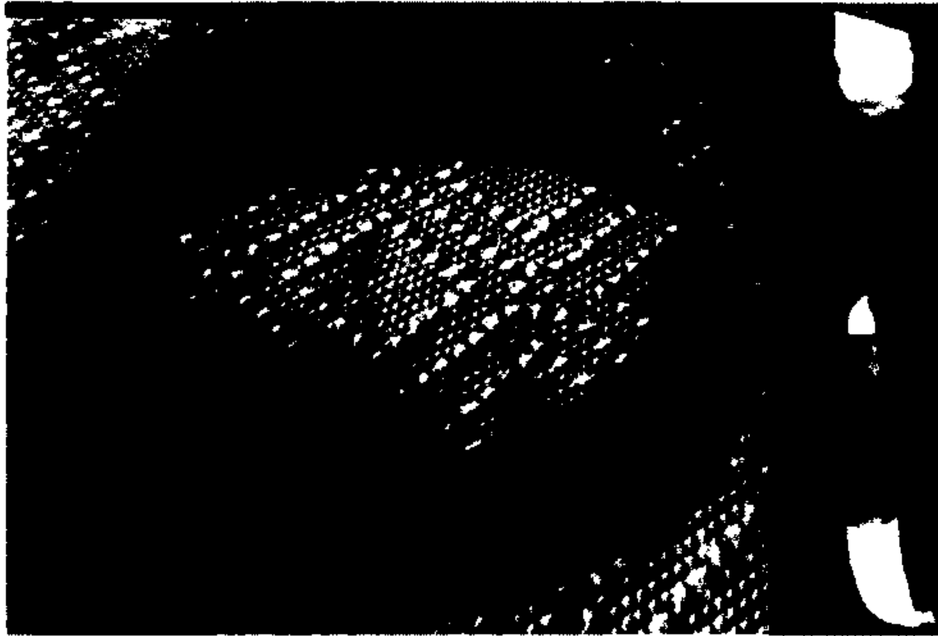

FIG. 51: Image of the Nb sample closest to the gas flow inlet: before plasma etching (left) and after plasma etching (right).

When the shorter corrugated inner electrode was moved inside the pill-box cavity filled with Nb samples, the sample placed inside the beam tube diameter cavity was etched completely as shown in Fig. 51 (right), while the Nb sample placed inside the cell diameter cavity was not etched significantly similar as shown in Fig. 51 (left). Therefore, it turned out to be necessary to establish the synchronous step-wise movement of both the electrode and the gas inlet.

7.1.4 ELECTRODE AND GAS FLOW INLET MANIPULATION

In the present setup, the inner electrode and the gas inlet have been moved so that the gap between them remained constant. Sole sequential movement of the inner electrode without the gas inlet movement could not result in the uniform etching. Even though the inner electrode is further away from the gas flow inlet, due to the low pressure environment, the plasma formation around the first Nb sample could not be prevented. In summary, the uniform etching of the single cell pill-box cavity is faced with a combination of two challenges. First is the variation in asymmetry, as the varied diameter cell plasma is much more asymmetric than the beam tube

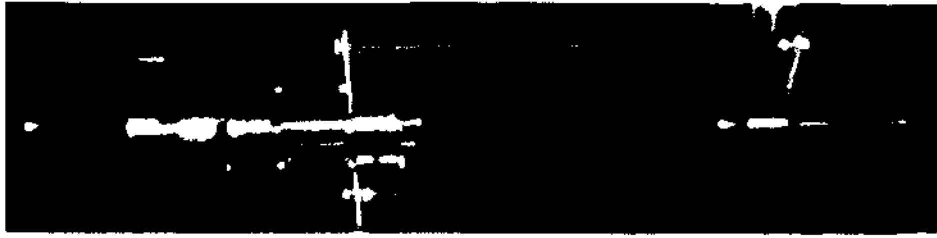

FIG. 52: Image of moving gas flow inlet setup.

diameter plasma. Consequently, the etch rate of Nb may be much higher at the beam tube than at the cell even when the sample was located at a longer distance from the gas flow inlet. The second challenge is in the immediate consumption of the fresh radicals by the Nb sample located closest to the gas inlet.

To overcome these issues, several steps were taken. First, the shape of the gas flow inlet was changed. It was partially enclosed and fixed to the bellows to have synchronous movement with the inner electrode. The moving gas flow inlet arrangement is shown in Fig. 52. The gas flow inlet (0.64 cm tube) was placed in a double conical-shape stainless steel funnel to give an outward directional flow to the gas. The diameter of the conical funnel is kept around 5.0 cm (inner electrode diameter) to stop the reflection of gas flow due to obstruction by the inner electrode. The distance between the gas flow inlet and the inner electrode was around 5.0 cm and the inner electrode and the gas flow inlet were moved at the same time. Step-wise sequential plasma generation enabled the plasma processing of the large diameter cell region only for a longer time, as the beam tube section of the pill-box cavity was etched a lot faster. Hence the processing of the cell region consumes most of the etching time, while much less time is needed when the inner electrode was inside the beam tube diameter. The experiment setup with the inner electrode movement and gas flow inlet movement is shown in Fig. 53.

The simultaneous movement of the gas flow inlet and the inner electrode, the maximum plasma exposure to cell structure, and the heating of the cell only helps in reducing the extreme non-uniformity in plasma surface interaction between the beam tube diameter and cell structure. With these steps, the etching of the Nb samples placed on the cell diameter cylindrical cavity and the samples placed on the transition flanges were possible.

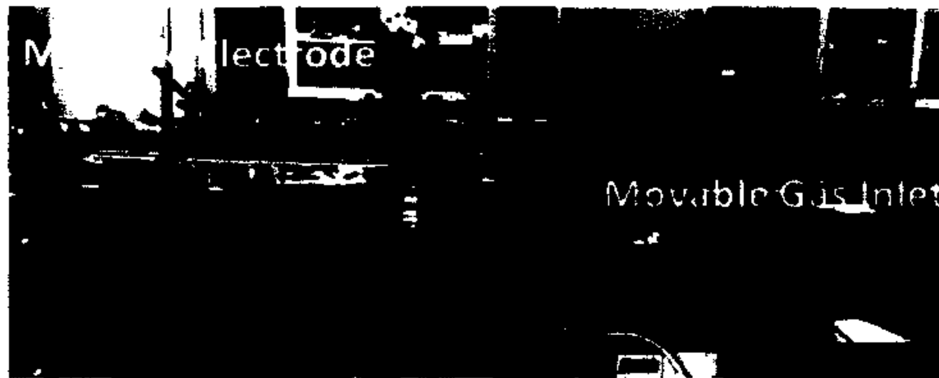

FIG. 53: Pill-box cavity with movable inner electrode and movable gas flow inlet.

FIG. 54: Pill-box cavity with plasma.

7.1.5 HEATING

The etch rate increases exponentially with the temperature [8]. In order to reduce the etch rate on the beam tube and increase the etch rate on the larger diameter cell structure, the heating tape was applied only to the middle section of the cavity with a large diameter. Although the cavity is a metallic structure and the temperature would reach equilibrium, there is a temperature difference between the sections opposite the inner electrode that interact with plasma and those that do not interact with plasma. The plasma produced in the pill-box cavity is shown in in Fig. 54.

Figure 54 indicates that the plasma intensity is higher at the third and fourth

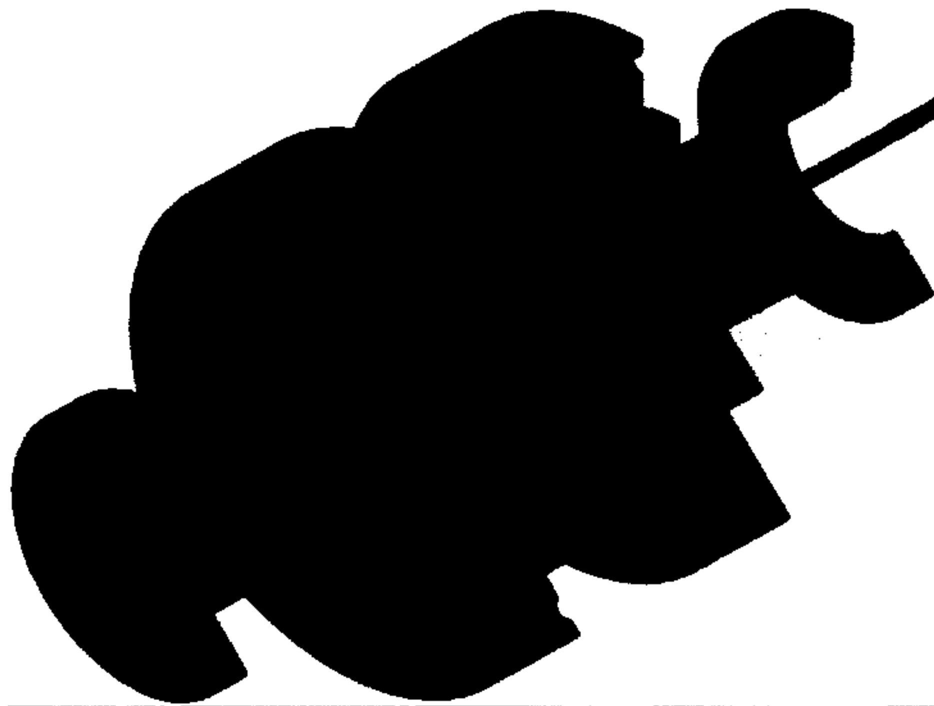

FIG. 55: Schematic diagram of the inner electrode, gas flow inlet and pill-box cavity during plasma processing.

window from the left as the inner electrode was positioned at that section as shown in Fig. 55.

7.2 SUMMARY

The plasma based surface etching of cylindrical three-dimensional structures is challenging, particularly for the structures with varying shape geometry, including the elliptical SRF cavities. The concept of the pill-box cavity with multiple ports for diagnostic and sample holding purposes has been chosen to test the plasma surface interaction. Capacitive coupled rf plasma of Ar/Cl_2 is utilized with the grounded pill-box cavity and powered electrode inside. Here are the most important facts:

(1) The method was developed using a stainless steel pill-box cavity setup that is aligned with the segmented Nb ring samples. It enables the study of the process parameters and the etching rate for a defined part of the cavity inner surface.

(2) Special emphasis was given to the dimension and structure of the powered electrode to reduce the complexity in plasma asymmetry due to the inner and outer

electrodes surface area variation.

(3) Segmented plasma-surface interaction is implemented for efficient and uniform etching process. This was achieved by synchronously moving the powered electrode and the conical shape gas flow inlet. The shape of the gas flow inlet is modified to avoid the reflection from the inner electrode and to act as a barrier for the plasma to spread beyond the gas flow inlet.

(4) A non-dissipative, movable atmospheric pressure rf power feedthrough is developed. Its coupling to the powered electrode is established.

The described procedures have proven to be effective for removal of bulk and impurity material on elliptical SRF cavities. This same procedure shows promise to become a tool for processing any concave cylindrical surface, including controlled surface modification and uniform thin film deposition.

CHAPTER 8

RF TEST OF THE PLASMA ETCHED CAVITY AT CRYOGENIC TEMPERATURE

At cryogenic temperature, rf performence of an actual plasma etched SRF cavity remained the only test left for comparison with wet etching technologies of SRF cavity. The approach to compare the rf test result was to use a single cell SRF cavity and test it at cryogenic temperature after wet etching, and retest the same cavity after plasma etching. The rf testing of a newly made and welded cavity without chemical etching would not provide rf test data that could be used as a reference. It was the reason why a BCP cavity was adopted to test plasma etching process. To test the effect of the plasma etching on the cavity rf performance, a single cell SRF cavity of 1497 MHz is used. The single cell cavity is mechanically polished and buffer chemically etched afterwards. The cavity is rf tested at cryogenic temperatures. This cavity is then plasma processed. The processing was accomplished by moving axially step-wise the inner electrode and the gas flow inlet to establish segmented plasma columns. The cavity is rf tested afterwards at cryogenic temperature. The rf test data, surface condition data is presented in this chapter.

8.1 EXPERIMENT AND METHOD

The apparatus, shown in Fig. 56, was used to plasma etch a single cell SRF cavity. It consists of a rf power supply, which is equipped with a matching network and connected in series with a dc power supply that provides positive dc bias on the inner electrode. rf power is coupled to the inner (driven) electrode with a coaxial atmospheric pressure rf feedthrough. The feedthrough and the inner electrode are attached to a controllable axially moving manipulator, which is shown in the left side of the Fig. 56. The cavity, acting as a vacuum vessel, is connected through the antechamber to the pumping system, which consists of a turbo molecular vacuum pump and a roughing pump with vacuum valves and diagnostic gauges. The exhaust gases are collected and processed in a homemade scrubber that is filled with sodium hydroxide solution in water. Gas is fed to the system through a mixing manifold and

FIG. 56: Experimental setup to plasma etch single cell SRF cavity.

a specially designed gas inlet, which disperses the gas mixture. The gas flow inlet is connected to a second controllable axially moving manipulator, synchronized with the first manipulator, which is shown in the right side of the Fig. 56. The gas flow inlet is a double conical structure shaped as described in Section 7 and reported in Ref. [11]. The gas flow inlet is part of the experimental setup, which is electrically grounded. The inner electrode is a corrugated structure and made of stainless steel. The inner electrode is 9.0 cm in length, which is smaller than the length of the cell structure.

The cavity wall is electrically grounded and serves as the outer electrode of the cylindrical rf discharge. A heating tape attached to a variable autotransformer to control the surface temperature during the etching process is used. The cavity surface temperature is measured and monitored with the help of a thermocouple and a multimeter.

8.2 RESULTS AND DISCUSSIONS

A single cell 1497 MHz SRF cavity was mechanically (centrifugally barrel polishing) polished and then buffered chemically (BCP) etched for 60 micron. The single cell cavity is heat treated in a vacuum furnace at 600^0 C for 10 hours, then degreased and high-pressure water rinsed. The cavity is rf tested at cryogenic temperatures at the JLab VTA facility. The cavity showed field emission around 15 MV/m. The test

results are shown in the Fig. 59. The rf test data at 1.8 K for BCP cavity is shown by the curve with date (8/27/2014).

The cavity is brought back to ODU and plasma etched for 24 hours. The conditions during plasma etching were, pressure, 50 mTorr; rf power, 160 watt; dc bias, 320 volt; temperature, 232^0 K; and dc current, 0.930 A. The gas flow rate in the mass flow controller was 0.43 l/min and the gas used was of 15% chlorine mixed with Argon. The uncertainty of Cl_2 concentration was 2%; in rf power, 10 W; in pressure, 4 mTorr; in dc bias, 10 V; and in dc current, 10 mA. The niobium removed from the cell structure was in the order of 10 microns, while the material removed from the beam tube was in the order of 100 microns. The separation between inner electrode and gas flow inlet during the plasma etching process was kept constant at 5 cm and the movement of the powered electrode was started at the beginning of the cell and finished at the end of the cell. The beam tube plasma etching happend even though the powered electrode was not present in that section.

After 24 hours of plasma etching, heating tape was on for 10 hours and the vacuum pumping system was on for 8 hours after switching off the heating tape. The cavity is open to atmospheric pressure afterwards. There was a thick black residue found on the cavity surface when it was open to atmospheric pressure. This residue is collected and analysed by surface diagnostics tools. The post plasma etched cavity looks dirty as shown in the Fig. 57.

The surface analysis of the residue shows it to be Fe, Ni, Cr and chlorine, which suggest that the inner electrode and gas flow inlet, which were made of stainless steel got plasma etched and the residue fell on the SRF cavity surface. The visible inspection of the gas flow inlet confirms that as well as the elemental analysis of the residue collected from the cavity surface. The images from the surface analysis are shown in Fig. 58.

The plasma-etched cavity was taken to JLab, water rinsed, ultrasonically cleaned and high-pressure water rinsed. The cavity is then rf tested at cryogenic temperatures including 1.8 K. The test result at 1.8 K show the quality factor of plasma etched cavity, an order of magnitude lower compared to the BCP cavity and quenching around 20 MV/m. One of the possible reasons was the deposition of the non-superconducting material on the cavity surface. This test result is shown in the graph with the date (2/2/2015). The cavity was parked at 77 K for 12 hours and tested for hydrogen disease and test results did not show hydrogen disease, as the Q curve was exactly

FIG. 57: Images of a single cell cavity (left) plasma etched (right) (BCP).

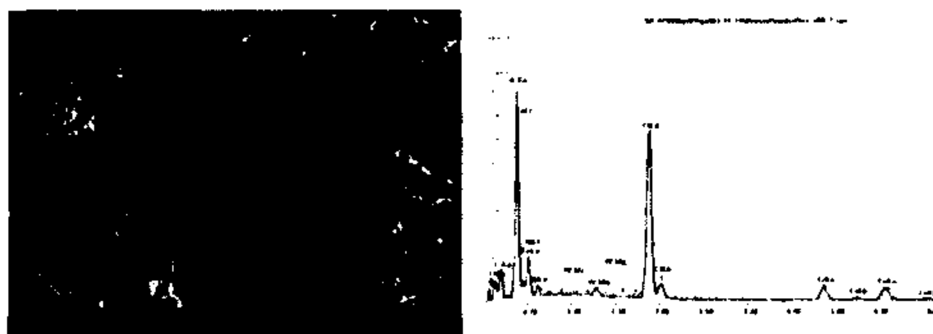

FIG. 58: Images of surface analysis of residue from plasma etched cavity.

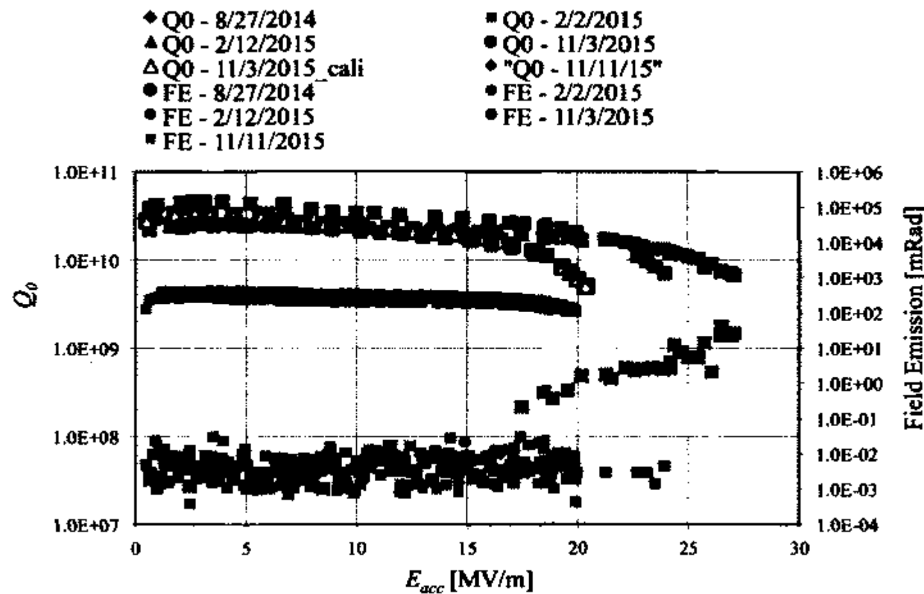

FIG. 59: rf test results of the plasma etched SRF cavity. Black, green, blue and yellow markers indicate performence data of the plasma etched single cell SRF cavity at various stages of the test.

the same as the fast cooled down cavity as shown in the curve plotted with the date (2/12/2015).

To remove the stainless steel residue, aquaregia solution and phosphoric acid chemical cleaning was opted [114, 115]. The use of HF was avoided in order to not disturb the niobium surface. The cavity was chemically cleaned with concentrated aquaregia solution and phosphoric acid. During the phosphoric acid cleaning, the temperature of the acid was raised to 100^0 C. The cavity was degreased and high pressure water rinsed and tested again. The removal of stainless steel residue helped and the quality factor of the cavity came back to the BCP cavity level. There was no sign of field emission during this chemically cleaned plasma etched cavity test as shown in Fig. 59. The test data of date (8/27/14) shows BCP cavity rf performence, test data of date (2/2/15) shows after plasma etching rf test and the test data of (11/3/15) show the rf test after BCP, plasma etching and aquaregia and phosphoric acid cleaning.

This shows that the earlier degradation of the Q factor was due to the stainless steel residue deposition on the surface of the SRF cavity. The component (inner

electrode, gas flow inlet) used in future plasma etching apparatus should be made of niobium and electrically biased so that they should not get etched. The purity of the cavity could be improved by raising the temperature, using higher pumping speed pumps. It seems that all the etched niobium material is not pumped out through the vacuum pumping system due to large amounts of niobium etching and the coaxial nature of the system with limited throughput.

8.3 CONCLUSION

In this Section, we presented the experimental setup to etch a single cell SRF cavity. We presented the rf test of the first plasma etched SRF cavity at cryogenic temperature. The test results show that the plasma-etched cavity would perform as good as the chemically etched cavity if the components used during the processing are made of niobium and are electrically isolated, so that the processing plasma should not etch the other components used for plasma etching. The plasma etched cavity before and after chemical cleaning shows no field emission. It shows that the plasma processing of the cavity might reduce the field emission in SRF cavities. Field emission did not go up even after multiple chemical cleaning and testing which suggest that the plasma is changing some material properties. This is the very first test result of the plasma etched cavity and further tests are required to evaluate the quantity of the reduction and understand the mechanism of reduction. This promising result shows that dry, plasma etching has the potential to be viable for environment friendly and less expensive technology compared to wet etching technology. It also holds promise to implement tailoring of the surface for better superconducting properties.

CHAPTER 9

SUMMARY AND CONCLUSIONS

This dissertation presents the development of plasma processing of SRF cavities in multiple stages. The technology in all its stages would not only help SRF cavities or any 3D structure for etching purposes, but any kind of plasma surface interaction in three dimensional structures. In view of the complex technological challenges facing the development of plasma-assisted SRF surface etching, we have adopted a multi step approach to transition from flat disk coupons to ring samples to pill box cavity to the full scale treatment of large cavity surfaces. The experiment on the flat sample shows that the Ar/Cl_2 combination can etch the bulk niobium surface and the surface roughness of the plasma etched niobium is better or equal to the chemically etched or polished niobium.

We completed the intermediary step of the transition from planar to cylindrical geometry, where a curved Nb sample with the surface area substantially larger than flat disk samples was successfully processed. To plasma etch a grounded wall which has a higher surface area than the inner electrode in a rf coaxial capacitively coupled plasma, the inner electrode has to be biased at a certain positive dc potential with the help of an external dc power supply. We have measured the dependence of the etching rate on the driven electrode diameter, rf power, gas pressure, and chlorine concentration. The conditions for etching are favorable at a large electrode radius, where the self-bias voltage is smaller. We note that the asymmetry is reduced at a higher diameter of the driven electrode. This result also means that the sheath voltage amplitude at the grounded electrode is relatively higher, which is a more favorable condition for the reactive ion etching. The increase of the etching rate is expected to somewhat slow down at higher power, but will certainly provide satisfactory etching rates when combined with temperature and pressure adjustments. Experiments on gas pressure variation indicate favorable conditions at low pressure, as observed in a number of works in planar technology.

The understanding of the etch mechanism is very important. The results suggests that the Nb etch rate can be increased by increasing the temperature of the Nb. The temperature dependence curve follows the Arrhenius type dependence and indicates

the chemical nature of the etching mechanism. The Nb etch rate can also be increased by increasing the positive bias on the inner electrode of the coaxial plasma as it increases the ion incidence energy on the surface. The almost square root dependence on the bias shows the mechanical impact nature of the mechanism, which indicates that there is a physical component to the etching mechanism. The temperature, bias, and gas variation shows that the Nb etching mechanism is neither purely physical etching nor purely chemical. Therefore, we identify it as ion assisted etching, or reactive ion etching.

The experiments on the etching of three-dimensional Nb structures show certain limitations of the coaxial rf plasma reactor. The etch rate non-uniformity experiments show that it will be challenging to uniformly etch an elongated cylindrical structure using a coaxial capacitively coupled rf discharge. To uniformly etch a cylindrical structure, the pressure, gas flow rate, and chlorine concentration have to be high as shown in the etch rate dependence curve in Fig. 26 and Fig. 27, while the diameters of the inner electrode, rf power, temperature, and dc bias have to be low as shown in Fig. 28, Fig. 25, Fig. 23 and Fig. 24. The exact value of these parameters will vary depending on the diameter of the cylindrical cavity to be etched.

This dissertation also presents the self-bias dependence in cylindrical coaxial capacitively coupled plasma on gas pressure and rf power using different diameters of the inner electrode. The self-bias data shows the difference between the Ar and Ar/Cl_2 plasma and offers an explanation for this difference. This study also presents the variation in dc current required for making self-bias potential zero or positive for the Ar and Ar/Cl_2 plasma and the role of plasma density in this variation. It also leads to the observation that positive dc bias increases the plasma density together with plasma potential, which is beneficial in etching the inner surface of the outer cylindrical structure.

We have also studied the possibility to reduce the asymmetry in a coaxial CCP reactor by geometrical enhancement of the surface area of the inner electrode. The geometrical modification of the inner electrode surface area to change the asymmetry of the coaxial cylindrical discharge is a novel concept. The effect of differently shaped inner electrodes on the self-bias potential at different pressure and rf power is measured and the corrugated structure is found to be optimal for reducing and reversing the asymmetry. The addition of Cl_2 makes the asymmetry significantly

smaller at higher pressure and rf power. It is found that for the DLCS inner electrode there is no need to provide additional current to zero the self-bias potential. At higher pressure the Ar/Cl_2 plasma, the dc self-bias potential, which is negative, with a powered inner electrode, reacts to the reversal of the asymmetry in the plasma by becoming positive. The etch rate was measured for the same positive dc bias at lower pressure for various structured inner electrodes. The etch rate is higher for the DLCS electrode due to the reduction in plasma asymmetry.

Uniform plasma processing of cylindrical three-dimensional structures is challenging, particularly for the structures with varying shape geometry, including the elliptical SRF cavities. The concept of the pill box cavity with multiple ports for diagnostic and sample holding purposes has been chosen to test the plasma surface interaction. The method was developed using a steel pill box cavity setup that is aligned with the segmented Nb ring samples. It enables the study of the process parameters and the etching rate for a defined part of the cavity inner surface. Special emphasis was given to the dimension of the powered electrode to reduce the complexity in the plasma asymmetry due to the inner and outer electrodes surface area variation. Segmented plasma-surface interaction was achieved by synchronously moving the powered electrode and the conical shape gas flow inlet. The shape of the gas flow inlet is modified to avoid the reflection from the inner electrode and to act as a barrier for plasma to spread beyond the gas flow inlet. This procedure shows promise to become a tool for processing any concave cylindrical surface, including the controlled surface modification and uniform film deposition.

We have rf tested the first plasma etched SRF cavity at cryogenic temperatures. After removal of the stainless steel residue accumulated due to etching of the steel inner electrode and gas flow inlet by chemical cleaning, the test results show that the plasma-etched cavity would perform as good as the chemically etched cavity if the components used during the processing are made of niobium and are electrically isolated to ensure that the processing plasma should not etch the components other than the SRF cavity. The plasma etched cavity before and after chemical cleaning shows no field emission. Field emission did not increase even after multiple chemical cleaning and testing. Though more tests are needed to show that the plasma etched cavity would eliminate field emission problem. This is the very first test result of the plasma etched cavity and it shows promising results to be viable for environment friendly and less expensive technology compared to wet etching technology. It also

holds the promise to implement the tailoring of the inner surfaces of SRF cavities for better superconducting properties.

BIBLIOGRAPHY

[1] H. Padamsee, J. Knobloch, and T. Hays, (2008).

[2] H. K. Onnes, Comm. Phys. Lab. Univ. Leiden **122**, 124 (1911).

[3] W. Meissner and R. Ochsenfeld, Naturwissenschaften **21**, 787 (1933).

[4] M. Tinkham, *Introduction to superconductivity* (Courier Corporation, 2012).

[5] A. C. Rose-Innes, *Introduction to superconductivity*, Vol. 6 (Elsevier, 2012).

[6] C. Gorter and H. Casimir, Phys **12**, 539 (1934).

[7] F. London and H. London, in *Proceedings of the Royal Society of London A*, Vol. 149 (1935) pp. 71–88.

[8] G. Ciovati, *Investigation of the superconducting properties of niobium radio-frequency cavities* (2005).

[9] A. Pippard, in *Proceedings of the Royal Society of London A*, Vol. 216 (1953) pp. 547–568.

[10] L. D. Landau and V. Ginzburg, Zh. Eksp. Teor. Fiz. **20**, 1064 (1950).

[11] J. Bardeen, L. N. Cooper, and J. R. Schrieffer, Physical Review **108**, 1175 (1957).

[12] J. Knobloch, *Advanced thermometry studies of superconducting radio-frequency cavities*, Ph.D. thesis, Cornell University (1997).

[13] D. Proch, Reports on Progress in Physics **61**, 431 (1998).

[14] J. Halbritter, Zeitschrift für Physik **238**, 466 (1970).

[15] B. Piosczyk and P. Kneisel, (1973).

[16] R. H. Fowler and L. Nordheim, in *Proceedings of the Royal Society of London A*, Vol. 119 (1928) pp. 173–181.

[17] P. Kneisel, **13**, 27 (1980).

[18] P. Kneisel, Nucl. Instrum. Methods **557**, 250 (2006).

[19] K. Saito, H. Inoue, E. Kako, T. Fujino, S. Noguchi, M. Ono, and T. Shishido, *RF superconductivity. Proceedings, 8th Workshop, Abano Terme, Padua, Italy, October 6-10, 1997.*, Part. Accel. **60**, 193 (1998).

[20] Y. P. Raizer and J. E. Allen, *Gas discharge physics*, Vol. 2 (Springer Berlin, 1997).

[21] D. M. Manos and D. L. Flamm, *Plasma etching: an introduction* (Elsevier, 1989).

[22] B. Chapman, *Glow discharge processes: sputtering and plasma etching* (Wiley-Interscience, 1980).

[23] S. M. Rossnagel, in *Thin Film Processes II* (Academic Press New York, 1991) pp. 11–77.

[24] F. F. Chen and J. P. Chang, *Principles of plasma processing* (2002).

[25] M. A. Lieberman and A. J. Lichtenberg, *Principles of plasma discharges and materials processing*, Vol. 30 (Cambridge Univ Press, 1994) pp. 899–901.

[26] A. Bogaerts, E. Neyts, R. Gijbels, and J. van der Mullen, Spectrochimica Acta Part B: Atomic Spectroscopy **57**, 609 (2002).

[27] D. L. Flamm and V. M. Donnelly, Plasma Chem. Plasma Process. **1**, 317 (1981).

[28] J. Coburn, Plasma Chem. Plasma Process. **2**, 1 (1982).

[29] H. Lehmann, Academic Press, Inc., Thin Film Processes II(USA), 1991, , 673 (1991).

[30] C. Cardinaud, M.-C. Peignon, and P.-Y. Tessier, Appl. Surf. Sci. **164**, 72 (2000).

[31] V. M. Donnelly and A. Kornblit, J. Vac. Sci. Technol. A **31**, 050825 (2013).

[32] Y. P. Raizer, M. N. Shneider, and N. A. Yatsenko, *Radio-frequency capacitive discharges* (CRC Press, 1995).

[33] N. L. Bassett and D. J. Economou, J. Appl. Phys. **75**, 1931 (1994).

[34] G. Franz, J. Vac. Sci. Technol. A **23**, 369 (2005).

[35] Plasma Sources Sci. Technol. **11**, A31 (2002).

[36] W. J. Goedheer, Plasma Sources Sci. Technol. **9**, 507 (2000).

[37] H. Koenig and L. Maissel, IBM Journal of research and development **14**, 168 (1970).

[38] M. Cooke and J. Pelletier, Appl. Phys. Lett. **53**, 19 (1988).

[39] R. A. Gottscho, Phys. Rev. A **36**, 2233 (1987).

[40] R. A. Gottscho and C. E. Gaebe, IEEE Trans. Plasma Sci. **14**, 92 (1986).

[41] K. Köhler, J. Coburn, D. Horne, E. Kay, and J. Keller, J. Appl. phys. **57**, 59 (1985).

[42] A. Garscadden and K. G. Emeléus, Proceedings of the Physical Society **79**, 535 (1962).

[43] M. V. Alves, M. A. Lieberman, V. Vahedi, and C. K. Birdsall, J. Appl. Phys. **69**, 3823 (1991).

[44] M. Lieberman and S. Savas, J. Vac. Sci. Technol. A **8**, 1632 (1990).

[45] M. Lieberman *et al.*, IEEE Trans. Plasma Sci. **16**, 638 (1988).

[46] M. A. Lieberman, J. Appl. Phys. **65**, 4186 (1989).

[47] E. Kawamura, M. Lieberman, A. Lichtenberg, and E. Hudson, J. Vac. Sci. Technol. A **25**, 1456 (2007).

[48] D. Gahan and F. SoberÃn, J. Appl. Phys. **101**, 023303 (2007).

[49] S. Yonemura, K. Nanbu, and N. Iwata, J. Appl. Phys. **96**, 127 (2004).

[50] M. Chandhok and J. W. Grizzle, IEEE Trans. Plasma Sci. **26**, 181 (1998).

[51] Z.-G. Li and Y. Ding, Surf. Coat. Technol. **200**, 5655 (2006).

[52] Y. Du and Y. Li, in *Proceedings of World Academy of Science, Engineering and Technology*, 71 (2012) p. 919.

[53] M. Nachman and P. C. Thanh, IEEE Trans. Plasma Sci. **19**, 423 (1991).

[54] M. M. Salem and J. Loiseau, J. Phys. D: Appl. Phys. **29**, 1181 (1996).

[55] G. Franz, A. Kelp, and P. Messerer, J. Vac. Sci. Technol. A **18**, 2053 (2000).

[56] A. Efremov and K.-H. Kwon, JSTS: Journal of Semiconductor Technology and Science **1**, 197 (2001).

[57] K. Takizawa, A. Kono, and K. Sasaki, Appl. Phys. Lett. **90** (2007).

[58] H. Park, C. Garvin, D. Grimard, and J. Grizzle, J. Electrochem. Soc. **145**, 4247 (1998).

[59] M. Zeuner, H. Neumann, and J. Meichsner, J. Appl. Phys. **81**, 2985 (1997).

[60] J. N. Sasserath, J. Appl. Phys. **68**, 5324 (1990).

[61] A. Lichtenberger, D. Lea, and F. Lloyd, IEEE Trans. Appl. Supercond. **3**, 2191 (1993).

[62] T. Harada, K. Gamo, and S. Namba, Jpn. J. Appl. Phys. **20**, 259 (1981).

[63] T. T. Foxe, B. D. Hunt, C. Rogers, A. W. Kleinsasser, and R. A. Buhrman, J. Vac. Sci. Technol. **19**, 1394 (1981).

[64] S. Reible, IEEE Trans. Magnetics **17**, 303 (1981).

[65] M. Chen and Y. H. Lee, J. Electrochem. Soc. **131**, 2118 (1984).

[66] R. Ranade, S. Ang, and W. Brown, J. Electrochem. Soc. **140**, 3676 (1993).

[67] D. Danner and D. Hess, J. Electrochem. Soc. **133**, 151 (1986).

[68] C. Pypen, H. Plenk Jr, M. Ebel, R. Svagera, and J. Wernisch, J. Mater. Sci.-Mater. Med. **8**, 781 (1997).

[69] N. M. Muthukrishnan, K. Amberiadis, and A. ElshabiniRiad, J. Electrochem. Soc. **144**, 1780 (1997).

[70] J. C. Martz, D. W. Hess, and W. E. Anderson, J. Appl. Phys. **67**, 3609 (1990).

[71] Y. Kuo, J. Electrochem. Soc. **144**, 1411 (1997).

[72] M. Rašković, L. Vušković, S. Popović, L. Phillips, A.-M. Valente-Feliciano, S. Radovanov, and L. Godet, Nucl. Instrum. Methods **569**, 663 (2006).

[73] T. Shiota, T. Imamura, and S. Hasuo, Appl. Phys. Lett. **58**, 750 (1991).

[74] S. Popović, J. Upadhyay, J. Mammosser, M. Nikolić, and L. Vušković, J. Appl. Phys. **116**, 173301 (2014).

[75] H. B. Pogge, J. A. Bondur, and P. J. Burkhardt, J. Electrochem. Soc. **130**, 1592 (1983).

[76] V. M. Donnelly, D. L. Flamm, C. W. Tu, and D. E. Ibbotson, J. Electrochem. Soc. **129**, 2533 (1982).

[77] W. T. Lim, I. K. Baek, J. W. Lee, E. S. Lee, M. H. Jeon, G. S. Cho, Y. W. Heo, D. P. Norton, and S. J. Pearton, Appl. Phys. Lett. **83**, 3105 (2003).

[78] S. C. McNevin and G. E. Becker, J. Appl. Phys. **58**, 4670 (1985).

[79] Y. Im, C. Choi, and Y. Hahn, J. Korean Phys. Soc. **39**, 617 (2001).

[80] J. Lee, J. Hong, and S. Pearton, Appl. Phys. Lett. **68**, 847 (1996).

[81] M. Rašković, S. Popović, J. Upadhyay, L. Vušković, L. Phillips, and A.-M. Valente-Feliciano, J. Vac. Sci. Technol. A **27**, 301 (2009).

[82] M. Rašković, J. Upadhyay, L. Vušković, S. Popović, A.-M. Valente-Feliciano, and L. Phillips, Phys. Rev. ST Accel. Beams **13**, 112001 (2010).

[83] P. Duval, J. Vac. Sci. Technol. A **1**, 233 (1983).

[84] J. W. Coburn and E. Kay, J. Appl. Phys. **43**, 4965 (1972).

[85] J. Vossen, J. Electrochem. Soc. **126**, 319 (1979).

[86] C. M. Horwitz, J. Vac. Sci. Technol. A **1**, 60 (1983).

[87] M. Malyshev and V. Donnelly, J. Appl. Phys. **90**, 1130 (2001).

[88] C. J. Mogab, J. Electrochem. Soc. **124**, 1262 (1977).

[89] S. H. Lee, H. P. Gillis, and C. Ratsch, Appl. Phys. Lett. **88**, 161916 (2006).

[90] J. Upadhyay, D. Im, S. Popović, L. Vusković, A. Valente-Feliciano, and L. Phillips, in *Proc SRF*, Vol. 580 (2013) p. 2013.

[91] D. L. Flamm, Pure Appl. Chem. **62**, 1709 (1990).

[92] J. W. Coburn, H. F. Winters, and T. J. Chuang, J. Appl. Phys. **48**, 3532 (1977).

[93] J. W. Coburn and H. F. Winters, J. Appl. Phys. **50**, 3189 (1979).

[94] D. L. Flamm, V. M. Donnelly, and D. E. Ibbotson, J. Vac. Sci. Technol. B **1**, 23 (1983).

[95] S. J. Pearton, A. B. Emerson, U. K. Chakrabarti, E. Lane, K. S. Jones, K. T. Short, A. E. White, and T. R. Fullowan, J. Appl. Phys. **66**, 3839 (1989).

[96] C. T. Nelson, L. J. Overzet, and M. J. Goeckner, J. Vac. Sci. Technol. A **30**, 041305 (2012).

[97] A. Durandet, O. Joubert, J. Pelletier, and M. Pichot, J. Appl. Phys. **67**, 3862 (1990).

[98] H. Kawata, K. Murata, and K. Nagami, J. Electrochem. Soc. **132**, 206 (1985).

[99] R. Bruce and A. Reinberg, J. Electrochem. Soc. **129**, 393 (1982).

[100] A. Ayon, R. Braff, R. Bayt, H. Sawin, and M. Schmidt, J. Electrochem. Soc. **146**, 2730 (1999).

[101] B. N. Chapman, T. A. Hansen, and V. J. Minkiewicz, J. Appl. Phys. **51**, 3608 (1980).

[102] J. Karttunen, J. Kiihamaki, and S. Franssila, Proceedings. SPIE **4174**, 90 (2000).

[103] J. Upadhyay, D. Im, S. Popović, A.-M. Valente-Feliciano, L. Phillips, and L. Vušković, Phys. Rev. ST Accel. Beams **17**, 122001 (2014).

[104] Y. P. Raizer and M. Shneider, Plasma Sources Sci. Technol. **1**, 102 (1992).

[105] R. Hytry and D. Boutard-Gabillet, Appl. Phys. Lett. **69**, 752 (1996).

[106] L. J. Overzet and L. Luo, Appl. Phys. Lett. **59**, 161 (1991).

[107] E. Barnat, G. Laity, and S. Baalrud, Phys. Plasmas **21**, 103512 (2014).

[108] N. Schmidt, J. Schulze, E. Schüngel, and U. Czarnetzki, J. Phys. D: Appl. Phys. **46**, 505202 (2013).

[109] J. Upadhyay, D. Im, S. Popović, A.-M. Valente-Feliciano, L. Phillips, and L. Vušković, arXiv preprint arXiv:1506.05167 (2015).

[110] J. Upadhyay, D. Im, S. Popović, L. Vušković, A.-M. Valente-Feliciano, and L. Phillips, J. Vac. Sci. Technol. A **33**, 061309 (2015).

[111] J. Upadhyay, D. Im, S. Popović, A.-M. Valente-Feliciano, L. Phillips, and L. Vušković, J. Appl. Phys. **117**, 113301 (2015).

[112] M. A. Wolak, T. Tan, A. Krick, E. Johnson, M. Hambe, K. Chen, and X. X. Xi, Phys. Rev. ST Accel. Beams **17**, 012001 (2014).

[113] A. Hershcovitch, M. Blaskiewicz, J. M. Brennan, A. Custer, A. Dingus, M. Erickson, W. Fischer, N. Jamshidi, R. Laping, C.-J. Liaw, W. Meng, H. J. Poole, and R. Todd, Phys. Plasmas **22**, 057101 (2015).

[114] K. R. Williams and R. S. Muller, Journal of Microelectromechanical Systems **5**, 256 (1996).

[115] K. R. Williams, K. Gupta, and M. Wasilik, Journal of Microelectromechanical Systems **12**, 761 (2003).

VITA

Janardan Upadhyay
Department of Physics
Old Dominion University
Norfolk, VA 23529

Education

2016	Ph.D. Physics, Old Dominion University, Norfolk, VA.
2008	M.S. Physics, Old Dominion University, Norfolk, VA.
2001	M.Sc. Physics, Gorakhpur University, Gorakhpur, India.
1999	B.Sc. Physics, Math, Gorakhpur University, Gorakhpur, India.

Publications in Refereed Journals

J. Upadhyay, D. Im, J. Peshl, M. Basovic, S. Popovi, A.-M. Valente-Feliciano, L. Phillips, and L. Vuskovi, "Apparatus and Method for Plasma Processing of SRF Cavities, Nucl. Instr. Meth. Phys. Res. A 818, 76-81 (2016).

J. Upadhyay, D. Im, S. Popovic, A.-M. Valente-Feliciano, L. Phillips, and L. Vuskovic, "Reversal of the Asymmetry in a Cylindrical Coaxial Capacitively Coupled Ar/Cl2 Plasma", J. Vac. Sci. Technol. A 33 (2), 061309 (2015).

J. Upadhyay, D. Im, S. Popovic, A.-M. Valente-Feliciano, L. Phillips, and L. Vuskovic, "Etching Mechanism of Niobium in Coaxial Ar/Cl2 RF Plasma", J. Appl. Phys. 117, 113301 (2015).

J. Upadhyay, D. Im, S. Popovic, A.-M. Valente-Feliciano, L. Phillips, and L. Vuskovic, "Plasma Processing of Large Curved Surfaces for SRF Cavity Modification", Phys. Rev. ST Accel. Beams 17, 122001 (2014).

Typeset using LaTeX.

Janardan Upadhyay